Max-Planck-Institut
für Meteorologie

MAX-PLANCK-GESELLSCHAFT

International Max Planck Research School
on Earth System Modelling

On Entrainment in Sheared Convective Boundary Layers

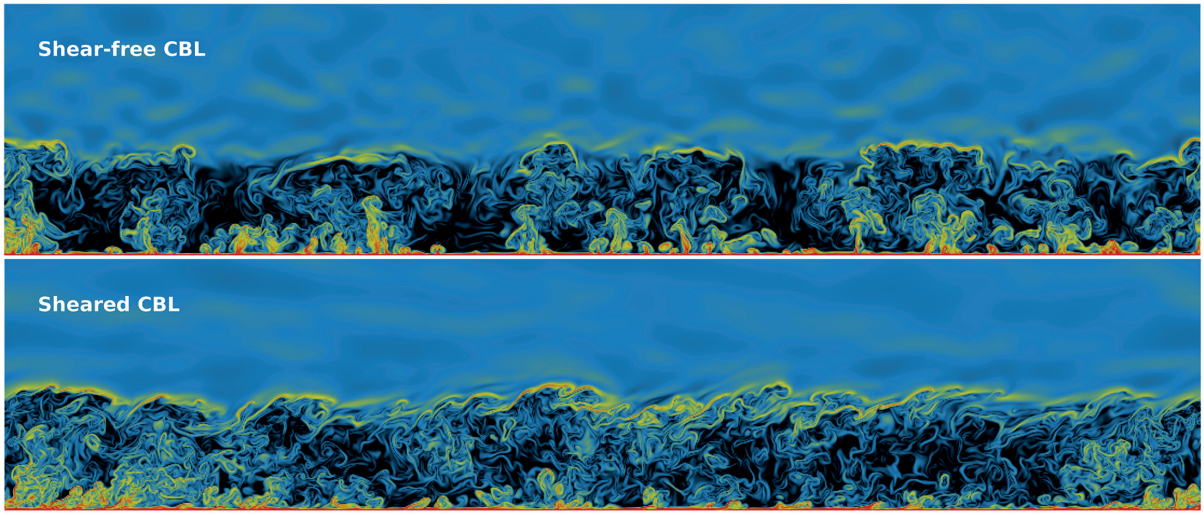

Armin Haghshenas

Hamburg 2019

Berichte zur Erdsystemforschung
Reports on Earth System Science

218
2019

Hinweis

Die Berichte zur Erdsystemforschung werden vom Max-Planck-Institut für Meteorologie in Hamburg in unregelmäßiger Abfolge herausgegeben.

Sie enthalten wissenschaftliche und technische Beiträge, inklusive Dissertationen.

Die Beiträge geben nicht notwendigerweise die Auffassung des Instituts wieder.

Die "Berichte zur Erdsystemforschung" führen die vorherigen Reihen "Reports" und "Examensarbeiten" weiter.

Notice

The Reports on Earth System Science are published by the Max Planck Institute for Meteorology in Hamburg. They appear in irregular intervals.

They contain scientific and technical contributions, including Ph. D. theses.

The Reports do not necessarily reflect the opinion of the Institute.

The "Reports on Earth System Science" continue the former "Reports" and "Examensarbeiten" of the Max Planck Institute.

Anschrift / Address

Max-Planck-Institut für Meteorologie
Bundesstrasse 53
20146 Hamburg
Deutschland

Tel./Phone: +49 (0)40 4 11 73 - 0
Fax: +49 (0)40 4 11 73 - 298

name.surname@mpimet.mpg.de
www.mpimet.mpg.de

Layout

Bettina Diallo and Norbert P. Noreiks
Communication

Copyright

On Entrainment in Sheared Convective Boundary Layers

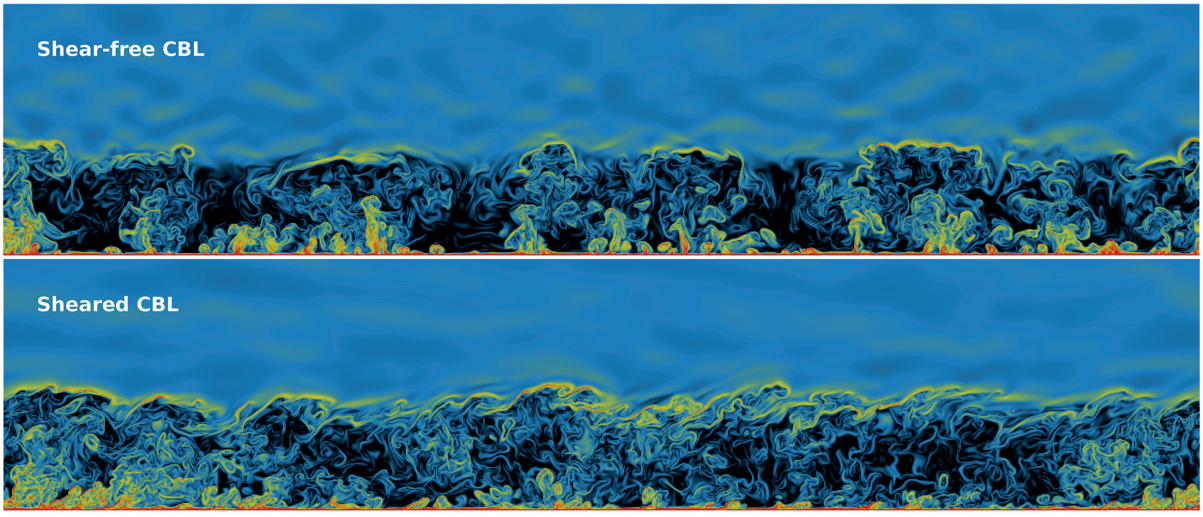

Armin Haghshenas

Hamburg 2019

Armin Haghshenas
aus Ghochan, Iran

Max-Planck-Institut für Meteorologie
The International Max Planck Research School on Earth System Modelling
(IMPRS-ESM)
Bundesstr. 53
20146 Hamburg

Universität Hamburg
Geowissenschaften
Meteorologisches Institut
Bundesstr. 55
20146 Hamburg

Tag der Disputation: 4. April 2019

Folgende Gutachter empfehlen die Annahme der Dissertation:
Prof. Dr. Felix Ament
Prof. Dr. Juan Pedro Mellado

Vorsitzender des Promotionsausschusses:
Prof. Dr. Dirk Gajewski

Dekan der MIN-Fakultät:
Prof. Dr. Heinrich Graener

Berichte zur Erdsystemforschung / Max-Planck-Institut für Meteorologie 218
Reports on Earth System Science / Max Planck Institute for Meteorology 2019

ISSN 1614-1199

Armin Haghshenas

Max-Planck-Institut für Meteorologie
Bundesstrasse 53
20146 Hamburg

The figure on the front page of the dissertation presents a cross-section of the logarithm of the magnitude of the buoyancy gradient for the shear-free and sheared CBLs. Typeset using the classicthesis template developed by André Miede, available at: https://bitbucket.org/amiede/classicthesis/

ABSTRACT

The purpose of this dissertation is to advance our knowledge of wind-shear effects on entrainment in a convective boundary layer (CBL) and to synthesize this new knowledge in the form of closure equations for bulk models. It is well-known that wind shear generally enhances entrainment, which thickens the entrainment zone and increases the growth rate of the CBL. Although previous work has identified major sensitivities of entrainment, and accordingly of sheared CBL properties, to changes in environmental conditions, the characterization of the shear enhancement of entrainment and of its dependence on environmental conditions remains elusive. In particular, scaling laws for different properties of sheared CBLs as functions of the surface and free-atmosphere conditions are lacking. Given that local scales within the entrainment zone become more relevant in sheared CBLs than in shear-free CBLs, one potential reason for the lack of a characterization of wind-shear effects on CBLs is the limitation of previous single-case studies in resolving the required small scales, which are of the order of tens of meters. We use direct numerical simulation and dimensional analysis, for the first time in the context of sheared CBLs, to reduce the uncertainty associated with small scales and to perform a systematic study.

We scrutinize the vertical structure of the sheared CBL and show that wind-shear effects on the CBL structure remain constrained within the entrainment zone. We further show that the entrainment zone in sheared CBLs, consistent with shear-free CBLs, is better described as a composition of two sublayers. However, contrary to shear-free CBLs in which only the upper entrainment-zone sublayer is characterized by a local length scale, we demonstrate that both lower and upper entrainment-zone sublayers in sheared CBLs are characterized by local length scales. We perform an integral analysis of the turbulence kinetic energy budget and find an independent variable that fully embeds the dependence of sheared CBL properties on environmental conditions. The reduction in the number of independent variables to one enables us to provide the scaling laws for different CBL properties, such as different definitions of the CBL height and the entrainment-flux ratio, as functions of environmental conditions. These scaling laws allow us to tackle a major long-standing limitation of previous bulk models, which is the singularity at a finite wind strength, and to propose non-singular bulk models of sheared CBLs. We argue that zero-order bulk models, despite their simplicity compared to higher-order models, can accurately predict bulk properties of sheared CBLs when the relevant features of the actual entrainment zone are considered in the entrainment closures.

ZUSAMMENFASSUNG

Das Ziel dieser Dissertation ist es, besser zu verstehen, wie Windscherung Entrainment in einer atmosphärischen konvektiven Grenzschicht beeinflusst und dieses neue Wissen im Form der Schließungsgleichungen für Massenmodelle zu synthetisieren. Es ist bekannt, dass Windscherung Entrainment im Allgemeinen verstärkt und dadurch die Dicke der Entrainmenzone und die Wachstumsrate der konvektiven Grenzschicht erhöht. Obwohl frühere Forschungsarbeiten herausgefunden haben, wie Entrainment — und somit die Eigenschaften einer gescherten konvektiven Grenzschicht im Allgemeinen — von den Umgebungsbedingungen abhängen, bleibt es schwierig diese Effekte zu charakterisieren. Insbesondere fehlen Skalierungsgesetze, welche beschreiben, wie verschiedene Eigenschaften der gescherten konvektiven Grenzschicht von den Oberflächen und Atmosphäreneigenschafen abhängen. Die Tatsache, dass Wind die Bedeutung der lokalen Skalen innerhalb der Entrainmentzone erhöht, legt nahe, dass der Grund für die fehlende Charakterisierung von Windscherungseffekten, in der Unfähigkeit früherer Studien liegt, diese kleinskaligen Prozesse darzustellen. Daher verwendet diese Dissertation das erste Mal direkte numerische Simulationen um die Unsicherheiten, welche als Folge kleinskaliger Prozesse entstehen, zu reduzieren. Des weiteren führen wir eine Dimensionsanalyse durch, um Windscherungseffekte systematisch zu analysieren.

Wir untersuchen die vertikale Struktur der gescherten konvektiven Grenzschicht und zeigen, dass Windscherungseffekte in der Entrainmentzone lokalisiert bleiben. Des weiteren zeigen wir, dass sich die Entrainmentzone, auch in der Gegenwart von Wind, gut als Zusammensetzung von zwei Teilschichten beschreiben lässt. Allerdings ändert Wind die Skalierung der unteren Teilschicht. Während sich in der scherfreien konvektiven Grenzschicht nur die obere Teilschicht mit einer lokalen Längenskala charakterisieren lässt, lassen sich in einer gescherten konvektiven Grenzschicht beide Teilschichten mit Hilfe lokaler Längenskalen charakterisieren. Darüber hinaus zeigt eine Integralanalyse des Turbulenz-Energiebudgets, dass sich verschiedene Eigenschaften einer gescherten konvektiven Grenzschicht als Funktion einer einzigen unabhängigen Variable charakterisieren lassen. Diese neuen Skalierungsgesetze erlauben es uns, eine bekannte Schwachstelle bestehender Massenmodelle zu beheben. Diese Schwachstelle besteht darin, dass bisherige Massenmodelle aufgrund einer Singularität bei einer endlichen Windstärke divergieren. Wir führen ein Massenmodell nullter Ordnung ein, welches frei von einer solchen Singularität ist. Des weiteren zeigen wir, dass dieses Massenmodell, trotz seiner Einfachheit im Vergleich zu Massenmodellen höherer Ordnung, die Eigenschaften einer gescherten konvektiven Grenzschicht akkurat darstellt. Dies folgt daraus, dass die verwendete Schließungsgleichung relevante Eigenschaften der Entrainmentzone implizit berücksichtigt.

PUBLICATIONS RELATED TO THIS DISSERTATION

Haghshenas, A., Mellado, J.P., "Characterization of wind-shear effects on entrainment in a convective boundary layer", J. Fluid Mech., 858, 145-183 (2019). See Appendix A.

Haghshenas, A., Mellado, J.P., Hartmann, M., "Non-singular zero-order bulk models of sheared convective boundary layers", J. Atm. Sci., (In review). See Appendix B.

CONTENTS

I UNIFYING TEXT

1 ON THE RELEVANCE OF SMALL-SCALE MIXING IN SHEARED CBLS 1
- 1.1 Importance of atmospheric boundary layers . . . 1
- 1.2 Entrainment in sheared convective boundary layers . . . 2
- 1.3 Current knowledge on entrainment in sheared CBLs . . . 5
- 1.4 Research proposition . . . 9
- 1.5 Research formulation . . . 11
- 1.6 Summary of results . . . 14
- 1.7 Outlook . . . 23

BIBLIOGRAPHY 27

II APPENDICES

A CHARACTERIZATION OF WIND-SHEAR EFFECTS ON ENTRAINMENT IN A CBL 1
- A.1 Introduction . . . 3
- A.2 Problem definition . . . 6
- A.3 Wind-shear effects on buoyancy and velocity . . . 16
- A.4 Wind-shear effects on the entrainment-zone vertical structure . . . 20
- A.5 Quantifying wind-shear effects on entrainment-zone properties . . . 26
- A.6 Discussion . . . 34
- A.7 Summary and conclusions . . . 38

B NON-SINGULAR ZERO-ORDER BULK MODELS OF SHEARED CBLS 1
- B.1 Introduction . . . 3
- B.2 Formulation . . . 5
- B.3 Zero-order bulk model . . . 8
- B.4 Non-singular entrainment-closure schemes . . . 11
- B.5 Evaluation of ZOM predictions . . . 15
- B.6 Discussion . . . 18
- B.7 Summary and conclusions . . . 23

LIST OF FIGURES

Figure 1 Sketch of the diurnal variation of the ABL over land and of its vertical structure. . . . 3
Figure 2 Sketch of the cloud-free barotropic CBL in the quasi-steady regime considered in this work. . . . 11
Figure 3 Vertical profiles of the TKE budget terms normalized by the surface buoyancy flux. . . . 15
Figure 4 Temporal evolution of the height of the minimum buoyancy flux normalized by the encroachment length scale. . . . 16
Figure 5 Sketch of the vertical structure of the CBL-top region, including the top part of the mixed layer and both EZ sublayers. . . . 17
Figure 6 Verification of the scaling laws for different definitions of the CBL height with DNS data. . . . 19

ACRONYMS

ABL	Atmospheric boundary layer
CBL	Convective boundary layer
DNS	Direct numerical simulation
EZ	Entrainment zone
FOM	First-order bulk model
LES	Large eddy simulation
RANS	Reynolds-averaged Navier Stokes
TKE	Turbulence kinetic energy
ZOM	Zero-order bulk model

Part I

UNIFYING TEXT

1

ON THE RELEVANCE OF SMALL-SCALE TURBULENT MIXING IN SHEARED CONVECTIVE BOUNDARY LAYERS

The **atmosphere boundary layer** (ABL) is of significant importance for the climate system as it regulates the exchange of energy, momentum, moisture, and other scalars between the Earth's surface and the **free atmosphere**. Despite continuing efforts in the past decades, uncertainties still remain in different aspects of ABLs. **Entrainment** is one key aspect of ABLs that still remains a challenge. There is emerging evidence that the still incomplete characterization of entrainment stems from the limited understanding of small-scale turbulent mixing in stably-stratified environments (Driedonks & Tennekes, 1984; Mellado, 2017; Reeuwijk et al., 2018; Mellado et al., 2018). Indeed, difficulties in obtaining accurate data at the required small scales, which are of the order of tens of meters, account for the lack of complete understanding and quantification of entrainment. In this regard, entrainment often compounds turbulent mixing with other complex phenomena such as wind shear and clouds (Stull, 1988; Garratt, 1992). The presence of wind shear within the ABL strengthens the relevance of local small scales, as wind shear locally generates turbulence on smaller scales compared to convection (Kim et al., 2003; Fedorovich & Conzemius, 2008). The presence of clouds at the ABL top reinforces the importance of local small scales even more substantially, given that radiative and evaporative cooling near the cloud top generates convective instabilities, and accordingly turbulence, on meter and submeter scales (VanZanten, 2002; Wood, 2012; Mellado, 2017). This dissertation elaborates on fluid mechanical aspects associated with the effects of wind shear on entrainment in a cloud-free ABL, arguing that studying entrainment in this simplified case, i.e. the cloud-free limit, helps to better understand cloud formation and entrainment in cloud-top ABLs.

***Atmospheric boundary layer**: the bottom, often turbulent part of the atmosphere that is directly influenced by the Earth's surface and by the diurnal cycle.*

***Free atmosphere**: the often quiescent and stably stratified part of the atmosphere, which is located immediately above the ABL.*

***Entrainment**: the process by which a non-turbulent fluid is incorporated and mixed into a turbulent fluid such that the former non-turbulent fluid becomes a part of the turbulent fluid.*

This dissertation is written in a cumulative way, comprising a unifying text and two appendices. The appendices contain two journal papers (one published and one submitted) that are the cornerstones of the unifying text.

1.1 IMPORTANCE OF ATMOSPHERIC BOUNDARY LAYERS

Given that most living entities are within the ABL, an understanding of ABL processes and their potential influence on life on Earth is of great significance. The ABL plays a vital role in controlling key aspects of many disciplines, including urban meteorology, mesoscale meteorology, agricultural science, hydrology, renewable energy, weather forecasting and climate, etc. For instance, the structure and dynamics of the ABL are fundamental to air quality issues, since the ABL acts as a buffer region between the Earth's surface and the free atmosphere. Knowledge on the ABL is, hence, essential for urban meteorology as the depth of the ABL regulates the concentration of air pollution.

In this regard, the need for better understanding of the controlling factors of the ABL depth becomes more critical, and studies of the ABL become increasingly in demand as cities become larger and more polluted (Yu et al., 2013; Barlow, 2014). Agriculture and hydrology are also highly associated with the ABL and its different processes such as dispersion and deposition of atmospheric pollutants to crops, evaporation, frost formation and rainfall (Camillo et al., 1983; Fritz & Hoffmann, 2008). Natural hazards such as floods, thunderstorms and wildfires that might threaten terrestrial life are largely affected by the ABL (Zampieri et al., 2005; Sun et al., 2009; Nowotarski et al., 2014). Better understanding of the structure and dynamics of the ABL is key for continuing the rapid expansion of renewable energy. Optimizing the efficiency of wind farms considerably relies on the accurate prediction of ABL flow and its interactions with wind turbines at a wide range of spatial and temporal scales (Burton et al., 2011; Porté-Agel et al., 2014).

The importance of the ABL as a critical component of the climate system has been recognized since the pioneering work of Manabe & Strickler (1964). About half of the kinetic energy of the atmosphere is dissipated in the ABL, and it is the major sink of momentum for the atmosphere (Stull, 1988; Garratt, 1992). One key challenge in atmospheric science and related disciplines is that resolution in large-scale atmospheric models is far beyond the dynamically relevant scales of the ABL. This means that the ABL needs to be accurately parameterized to be reasonably represented in large-scale models, given that no large-scale model is conceptually complete without representation of ABL effects, and that any prediction model is condemned to failure without a sufficiently accurate parameterization of the ABL (Stewart, 1979). Despite considerable progress in the past decades, uncertainties associated with ABL parameterization remain one of the primary sources of inaccuracies in large-scale models (Ayotte et al., 1996).

Better understanding of ABL processes and more accurate ABL parameterization schemes are becoming increasingly in demand with the growing relevance of mesoscale numerical modeling to climate science and the development of high-resolution large-scale models (Baklanov et al., 2011). In this regard, since much of the incomplete characterization of ABL processes arises from uncertainties in the understanding of small-scale turbulent mixing within the ABL, information on very small spatial and temporal scales is highly critical. Following this line of argumentation, this dissertation aims at providing better understanding of prevailing daytime ABL processes and more accurate daytime ABL parameterization schemes by analyzing data obtained on very small spatial and temporal scales.

1.2 ENTRAINMENT IN SHEARED CONVECTIVE BOUNDARY LAYERS

This section restricts the research context and introduces the specific problem concerning this dissertation. The turbulent nature of the ABL is its most conspicuous feature, which is driven by two main forcing mechanisms: wind shear and buoyancy. However, buoyancy can also play a damping role on turbulence under some circumstances. The ABL is commonly classified into three main groups based on the role of buoyancy in the ABL evolution (Garratt, 1994):

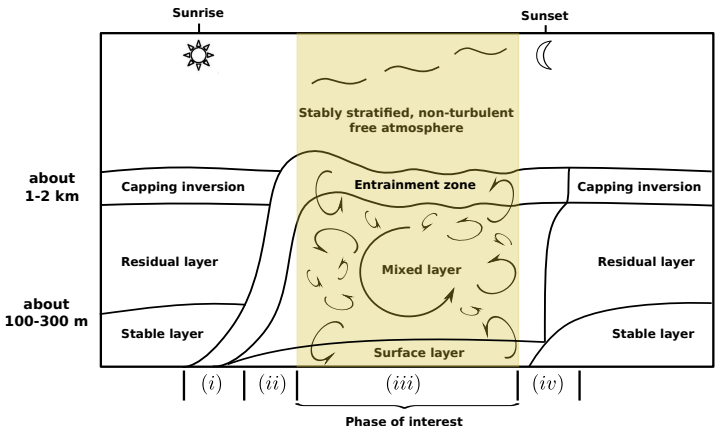

Figure 1: Sketch of the diurnal variation of the ABL over land and of its vertical structure. This research work focuses on the third phase of the CBL evolution, which is shaded in yellow. Strong turbulent mixing and slow growth of the CBL by entrainment are the main characteristics of the CBL in this phase. [Figure adopted from Stull (1988)].

- The unstable ABL: when buoyancy triggers turbulence, resulting from the strong underlying surface heating that produces thermal instability and convection in the form of plumes and thermals.
- The stable ABL: when buoyancy hampers turbulence, resulting from the strong underlying surface cooling that produces thermal stability.
- The neutral ABL: when buoyancy plays no role in triggering or hampering turbulence, resulting from the situation in which there is no flux of buoyancy from the underlying surface.

Wind shear that originates from the vertical gradient of the horizontal wind due to surface friction is the only driving mechanism of turbulence in the last two groups. The unstable ABL occurs during the day time and the neutral and stable ABL occur mostly, though not exclusively, during the night time. The unstable ABL—also referred to as the convective boundary layer (CBL)—is itself classified into the shear-free and sheared CBL, depending on the presence of wind shear within the CBL. Arguing that the shear-free CBL is very rare in nature, the subject of this research work is the sheared CBL in which both buoyancy and wind shear drive turbulence. We approach the sheared CBL such that we consider buoyancy as the prevailing forcing mechanism of turbulence, and we perturb the system by adding first weak and then gradually stronger wind shear. We then investigate how wind shear affects the structure and dynamics of the CBL.

The diurnal cycle of solar heating in the daytime and longwave cooling in the nighttime is one of the important factors in determining the ABL evolution and structure (Stull, 1988). The evolution of CBLs over land is generally described in four phases (see figure 1) : (*i*) during the early morning the CBL is shallow and it grows slowly into the strongly stable boundary layer that was formed in the previous night; (*ii*) by the late morning, the stable layer is fully eroded, and the CBL starts to penetrate into the residual layer, a weakly stratified layer that is left from the CBL of the previous afternoon. The CBL in this phase grows rapidly until it fully devours the residual layer; (*iii*) the CBL encounters the capping inversion at the top of the

residual layer. The capping inversion, which is also a remnant of the CBL from the previous afternoon, hinders the CBL growth rate. The rising thermals, however, tend to overshoot and penetrate through the free atmosphere, causing a slow growth of the CBL. This phase lasts over most of the afternoon and results in the conventional conceptual structure of the CBL that comprises three sublayers: the **surface layer**, the **mixed layer**, and the **entrainment zone** (EZ); and (*iv*) buoyancy-generated turbulence decays as the underlying surface heating diminishes after sunset. This leads to the formation of the stable layer near the Earth's surface and to the collapse of the CBL through most of the boundary layer.

***Surface layer**: the shallow layer above the Earth's surface, where the vertical gradients of CBL properties are large.*

***Mixed layer**: the thick layer above the surface layer, where the vertical gradients of CBL properties are, due to strong turbulent mixing, relatively small.*

***Entrainment zone**: the layer of negative buoyancy flux at the CBL top, where the vertical gradients, due to the suppression of vertical mixing, are once again large.*

In this study, we focus on the third phase, i.e., when the CBL has already penetrated into the stably stratified free atmosphere and grows slowly (see figure 1). The reason to consider this phase is that it accounts for a large period of the day, covering from the late morning till the late afternoon. We refer to this phase as the quasi-steady (equilibrium) entrainment regime that is defined by three characteristics (Fedorovich et al., 2004a). First, CBL properties should evolve on time scales much larger than the eddy turnover time of the large, energy-containing motions; second, there should be a balance between the bulk shear production, buoyancy production and viscous dissipation of the turbulence kinetic energy (TKE); and third, the profiles of different properties, when appropriately normalized, should behave approximately self-similarly. Hereafter, we call this regime the "quasi-steady regime", for simplicity.

One of the most important aspects of the CBL in the quasi-steady regime is entrainment, the process by which air from the free atmosphere is incorporated and mixed into the boundary-layer interior. This work focuses on this process, among different important topics[1] in the context of CBLs that have attracted attention in previous literature. Entrainment is relevant for the structure and dynamics of CBLs because first, the engulfment of non-turbulent air into the CBL causes the CBL to grow slowly, and second, the non-turbulent air in the free atmosphere often has different properties than the air within CBLs. This means that entrainment substantially modifies mean properties of CBLs and plays a critical role in cloud formation and desiccation at the boundary-layer top, in the evolution of mixed-layer properties, and in surface processes. Entrainment influences the atmospheric system on both short and long time scales (Wulfmeyer et al., 2016). On short time scales, entrainment controls the evolution of CBL properties as well as the convective available potential energy and convective inhibition. On longer time scales, entrainment determines the vertical distribution of moisture and accordingly the formation, maintenance, and desiccation of clouds and precipitation.

Entrainment has been investigated in the past decades in both the fields of fluid mechanics and meteorology. In fluid mechanics, entrainment in a stably stratified environment has often been studied in idealized configurations where the turbulence is forced by a grid or by an imposed mean shear (e.g., Fernando, 1991; Strang & Fernando, 2001; Peltier & Caulfield, 2003; Chung & Matheou, 2012, and references therein). The emphasis in these studies lies on understanding various mixing mecha-

1 A list of the most important topics on CBLs includes formation, maintenance, and dissipation of clouds and their realistic representations in large-scale models (Suarez et al., 1983), vertical transport of properties across CBLs and development of turbulent closures (Louis, 1979), Monin-Obukhov similarity theory (Maronga, 2014) and its breakdown in highly unstable conditions, flow over orography and complex terrain (Grant & Mason, 1990), the interaction between the CBL and the free atmosphere (Sullivan et al., 1998), and development of bulk models of CBLs (Conzemius & Fedorovich, 2006b).

nisms and deriving entrainment-rate laws depending on the stratification conditions. In meteorology, however, entrainment is studied in the context of the CBL, and it remains difficult to extend the results of entrainment in fluid mechanics to entrainment in CBLs. For instance, these previous studies in fluid mechanics indicate that the buoyancy Reynolds number, defined as the ratio of the dissipation rate to the molecular buoyancy flux, should be on the order of 100 for large patches of turbulence to be sustained (Smyth & Moum, 2000a; Portwood et al., 2016), whereas buoyancy Reynolds numbers on the order of 10 are sufficient in the entrainment zone of CBLs (Garcia & Mellado, 2014). The reason for this difference is that large-scale updrafts in the CBL continuously transport turbulence into the entrainment zone. Besides, turbulence in the CBL has its distinct properties, such as the large-scale organization of the flow in convective rolls and the possible interaction between entrainment and near-surface dynamics (LeMone, 1973; Boer et al., 2014; Salesky et al., 2017).

Although previous work has made considerable efforts in studying entrainment in CBLs, uncertainties still remain in key aspects associated with understanding and quantifying entrainment and its parameterization. Having critically reviewed and evaluated ABL parameterization schemes, Ayotte et al. (1996) found that all ABL parameterization schemes have difficulty with representing entrainment even in the cloud-free boundary layer. Characterization of entrainment in CBLs is difficult owing to the complexity and diversity of the influential phenomena in CBLs, namely, turbulent mixing within a stratified medium, convective and shear instabilities, cloud formation and gravity waves. The uncertainties associated with entrainment mostly arise from the limited understanding of small-scale turbulent mixing at the CBL top and challenges in obtaining accurate turbulent quantities, such as variances and covariances, for both simulations and measurements (Driedonks & Tennekes, 1984; Mellado et al., 2018). Given that entrainment in the shear-free cloud-free CBL is relatively well understood and characterized (Fedorovich et al., 2004a; Garcia & Mellado, 2014), this dissertation introduces one extra degree of freedom, i.e. shear instability, and investigates wind-shear effects on entrainment in a cloud-free CBL.

1.3 CURRENT KNOWLEDGE ON ENTRAINMENT IN SHEARED CBLS

In this section, we briefly discuss the current knowledge on the characterization of entrainment in sheared CBLs and its parameterization in large-scale models.

Characterization of wind-shear effects on entrainment

Our knowledge of wind-shear effects on entrainment in CBLs is shaped primarily by three tools: atmospheric measurements, laboratory experiments, and numerical simulations (see review in Conzemius & Fedorovich, 2006a; Pino & Vilà-Guerau De Arellano, 2008; Fedorovich & Conzemius, 2008, and references therein). These studies have shown that, in addition to the surface wind shear, an elevated wind shear is developed across the entrainment zone. They have further shown that the entrainment-zone wind shear generally enhances entrainment, which thickens the entrainment zone and increases the growth rate of the CBL.

A quantitative analysis of wind-shear effects on entrainment in CBLs through atmospheric measurements proves difficult because first, isolating wind-shear effects from the influence of other processes determining the CBL evolution is challenging,

and second, collecting data with satisfactory spatial and temporal resolution, particularly within the entrainment zone, is demanding (Ayotte et al., 1996; Fedorovich & Conzemius, 2008). Sophisticated measurements, including measurements of different definitions of the CBL height, of the entrainment-zone thickness, and of turbulence and stability throughout the boundary layer and above, are required to investigate entrainment in detail (Träumner et al., 2011; Wulfmeyer et al., 2016). Fulfillment of such a complicated task is only feasible by the employment of state-of-the-art facilities such as in-situ aircraft, lidar and Doppler lidar. Early observational studies provided evidence of shear-generated turbulence in the surface layer but not in the entrainment zone (Lenschow, 1970; Pennell & LeMone, 1974). The reason was insufficient measurements at the CBL top to address shear generation of TKE in the entrainment zone (Fedorovich & Conzemius, 2008). It was shown, however, that most of the shear-generated turbulence in the surface layer is probably balanced by dissipation. Later studies in the 1980s, despite collection of sparse data, qualitatively indicated entrainment enhancement due to the presence of wind shear (Garratt et al., 1982; Boers et al., 1984). Although large **entrainment-flux ratios** were reported in some studies based on satellite data (Betts & Ball, 1994; Margulis & Entekhabi, 2004), the overall correlation between wind shear and entrainment-flux ratios was relatively weak. The most solid evidence of entrainment enhancement by wind shear was provided by the observational data of Angevine (1999) and Angevine et al. (2001).

***Entrainment-flux ratio**: the ratio between the minimum turbulent buoyancy flux and the surface buoyancy flux.*

Although laboratory experiments, in particular using the water tank, were successfully designed and conducted to study shear-free CBLs (Deardorff et al., 1969; Willis & Deardorff, 1974) and purely shear-driven boundary layers (Kato & Phillips, 1969; Kantha et al., 1977), few attempts have been made to investigate sheared CBLs. Particularly challenging, in this respect, is conducting a laboratory experiment to simulate the boundary layer growing into the stably stratified medium with wind shear and buoyancy forcings acting simultaneously. In wind-tunnel experiments, stratifying the air is demanding and in water-tank experiments, statistics might be significantly affected by several factors, including side walls and a different Prandtl number from air. Even though considering an annular tank might alleviate side-wall effects, it gives rise to a secondary circulation within the tank that might influence the results (Kato & Phillips, 1969). Despite the described intrinsic challenges in laboratory experiments, stratified wind tunnels have been utilized for studies of a horizontally evolving sheared CBL (Fedorovich & Kaiser, 1998; Fedorovich et al., 2001a,b). These studies have shown significant effects of wind shear on the CBL structure and heat flux at the CBL top. But direct quantification of wind-shear effects on the CBL growth rate were hindered due to the dominating effects of the flow contraction/expansion in the wind tunnel on entrainment (Fedorovich & Conzemius, 2008).

***Large eddy simulation**: simulation that requires a turbulence model to represent the effect of subgrid-scale motions on resolved-scale motions.*

Numerical simulation serves as a powerful tool to investigate systematically sheared CBLs for the following reasons. First, it enables us to conduct a simulation of sheared CBLs in a well-defined setup that is unaffected by the bounding geometry. Second, it allows us to isolate wind-shear effects from the influence of other processes affecting the CBL evolution. Third, it provides a full, three-dimensional set of variables over the entire parameter space for long averaging times. Nonetheless, today numerical simulations suffer from numerical artifacts and limited scale separation. These deficits, however, are becoming less and less with increasing computing power. **Large eddy simulation** (LES) is the numerical tool employed in almost all previous studies of

sheared CBLs. Only within the mixed layer could previous large-eddy simulations accurately reproduce the general vertical structure of shear-free and sheared CBLs and the behavior of relevant low-order statistics of buoyancy and velocity (Stull, 1988; Garratt, 1992; Zilitinkevich, 1991). The reason is that large-scale motions are dominant across the mixed layer, and subgrid-scale models play a relatively small role in that region. The role of small scales on the dynamics and structure of the CBL is, however, significant within the surface layer and the entrainment zone, where the gradients of CBL properties are very large. Hence, one key aspect to quantify the relevant processes affecting the dynamics and structure of the CBL in these regions is to obtain accurate data at the required small scales. These scales are of the order of tens of meters. Typical grid spacings in previous large-eddy simulations are usually of the order of ten meters or more, and hence simulated properties can be strongly influenced by the subgrid-scale models and numerical artifacts, as illustrated by the order-of-one intra-model variability of the minimum buoyancy flux in the inter-comparison study of Fedorovich et al. (2004b). Despite the explained limitation of previous large-eddy simulations, they have lent further evidence that wind shear generally enhances entrainment (Moeng & Sullivan, 1994; Pino & Vilà-Guerau De Arellano, 2008; Liu et al., 2016). They have illustrated that the entrainment enhancement due to wind shear leads to a thicker entrainment zone and a larger growth rate of the CBL. This entrainment enhancement has been attributed to the shear-generated turbulence in the entrainment zone, and not to the vertical transport of shear-generated turbulence from the surface layer. A consensus has been reached in the literature that the wind shear in the surface layer dissipates almost completely locally. Therefore, the surface wind shear affects entrainment mainly indirectly by slowing the flow in the CBL interior that gives rise to the formation of an elevated wind shear, and accordingly a localized shear layer, at the CBL top (Fedorovich & Conzemius, 2008).

Despite the fact that sheared CBLs have been an active research topic in the community of fluid mechanics and meteorology for several decades, some key aspects of sheared CBLs are still unclear. In particular, the quantification of the shear enhancement of entrainment and of its dependence on environmental conditions remains elusive. This work employs a new numerical tool in the context of sheared CBLs, namely **direct numerical simulation** (DNS), to revisit an old problem in the hope of better understanding and characterizing effects of wind shear on entrainment by resolving the required small scales.

Direct numerical simulation: *simulation that does not require a turbulence model as it resolves the whole range of scales from large, energy containing scales to the Kolmogorov scale.*

Parameterization of sheared CBLs in large-scale models

Several ABL parameterization schemes—also known as boundary-layer schemes—have been proposed in the literature to represent the ABL in a physically realistic way in large-scale models. Here, we discuss briefly the two most commonly-used ones.

The first scheme solves the Reynolds-averaged Navier-Stokes (RANS) equations using a turbulence closure (see Holt & Raman, 1988, for a review). (RANS equations are the governing equations of fluid motion subjected to time averaging based on Reynolds decomposition.) The order of prognostic equations that are retained in this approach determines the complexity of the approach. For instance, in the first-order approach the equations for the first moment are retained and any turbulence statistics of second or higher order that appear in the governing equations are replaced by approximations that depend only on first-order statistics. This approach makes the

number of unknown variables equal to the number of governing equations, allowing them to be mathematically closed. For the turbulence closure, the eddy-diffusivity approach, in which the turbulent flux is assumed to be equal to the product of local mean gradients and a turbulent eddy diffusivity, is commonly used. The symbol for eddy diffusivity is often chosen to be K, hence, this approach is also known as K-approach (see e.g. Louis, 1979; Holtslag & Boville, 1993). The eddy diffusivities for momentum, heat, and moisture, which vary in space and time, are determined by a combination of dimensional considerations and empirical measurements (Mason & Thomson, 2015). The eddy diffusivity is usually considered as a product of a length scale and a turbulent velocity scale. Near the surface, the distance from the surface is usually considered as the length scale, whereas within the middle of the boundary layer some length scale related to the boundary layer depth is taken into account. An estimate of the velocity scale is usually made from a mixing length model wherein the velocity scale is approximated as a product of a length scale and the velocity gradient. Despite severe challenges, the boundary-layer scheme based on a RANS approach suits better to neutral and stable ABLs, where the transition between the surface and the free atmosphere above is gradual, and the turbulence slowly dies off with height (Garratt et al., 1996). Although the RANS approach has been extensively modified to address its failure at the top of the mixed layer in CBLs by including a counter-gradient correction term (Deardorff, 1972), computational time is still wasted by having a fine vertical resolution across the mixed layer (Suarez et al., 1983).

***Zero-order model**: the model in which the transition layer is considered as an infinitesimally thin layer with a discontinuous variation of properties.*

***First-order model**: the model in which the transition layer is considered as a finite thickness with linear variation of properties.*

The second scheme is based on the bulk model, where the ABL bulk properties such as the ABL depth and the entrainment fluxes are explicitly predicted using the momentum, buoyancy, and moisture budgets (see e.g. Haltiner & Williams, 1980; Suarez et al., 1983). A very attractive aspect of bulk-model scheme is that interactions with the free atmosphere and processes associated with the ABL-top clouds can be explicitly formulated. The ABL in this conceptual framework is represented by a layer of height-constant properties (also referred to as the mixed layer), which is accompanied by a transition layer at the top. Bulk models are classified based on their degree of complexity in the representation of this transition layer. The simplest is the **zero-order model** (ZOM) (Lilly, 1968). Alternatively, the **first-order model** (FOM) (Betts, 1974) and higher-order models[2] (Deardorff, 1979) have been proposed, arguing that a more realistic representation of the transition layer between the mixed layer and the free atmosphere is required to better quantify CBL bulk properties. However, we show in this dissertation that this argument is not necessarily true and the infinitesimal transition-layer representation of the ZOM is sufficient to precisely reproduce bulk properties in the cloud-free sheared CBL. The set of equations in the zero-order model obtained from vertical integration of momentum, buoyancy, and specific humidity equations suffers from closure problems. These closure problems are associated with the surface and entrainment. For the surface closure, the surface-drag relation with a constant surface-drag coefficient is generally used (see e.g. Boers et al., 1984). For the entrainment closure, a parameterization for the entrainment-flux ratio—also referred to as the entrainment parameterization—is commonly derived by either using a local TKE budget (Zeman & Tennekes, 1977; Pino et al., 2003) or using an integrated TKE budget (Boers et al., 1984; Batchvarova & Gryning, 1994). It is important to note

2 The higher-order models are the models in which the transition layer between the mixed layer and free atmosphere is considered as a finite thickness with high-order polynomial variation of CBL properties.

that the quite flat vertical structure of conserved CBL quantities within the mixed layer makes the bulk model the most appropriate scheme to parameterize CBLs in large-scale models (Ayotte et al., 1996).

Following this line of reasoning, a great deal of effort has been devoted in previous literature to develop bulk models of CBLs. However, uncertainties still remain in some key aspects associated with closures in bulk models. This research work focuses on entrainment closure and is motivated by several challenges in previous work, namely, the lack of agreement on the minimum complexity of the bulk model that is necessary to accurately represent sheared CBLs (Pino et al., 2006; Liu et al., 2016), the large uncertainties in the empirical constants of the entrainment closure (see review in Conzemius & Fedorovich, 2006b), and the singularity of the entrainment closure at a finite wind strength (Driedonks, 1982; Conzemius & Fedorovich, 2004).

1.4 RESEARCH PROPOSITION

As indicated before, entrainment in sheared CBLs still poses challenges in two different aspects. The first aspect is concerned with the characterization of the dependence of entrainment, and accordingly of different properties of sheared CBLs, on environmental conditions. The second aspect is associated with parameterization of entrainment in sheared CBLs to develop bulk models. In the following, we raise four research questions that guide us to address the aforementioned two main challenges. We note that the first two questions are addressed in detail in Appendix A and the second two questions in Appendix B.

Q1: How does the two-layer structure of the entrainment zone in shear-free CBLs change with prescribing wind in the free atmosphere?

The entrainment-zone structure is a fundamental property of CBLs that is associated with entrainment. In shear-free CBLs, Garcia & Mellado (2014) have introduced a two-layer structure to describe the entrainment zone: (*i*) the lower sublayer is characterized by global scales, namely, by a length scale proportional to the CBL depth, and (*ii*) the upper sublayer acts as a transition layer between the turbulent region below and the non-turbulent stably stratified region above, and is characterized by local scales. Quantification of the characteristic scales for both sublayers helped them first, to rationalize the observation that the entrainment-zone thickness deviates from a constant fraction of the CBL depth, and second, to explain the dependence on weak and strong stratification regimes of local properties like the minimum buoyancy flux.

Because of the relevance of the local wind shear in the entrainment zone, understanding the vertical structure of the entrainment zone and quantifying characteristic scales are crucial to understand and characterize wind-shear effects on entrainment. In this work, we show that the entrainment zone in sheared CBLs is also better described as a two-layer structure. However, in addition to the upper entrainment-zone sublayer, the lower entrainment-zone sublayer is also characterized by a local length scale.

Q2: How can we characterize the dependence of different properties of sheared CBLs on environmental conditions?

Previous studies have identified major sensitivities of entrainment—and accordingly of sheared CBL properties—to changes in environmental conditions. For instance,

Scaling law: functional relationships between dependent and independent variables that are consistent with dimensional analysis.

Mean entrainment velocity: time rate of change of the ABL depth, caused by engulfment of air from the free atmosphere into the ABL.

Pino & Vilà-Guerau De Arellano (2008) showed that entrainment generally increases with the free-atmosphere wind velocity. Conzemius & Fedorovich (2006a) found that increasing the free-atmosphere stratification or decreasing the surface buoyancy flux enhances wind-shear effects, because a slower CBL growth permits the accumulation of more wind shear at the CBL top. However, characterization of the dependence of entrainment-zone properties on environmental conditions remains unclear.

In this work, using the new characterization of the entrainment-zone structure (Q1) and performing an integral analysis of the TKE budget, we find a single non-dimensional independent variable that solely characterizes wind-shear effects under arbitrary environmental conditions. We then derive explicit **scaling laws** for different sheared CBL properties, including the CBL depth, the entrainment-zone thickness, the **mean entrainment velocity**, and the entrainment-flux ratio as functions of that non-dimensional independent variable.

Q3: Why do previous bulk models of sheared CBLs suffer from a potential singularity at finite wind strength? How can this singularity be removed?

The potential singularity at finite wind strength in previous entrainment parameterizations is a major long-standing limitation of previous zero-order and first-order models (Driedonks, 1982; Conzemius & Fedorovich, 2004; Conzemius & Fedorovich, 2007). Indeed, the contribution of entrainment-zone shear to the entrainment flux, represented by a negative sign term in the denominator of previous entrainment parameterizations (entrainment closure), could cause the denominator to become zero and the entrainment-flux ratio to become unbounded. Such a singularity occurs not only under very strong shear conditions, but also under moderate shear conditions with initial conditions that are far away from the quasi-steady regime.

We show that the derivation of the entrainment parameterization in previous work in the idealized framework of bulk models—in particular, using the CBL depth as the characteristic length scale of the entrainment zone—accounts for the emergence of the singularity. Using the local length scale of the entrainment zone (Q1) in the integral analysis of the TKE budget solves the singularity issue and leads us to a new non-singular parameterization of entrainment properties (Q2).

Q4: What is the simplest bulk model of sheared CBLs that faithfully represents bulk properties?

The minimum complexity of the structure of the CBL bulk model to precisely predict the evolution of CBL bulk properties such as the CBL growth rate and entrainment fluxes is a controversial issue in previous literature. Betts (1974) argued that oversimplification of the CBL structure leads to misrepresentation of vital processes to the CBL evolution. Although the dependence of sheared entrainment on the entrainment-zone Richardson number, predicted by Mahrt & Lenschow (1976), might suggest that one needs, as a minimum, the FOM representation of the CBL in order to adequately capture the entrainment process in sheared CBLs, some recent work (Pino et al., 2006; Conzemius & Fedorovich, 2007) has found no substantial differences between the overall ability of the ZOM and FOM to predict sheared CBL bulk properties. However, Conzemius & Fedorovich (2007) found that the FOM largely mitigates—though not completely removes—the singularity of the ZOM at finite wind strength. Because of

Figure 2: Sketch of the cloud-free barotropic CBL in the quasi-steady regime considered in this work. The background is a cross-section of the logarithm of the magnitude of the buoyancy gradient for a strongly sheared CBL.

this advantage, they argued that the FOM is superior to the ZOM. Following this line of argumentation, most recent work made the effort to further develop a FOM (Sun & Xu, 2009; Huang et al., 2011; Liu et al., 2016).

In this work, we show that the infinitesimal transition-layer representation of the ZOM is sufficient to precisely reproduce bulk properties of cloud-free sheared CBLs, as long as the entrainment closure appropriately represents the local effects of wind shear on entrainment.

1.5 RESEARCH FORMULATION

In this section, we explain how we formulate the problem such that we can systematically investigate wind-shear effects on entrainment. We then shortly discuss the new research tools in the context of sheared CBLs employed in this work, namely direct numerical simulation and dimensional analysis, and their advantages. In addition, we elaborate on the dimensional analysis of the sheared CBL considered in this work; this discussion helps the reader to follow how we set up the simulations and how we characterize the problem on the basis of the dimensional analysis.

It is a general practice to analyze a simplified (reduced complexity) configuration of any problem, instead of studying it in its full complexity. This approach allows a systematic analysis of the problem. Convective boundary layers, in general, evolve as a result of a complex interaction of diverse phenomena (Stull, 1988). These phenomena include convective instabilities due to heating from the surface or radiative and evaporative cooling at the top, shear instabilities due to the presence of strong wind shear within CBLs, horizontal divergence or convergence of the CBL flow associated with subsidence or lifting at the CBL top, the stability of the free atmosphere and also the stability of the interface between the turbulent boundary layer and the free atmosphere, differential temperature advection, and entrainment. Additionally, the boundary-layer evolution of the previous day as well as terrain effects influence the CBL. In this dissertation, however, we consider a simplified configuration and retain only a subset of the aforementioned processes, namely, convective instability due to surface heating, shear instability, entrainment, and the free-atmosphere stability.

We consider a cloud-free CBL that develops over an aerodynamically smooth surface and that penetrates into a free atmosphere with constant buoyancy gradient, $\boldsymbol{N_0^2}$ (see figure 2). Here N_0 is the Brunt-Väisälä frequency. Convection is imposed and maintained by a constant and homogeneous surface buoyancy flux, $\boldsymbol{B_0}$. We consider barotropic conditions, i.e., the wind strength in the free atmosphere, $\boldsymbol{U_0}$,

$\boldsymbol{N_0^2}$: *the constant buoyancy gradient within the free atmosphere.*

$\boldsymbol{B_0}$: *the constant and homogeneous buoyancy flux at the surface.*

$\boldsymbol{U_0}$: *the height-constant wind velocity within the free atmosphere.*

is constant with height (Fedorovich & Conzemius, 2008; Pino & Vilà-Guerau De Arellano, 2008). In addition, we consider zero Coriolis parameter, which implies that the mean pressure gradient associated with the geostrophic balance is zero. The main reason not to include the Coriolis force in our configuration, despite its relevance for the dynamics of CBLs, is that only one degree of freedom, namely the wind, is intended to be added to the well-studied shear-free limit. Such an approach allows us to systematically study wind-shear effects on sheared CBLs and also provides a reference case to systematically study Coriolis effects in future. The considered simplified configuration is representative of CBLs in midday conditions at the equator over land. Nonetheless, results show that our simulations reproduce main features of barotropic CBLs in middle latitudes.

Research Tools

In this study, we systematically employ direct numerical simulation, a widely-used tool to study canonical problems in fluid mechanics (Moin & Mahesh, 1998), to investigate entrainment in sheared CBLs. Direct numerical simulation reduces the uncertainties associated with subgrid-scale models in previous work to only one non-dimensional parameter—the Reynolds number. In particular, the Reynolds number achieved in our simulations ($Re_* \sim 10^4$) is still orders of magnitudes smaller than in the atmosphere ($Re_* \sim 10^8$). Here Re_* is the convective Reynolds number defined by considering the depth of the CBL and the convective velocity scale (Deardorff, 1970) as the length and velocity scales, respectively. A careful assessment of the dependence of results on the Reynolds number is, hence, necessary to examine whether a tendency towards **Reynolds-number similarity** (Dimotakis, 2000) exists. An observation of this tendency justifies certain extrapolation of results to atmospheric conditions. We note that the discretization of the governing equations in our DNS code is carried out by sixth-order spectral-like compact schemes for the spatial derivatives (Lele, 1992) along with a low-storage fourth-order Runge–Kutta scheme to advance in time (Carpenter & Kennedy, 1994). Such a discretization method, compared to the typically-used second-order central scheme in previous LESs, considerably reduces the uncertainty associated with numerical artifacts.

***Reynolds-number similarity**: the theory, based on observation, that some statistics become independent of the Reynolds number once it is sufficiently large.*

In this study, we employ dimensional analysis, as another novelty of this work in terms of the research tools, to formulate the problem in terms of non-dimensional parameters. This approach enables us to perform a systematic study of wind-shear effects on the structure and dynamics of the CBL. We note that previous work has done only some single-case studies from which it is difficult to extrapolate the results for other environmental conditions. Dimensional analysis benefits this work in several aspects: (*i*) dimensional analysis simplifies the study of sheared CBLs, as it reduces the complexity of the problem by organizing the number of control parameters into a smaller number of dimensionless groups; (*ii*) dimensional analysis enables us to cover a wide range of the parameter space by few numerical simulations, because dimensional analysis generalizes the results such that any conclusion reached for the given values of the non-dimensional parameters is applicable for all different combinations of control parameters that create the given values of the non-dimensional parameters; and (*iii*) dimensional analysis provides the basis for the derivation of scaling laws for properties of interest, as every non-dimensional property is a function of non-dimensional parameters and independent variables.

Dimensional Analysis

The sheared CBL described in the previous section is completely governed by the control parameters $\{\nu, \kappa_b, B_0, N_0, U_0\}$ and the independent variables $\{z, t\}$, once the quasi-steady regime is reached. The parameters ν and κ_b are the kinematic viscosity and thermal diffusivity, respectively. The variables z and t represent the vertical distance from the surface and time, respectively. Dimensional analysis indicates that three non-dimensional parameters are sufficient to characterize the system: the reference buoyancy Reynolds number, the Prandtl number, and the reference Froude number, respectively, defined as

$$Re_0 \equiv \frac{(N_0 L_0) L_0}{\nu}\,, \qquad Pr \equiv \frac{\nu}{\kappa_b}\,, \qquad \text{and} \qquad Fr_0 \equiv \frac{U_0}{N_0 L_0}\,, \tag{1}$$

where

$$L_0 \equiv \left(\frac{B_0}{N_0^3}\right)^{1/2} \tag{2}$$

is the reference Ozmidov length, $\boldsymbol{L_{Oz}}$. Previous work has shown that $\boldsymbol{L_0}$ helps characterize main properties, such as the mean gradients and variances of temperature and specific humidity, in the upper region of the entrainment zone in shear-free CBLs (Garcia & Mellado, 2014; Mellado et al., 2017). The first two non-dimensional parameters, namely the reference buoyancy Reynolds number and the Prandtl number, fully characterize the shear-free limit, and the reference Froude number is introduced to characterize wind-shear effects. The reference Froude number can be rewritten as $U_0/(B_0 L_0)^{1/3}$, which compares the wind velocity in the free atmosphere with the velocity scale associated with motions of size L_0 in a turbulent cascade characterized by an energy transfer rate B_0.

$\boldsymbol{L_0}$: *a length scale that provides a relevant measure for the thickness of the upper region of the EZ in shear-free CBLs.*

$\boldsymbol{L_{Oz}}$: *a length scale that represents the size of the largest motions in a turbulent field unaffected by a background stratification.*

$\boldsymbol{z_{enc}}$: *an integral length scale that provides a relevant measure for the depth of the mixed layer in shear-free CBLs.*

We use $\{z/z_{\mathrm{enc}}, z_{\mathrm{enc}}/L_0\}$ as the non-dimensionalized form of the independent variables $\{z, t\}$. Obtained from the integral analysis of the buoyancy equation, the encroachment length scale, $\boldsymbol{z_{enc}}$, has an analytical relationship (Carson & Smith, 1975) as

$$z_{\mathrm{enc}} = \left[2\, B_0 N_0^{-2} (1 + Re_0^{-1})(t - t_0)\right]^{1/2}\,, \tag{3}$$

where t_0 is a constant of the integration, which quantifies the dependence of the encroachment length scale on the initial buoyancy profile. The independent variable z_{enc}/L_0 characterizes the state of the CBL development. Using z_{enc} instead of time as an independent variable proves useful because it enables us to simply make a one-to-one comparison with results from different numerical simulations conducted with different initial conditions and also with atmospheric measurements. We refer the reader to §A.2.2 in Appendix A for details of the dimensional analysis.

Dimensional analysis indicates that every non-dimensional variable, Π, in the sheared CBL is a function of the non-dimensional parameters and independent variables

$$\Pi(z, t) = f(Re_0, Pr, Fr_0; z/z_{\mathrm{enc}}, z_{\mathrm{enc}}/L_0)\,. \tag{4}$$

As explained in §1.4, one of the main aims of this research work is to characterize the dependence on environmental conditions of various sheared CBL properties by providing corresponding scaling laws.

Description of simulations

In our simulations, we fix $Pr = 1$ in the simulations, which is a good approximation for the Prandtl number of the air in the atmosphere. To systematically investigate the sheared CBL, we consider the shear-free limit, $Fr_0 = 0$, as the reference and gradually increase the reference Froude number. Under weak-wind conditions, effects of wind shear on the structure and dynamics of sheared CBLs are expected to be insignificant. However, we keep increasing the Froude number to observe order-of-one effects of wind shear. This approach allows us to scan a wide range of the parameter space—from strongly to weakly unstable conditions—occurring in the typical midday atmospheric conditions over land. In particular, we change the reference Froude number between zero (no wind condition) and 25 (strong wind condition that corresponds to $U_0 \simeq 15$ ms^{-1} for typical midday atmospheric conditions) in intervals of 5 [see table A.1 in Appendix A for more details]. We run the simulations from a shallow CBL, $z_{enc}/L_0 \simeq 5$, and reach $z_{enc}/L_0 \simeq 35$, covering in this way a large extent of the typical values observed in nature, i.e. $z_{enc}/L_0 \simeq 5 - 50$. As mentioned before, the reference Reynolds number is the only non-dimensional parameter that can not be matched between the conducted simulations and the real atmosphere. We perform the main analysis based on the simulations with $Re_0 = 25$ because these cases reach higher values of state of CBL development z_{enc}/L_0. In addition, we simulate some cases with $Re_0 = 42$ to study the sensitivity of the results to the Reynolds number. Although this range of Reynolds number is small, the observed tendency towards Reynolds number similarity (Dimotakis, 2000) is consistent with that observed in previous work in similar configurations, and supports the use of DNS to study some aspects of the atmospheric boundary layer (Jonker et al., 2013; Waggy et al., 2013; Garcia & Mellado, 2014; Van Heerwaarden & Mellado, 2016; Mellado et al., 2018).

1.6 SUMMARY OF RESULTS

In this section, we present the key results of this dissertation. The first part summarizes the general effects of the wind shear on the structure and dynamics of the CBL. The second part characterizes wind-shear effects on entrainment and answers in detail the first two scientific questions posed in §1.4 (see Appendix A for more details). The third part takes the advantage of this characterization to address the second two scientific questions (see Appendix B for more details).

The main features of barotropic CBLs in middle latitudes, despite neglecting Coriolis effects, are reproduced by the idealized CBL considered in this study (see figure 2). These features include:

1. Strong turbulent mixing within the interior of the CBL that leads to a well-mixed profile of buoyancy and velocity in the mixed layer and an elevated wind shear in the entrainment zone (Sorbjan, 2006; Pino & Vilà-Guerau De Arellano, 2008).

2. Low-speed streaks near the surface due to the presence of surface wind shear, that through interaction with convective cells, tend to form horizontal convective rolls (LeMone, 1973; Moeng & Sullivan, 1994; Salesky et al., 2017).

3. Sustainable patches of Kelvin-Helmholtz-like billows across the entrainment zone, which are induced by the elevated wind shear in a stratified region and

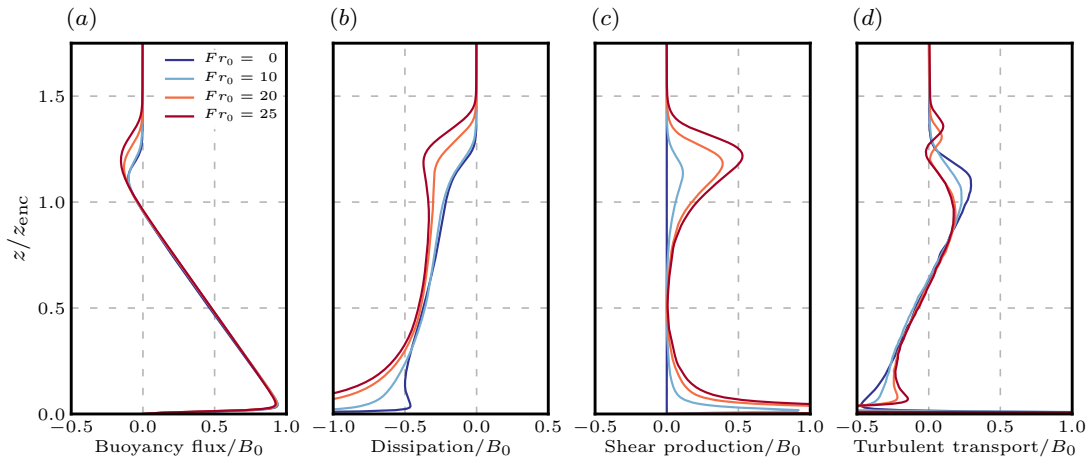

Figure 3: Vertical profiles of the TKE budget terms normalized by the surface buoyancy flux, B_0, for different Froude numbers at $z_{enc}/L_0 \simeq 25$.

are sustained by the interaction between the elevated wind shear and convective thermals impinging from below (Kim et al., 2003).

4. Enhanced gravity waves triggered at the CBL top with respect to shear-free CBLs due to the presence of patches of Kelvin-Helmholtz-like billows that radiate energy from the CBL into the free atmosphere (Schröter, 2018).

Consistently with previous studies of barotropic CBLs in middle latitudes (Pino & Vilà-Guerau De Arellano, 2008; Fedorovich & Conzemius, 2008), we observe that

1. Under all shear conditions considered in this work, some relevant properties, like buoyancy and vertical-velocity statistics, remain approximately unchanged within the mixed layer (see figure 3*a*).

2. Under weak-shear conditions characterized by small Froude numbers, wind-shear effects on the CBL structure and buoyancy properties are negligible over the whole depth of the CBL (see figure 3*a*).

3. Under moderate- and strong-shear conditions characterized by Froude numbers larger than 10, wind shear enhances entrainment. However, these effects on the structure and dynamics of the CBL remain constrained within the entrainment zone. Entrainment enhancement thickens the entrainment zone and increases the growth rate of the CBL (see figure 3).

The relevance of wind shear on the CBL for $Fr_0 \gtrsim 10$ is rationalized by examining wind-shear effects on the dynamics of the entrainment zone. In the shear-free limit, the turbulent transport term is the only source of turbulence across the entrainment zone (figure 3*d*). As wind is introduced in the free atmosphere, additional turbulence is generated through the elevated wind shear in the entrainment zone (figure 3*c*). The immediate effect of shear-generated turbulence on the dynamics of the entrainment zone is that the turbulent transport term reduces across the entrainment zone, meaning that less convectively-generated turbulence in the CBL interior is allowed to enter the entrainment zone. The amount of shear-generated turbulence increases with the Froude number, and therefore, the ratio between the turbulent-transport term and

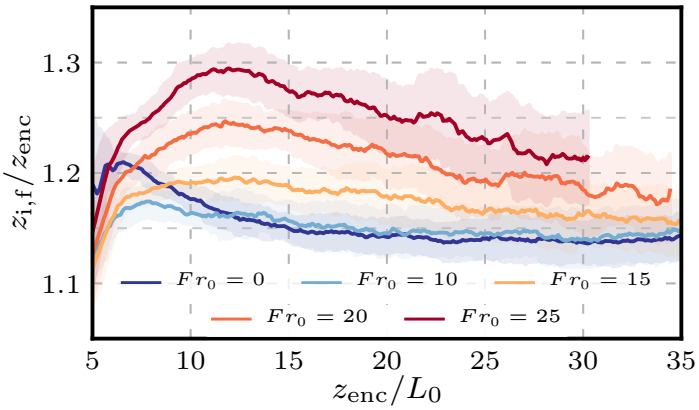

Figure 4: Temporal evolution of the height of the minimum buoyancy flux, $z_{i,f}$, normalized by the encroachment length scale, z_{enc}, for different Froude numbers. Lines indicate the average within an interval $\Delta z_{enc}/L_0 = 2$, and shadow regions indicate the interval of two standard deviations around that average.

the shear-production term decreases with the Froude number. This ratio becomes comparable at $Fr_0 \simeq 10$, which justifies why relevant effects of the wind shear start to emerge at this Froude number.

A key aspect of the barotropic CBL is that wind-shear effects diminish and eventually vanish as the CBL grows (see figure 4). The reason is that the wind velocity in the free atmosphere is constant, and therefore, wind shear is limited in the considered configuration, whereas convection caused by the constant surface buoyancy flux is unlimited and thermals ascending from the mixed layer become more vigorous and dominate mixing in the entrainment zone as time advances (Mahrt & Lenschow, 1976; Liu et al., 2016). Hence, as indicated in the dimensional analysis (cf. Eq. 4), wind-shear effects depend not only on the Froude number Fr_0, or, equivalently, the wind velocity in the free atmosphere, but also on the state of the CBL development, z_{enc}/L_0 (see figure 4). This fact complicates addressing the second research question in §1.4, namely, deriving scaling laws for different CBL properties.

$z_{i,0}$: *the zero-crossing height, where the buoyancy flux becomes zero.*

$z_{i,f}$: *the flux-based height, where the buoyancy flux is minimum.*

$z_{i,g}$: *the gradient-based height, where the mean buoyancy gradient is maximum.*

$z_{i,s}$: *the reference height that marks the transition from the lower EZ sublayer to the upper EZ sublayer.*

Q1: The two-layer structure of the entrainment zone in sheared CBLs

A property that proves useful for the analysis of wind-shear effects on entrainment is the CBL depth and the structure of the entrainment zone. Different definitions of the CBL height have been considered in the literature (see, e.g., Garratt, 1992; Sullivan et al., 1998), as they provide reference positions needed for the detailed analysis of the entrainment zone. In this work, we restrict ourselves to the buoyancy-related definitions of the CBL height, namely, the zero-crossing height, $z_{i,0}$, the flux-based height, $z_{i,f}$, and the gradient-based height, $z_{i,g}$. It is worthy of remark that these heights vary by a few hundred meters in midday atmospheric conditions over land. We follow the structural analysis in Garcia & Mellado (2014) and measure the deviations for different definitions of the CBL height with respect to the shear-free limit.

As explained in §1.4, Garcia & Mellado (2014) have shown that the entrainment zone in the shear-free limit is better described as a composition of two sublayers (see figure 5). The lower entrainment-zone sublayer is located around the height of the minimum buoyancy flux and its vertical structure is characterized by a global length

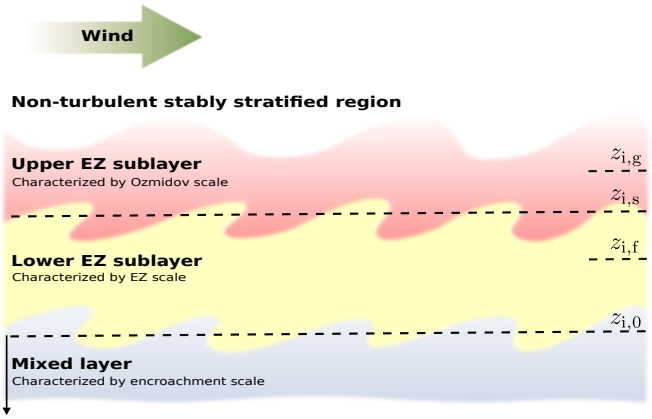

Figure 5: Sketch of the vertical structure of the CBL-top region. Here $z_{i,0}$ is the zero-crossing height, $z_{i,f}$ is the height of the minimum buoyancy flux, $z_{i,s}$ marks the transition from the lower to upper EZ sublayer, and $z_{i,g}$ is the height of maximum buoyancy gradient.

scale that is the encroachment length scale, z_{enc}. The upper EZ sublayer is centered around the height of the maximum buoyancy gradient and is characterized by a local length scale that is the Ozmidov length particularized at the height of the minimum buoyancy flux, $(L_{OZ})_{z_{i,f}}$. As another buoyancy-related definition of the CBL height that will prove useful in the characterization of the entrainment zone of sheared CBLs and also in bulk models, we define $\boldsymbol{z_{i,s}}$ that marks the transition from the lower to upper EZ sublayer (see figure 5).

Figure 4 illustrates that, in sheared CBLs under moderate- and strong-shear conditions, the height of the minimum buoyancy flux around which the lower EZ sublayer is formed is not anymore characterized by the encroachment length scale. Rather a local length scale governs the lower EZ sublayer. We argue that a shear layer is formed around the height of the minimum buoyancy flux, owing to the resemblance between the structure of the wind shear in the entrainment zone of the sheared CBL (see figure 2) and in a stably stratified shear layer (see e.g. Sherman et al., 1978; Peltier & Caulfield, 2003). Given that the vorticity thickness is the well-known characteristic length scale of the stably stratified shear layer, we introduce the local length scale

$$\Delta z_i \equiv \frac{\Delta u}{(\partial_z \langle u \rangle)_{z_{i,f}}} \tag{5}$$

to quantify how wind shear modifies the lower EZ sublayer. The variable Δu is the velocity difference across the entrainment zone. Our further analysis of the EZ structure confirms that Δz_i fully characterizes the whole lower EZ sublayer (for more details see figure A.12(*a*) and the corresponding discussion in Appendix A). Therefore, we choose to refer to Δz_i as the EZ scale.

We further find that the Ozmidov length particularized at the height of the minimum buoyancy flux, $(L_{OZ})_{z_{i,f}}$, characterizes the upper entrainment zone in the sheared CBL, supporting the interpretation of the upper EZ sublayer as a transition layer between the turbulent region below and the non-turbulent stably stratified region above (for more details see figure A.12(*b*) in Appendix A). As the turbulence intensity in the lower EZ sublayer increases due to extra shear-generated turbulence, the lower

EZ sublayer broadens and so does the upper EZ sublayer. The latter is because a stronger turbulence within the lower EZ sublayer results in a thicker transition layer.

Characterization of the whole vertical structure of the sheared CBL enables us to derive scaling laws for different definitions of the CBL height in terms of the characteristic length scales as

$$z_{i,f} \simeq 0.94\, z_{enc} + 0.8\, \Delta z_i \ , \tag{6a}$$

$$z_{i,s} \simeq 0.94\, z_{enc} + 1.0\, \Delta z_i \ , \tag{6b}$$

$$z_{i,g} \simeq 0.94\, z_{enc} + 1.0\, \Delta z_i + 1.78\, (L_{Oz})_{z_{i,f}} \ . \tag{6c}$$

The coefficients of proportionality are obtained from the DNS data. The term $0.94\, z_{enc}$ can be identified with $z_{i,0}$, the height of zero-crossing of the buoyancy flux, which marks the base of the entrainment zone (see figure 5). We find the limits of Δz_i for vanishingly weak- and strong-wind conditions, respectively, as

$$(\Delta z_i)_c \equiv 0.25\, z_{enc} \quad \text{and} \quad (\Delta z_i)_s \equiv \sqrt{1/3}\, \Delta u / N_0 \ , \tag{7}$$

where subscripts "c" and "s" denote convective and shear limit, respectively. The first relationship follows from Eq. (6a) and the observation that $z_{i,f} \simeq 1.14\, z_{enc}$ in the shear-free limit (see figure 4). The second relationship follows from Eq. (5) and the observation that with increasing wind condition the gradient Richardson number asymptotes toward $1/3$, while the buoyancy gradient at $z_{i,f}$ remains constant $\simeq N_0^2$.

Q2: Scaling laws for different properties os sheared CBLs

Although the scaling laws for different definitions of the CBL height, Eq. (6), help characterize wind-shear effects on entrainment, we are still lacking a scaling law for Δz_i and $(L_{Oz})_{z_{i,f}}$ in terms of environmental conditions. This means that the structure of the sheared CBL can not be reconstructed using the control parameters, unless the scaling laws for the characteristic length scales in terms of the control parameters are provided (cf. Eq. 4).

The TKE budget has proven a useful tool in the analysis of entrainment in the literature, since entrainment of more buoyant air into the CBL is associated with an expenditure of energy supplied by turbulence. This line of argumentation encourages us to turn to the budget of turbulent kinetic energy in the hope of deriving a scaling law for Δz_i. Although early studies considered the TKE budget equation at the height of the minimum buoyancy flux (Zeman & Tennekes, 1977; Tennekes & Driedonks, 1981), recent work has shown that a vertically integrated (bulk) energy budget is more practical because quantifying the integrated TKE budget is much easier than at a specific level (Kim et al., 2006; Conzemius & Fedorovich, 2006b).

The integral analysis of the TKE budget in the present work is different in various aspects from the approach in previous work, which considered the integrated TKE budget (Boers et al., 1984; Batchvarova & Gryning, 1994; Conzemius & Fedorovich, 2006b). First, we constrain the integral analysis within the entrainment zone, and second, we perform it with respect to the shear-free limit. In this way, wind-shear effects on entrainment are underlined and can be better investigated. Last but not least, we perform this analysis in the actual structure of the CBL, not in an idealized framework of bulk models as in previous work. In particular, we explicitly take the

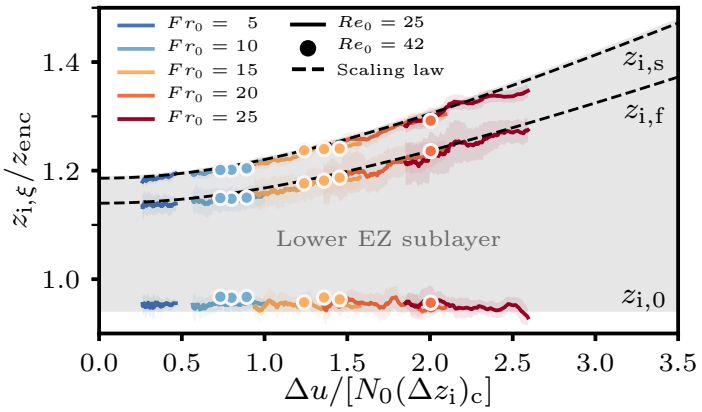

Figure 6: Verification of the scaling laws for different definitions of the CBL height (dashed lines) with DNS data (colored lines).

EZ scale into account to determine the integral of the negative buoyancy flux and of the shear production across the entrainment zone.

The integral analysis of the TKE balance along with the scaling of the relevant terms therein yield a relationship between the enhancement in the buoyancy flux and the shear production term (see Eq. (A.36) in Appendix A). This relationship implies that the entrainment enhancement in sheared CBLs is due to the additional TKE generated by the wind shear in the entrainment zone. We obtain the scaling law for the EZ scale as

$$\frac{\Delta z_i}{(\Delta z_i)_c} = \left[1 + 0.3\left(\frac{\Delta u}{N_0(\Delta z_i)_c}\right)^2\right]^{1/2}, \tag{8}$$

by employing the scaling arguments for the shear production and the buoyancy flux and solving the achieved equation for Δz_i. Recall that $(\Delta z_i)_c \equiv 0.25\, z_{enc}$ is the convective limit of the EZ scale. The proposed scaling law for Δz_i is supported in figure 6, where the reference heights $z_{i,f}$ and $z_{i,s}$ calculated from Eqs. (6a) and (6b) using Δz_i obtained from Eq. (8) agree with the DNS data. Comparison of the data from simulations with different Reynolds number supports the tendency towards Reynolds-number similarity and indicates that local effects of the Reynolds number are estimated to be commensurate to the achieved statistical convergence, i.e. approximately $10 - 20\%$. We employ Eq. (8) to provide the scaling laws for different properties of the sheared CBL, including the Ozmidov length, mean entrainment velocity and entrainment-flux ratio, as functions of $\Delta u/[N_0(\Delta z_i)_c]$. We argue that the proposed scaling laws in terms of $\Delta u/(N_0 L_0)$ and z_{enc}/L_0 remain approximately valid for different surface properties because the shear near the surface affects entrainment mainly indirectly through the change of Δu, and Eq. (8) and the other derived scaling laws depend explicitly on Δu. We refer to §A.5 in Appendix A for details of the integral analysis of the TKE budget and the derivation of scaling laws for different CBL properties.

One relevant implication of the derived scaling laws is that we found one single independent variable, $\Delta u/[N_0(\Delta z_i)_c]$, that embeds the dependence of mixed-layer and entrainment-zone properties on z_{enc}/L_0 and Fr_0 (cf. figure 4 and figure 6). This importance enables us to determine the critical condition to observe relevant wind-shear effects, i.e. $\Delta u/[N_0(\Delta z_i)_c] \simeq 0.6$ (see figure 6). This critical condition corresponds

to $\simeq 5$ ms^{-1} wind velocity in the free atmosphere for typical midday conditions, which is often considered as a reference value for wind effects to become relevant in unstable conditions (Stull, 1988). We note, however, that even such a weak wind could significantly affect the entrainment zone when the buoyancy forcing is weak, e.g., in the early morning or the late evening within the quasi-steady regime.

The scaling laws in terms of z_{enc}, N_0, and Δu for different CBL properties help characterize a barotropic CBL penetrating into a linearly stratified atmosphere in the quasi-steady regime. Nonetheless, we are still lacking a relationship between the velocity increment Δu, the control parameter Fr_0, and the independent variable z_{enc}/L_0 in order to quantify the dependence of CBL properties on the control parameters (cf. Eq. 4). This relationship could be obtained from the integral analysis of the momentum equation between the surface and the CBL top. This analysis, however, leads to a closure problem associated with the surface that requires the study of the friction velocity and its dependence on surface properties, e.g., on the Reynolds number for an aerodynamically smooth surface or on the roughness properties for an aerodynamically rough surface.

Even though studying the surface closure for the CBL over an aerodynamically smooth surface proves interesting, our preliminary analysis showed non-negligible sensitivities of surface-layer properties to low Reynolds numbers, generally because small-scale turbulent mixing near the surface is even more critical than across the entrainment zone. This dependence on low Reynolds number of surface-layer properties hinders us to study, in a systematic manner, the surface closure for the CBL over an aerodynamically smooth surface using the simulated cases. Higher Reynolds-number simulations are required in this respect. Therefore, in the following, to tackle this issue and also to examine the capability of the derived scaling laws and their sensitivities to surface properties, we develop bulk models and address the relationship between the velocity increment Δu, the control parameter Fr_0, and the independent variable z_{enc}/L_0 in the framework of bulk models of the CBL over an aerodynamically rough surface. Considering the aerodynamically rough surface, which is the more appropriate boundary condition for the land surface, allows us to simply consider the surface-drag relationship with a constant drag coefficient as the surface closure in dealing with the integral analysis of the momentum equation. This simplification, in addition, enables us to keep focusing on entrainment and investigate advantages of the derived scaling laws compared to previous entrainment parameterizations.

Q3: Singularity in previous bulk models of sheared CBLs

The crucial problem in previous bulk models of sheared CBLs, associated with the entrainment closure, arises from an incomplete characterization of wind-shear effects on entrainment. The singularity at finite wind strength in previous entrainment parameterizations is one manifestation of this incomplete characterization. We show that the singularity in previous entrainment closures takes place under a very strong-shear condition when the sheared CBL depth becomes nearly two times larger than the encroachment length scale or equivalently when $\Delta u/(N_0 z_{enc}) \simeq 1.8$. In addition, we show that considering initial conditions far away from the quasi-steady regime leads to the singularity at finite wind strength even in moderate-shear conditions. This limits the applicability of previous models to parametrize CBL bulk properties in

large-scale atmospheric models, since bulk models are likely initialized in large-scale models with initial conditions that are far away from the quasi-steady regime.

We find that this potential singularity has formed because previous work has derived the entrainment parameterization in the idealized framework of the bulk models. In the ZOM framework, the CBL depth—as the only length scale defined in this framework—is employed as the characteristic length scale in the scaling arguments of different TKE terms associated with the entrainment zone. In particular, the CBL depth is used in the scaling of the shear production at the CBL top in the local TKE approach (see e.g. Tennekes & Driedonks, 1981), and is used in the scaling of the integral of the negative buoyancy flux in the integrated TKE approach (see e.g. Boers et al., 1984). Increasing the complexity of the bulk model to the first-order or higher-order models does not help tackle the singularity issue as long as the CBL depth is deemed as the characteristic length scale of different TKE terms associated with the entrainment zone.

We have shown in the previous section that when the integral analysis of the TKE budget is done in the actual CBL structure, and in particular, when the local length scale of the entrainment zone is taken into account to determine the integral of the negative buoyancy flux and of the shear production across the entrainment zone, the singularity at finite wind strength in the scaling laws vanishes. For instance, the EZ scale, according to Eq. (8), grows monotonically with increasing the shear condition.

Q4: ZOM faithfully represents bulk properties of sheared CBLs

In this section, as the main implication of the derived scaling laws, we employ some of them to develop bulk models that are free from any singularity at finite wind strength. We develop two zero-order bulk models with different entrainment closures for a cloud-free barotropic convective boundary layer that grows over an aerodynamically rough surface into a linearly stratified atmosphere. As indicated before, considering the aerodynamically rough surface allows us to consider the surface-drag relationship with constant surface drag as the surface closure (see e.g. Kim et al., 2006).

In the first ZOM, referred to as the energetics-based model, we assume that the negative and positive areas of the buoyancy flux match between the model and the actual CBL. We derive a non-singular scaling law for the ratio of the actual negative and positive buoyancy flux and consider this scaling law as the entrainment-closure equation. The closure assumption in the energetics-based model is similar to the closure assumption in previous work, i.e., the bulk or local energetics between the model and the actual CBL were assumed to be equal (see e.g. Conzemius & Fedorovich, 2006b). Although the proposed entrainment-closure equation, and thus the proposed ZOM, are validated with the DNS data, we further evaluate this model by comparing its predictions with those obtained from previous models in the literature for a moderate-shear condition. This analysis enables us to further examine the capability and accuracy of the energetics-based model in the prediction of CBL bulk properties and also to better underline the advantage of this model with respect to models proposed in previous literature.

Our analysis shows that the temporal evolution of different CBL properties obtained from the energetics-based model agrees very well with predictions of those previous models that appropriately considered the contribution of the entrainment-zone shear in the entrainment-closure equation. The best match was observed with predictions of

Liu et al. (2016)'s model wherein 43% of generated turbulence by entrainment-zone shear was assumed to be available for the entrainment. The observed agreement between the prediction of the present and previous models might sound surprising because of the differences in entrainment closures, in particular, differences in the length scale used to estimate the various terms of the TKE budget equation in the entrainment zone. The reason for such an agreement is that under weak- and moderate-shear conditions, the CBL depth (applied in previous work) and the local length scale of the entrainment zone (applied in the present work) are approximately proportional to each other, which results in equally good predictions of CBL bulk properties from the present and previous models for moderate-shear conditions. Under a very strong-shear condition, however, these two length scales differ, and the CBL depth does not act as an appropriate proxy of the local length scale of the entrainment zone anymore. This different scaling eventually leads to the emergence of the singularity in models developed in previous work for very strong-shear conditions.

One potential disadvantage of the energetics-based model and models developed in previous literature is that the modeled CBL depth can not be *a priori* associated to any actual CBL height. This lack of knowledge has led to some controversy in previous work and might become important when the bulk model is intended to include more complexity like cloud formation. We develop the second ZOM, referred to as the geometric-based model, to address this issue. In this ZOM, instead of matching the energetics, we assume that the modeled CBL depth matches different definitions of the actual CBL height. We consider three options for the CBL depth in the geometric-based model, namely, the height of the minimum buoyancy flux, the height that marks the transition from the lower to upper entrainment-zone sublayer, and the height of the maximum buoyancy gradient. We employ the non-singular scaling laws for these properties [Eqs. (6) and (8)] as the entrainment-closure equation in this ZOM.

Predictions of the geometric-based model suggest that the CBL depth in the energetics-based model and models developed in previous work corresponds better to the height that marks the interface between the lower and upper entrainment-zone sublayers, rather than the height of the minimum buoyancy flux, as is typically considered in previous work. This finding helps explain the reported $\simeq 5\%$ deviation of the zero-order CBL depth from the height of the minimum buoyancy flux in sheared CBLs in Conzemius & Fedorovich (2007). This finding also indicates that Fedorovich et al. (2004a) have obtained 0.17 for the zero-order entrainment-flux ratio in the shear-free limit (which is 15% smaller than the generally-agreed value 0.2) just because they have assumed that the zero-order CBL depth corresponds to the height of the minimum buoyancy flux, and not because of statistical uncertainty.

An important conclusion of this study is that the zero-order bulk model, despite its simplicity, can faithfully represent CBL bulk properties. This means that a finite transition layer between the mixed layer and the free atmosphere, as is the case in the first- and higher-order bulk models, is not explicitly required. This is because the relevant shear-induced features of the actual entrainment zone are implicitly considered in the zero-order bulk models through the entrainment closures. If needed, the vertical structure of the actual entrainment zone of the sheared CBL can be reconstructed *a posteriori* using the zero-order CBL depth predicted from any of the ZOMs and using the relationships between the zero-order CBL depth and various actual heights of the CBL provided in Eqs. (6) and (8).

1.7 OUTLOOK

In this section, we make a number of suggestions for a potential continuation of this research work. The main suggestion is concerned with the elimination of main limitations of this project. These limitations are basically imposed by the simplifications in the considered configuration, including zero Coriolis force, the aerodynamically smooth surface, the constant and homogeneous surface buoyancy flux. Particularly important here is prioritizing these limitations based on their relevance for the application of the proposed characterization of entrainment.

The good agreement observed in the previous section between the predictions of the bulk models proposed in this work and of Liu et al. (2016)'s model can help us to anticipate the relevance of some of these simplifications on the characterization of entrainment and, in particular, on the derived scaling laws. The critical point is that Liu et al. (2016) have obtained the entrainment closure from a variety (twenty six cases) of simulated CBLs in the mid latitudes, including barotropic and equivalent-barotropic sheared CBLs over two aerodynamically rough surfaces, while we have derived the entrainment closures from few simulations of barotropic sheared CBLs without the Coriolis force over an aerodynamically smooth surface. The observed agreement is, hence, promising in two aspects. First, it confirms that the scaling laws in this work are independent of the surface properties, as they are explicitly expressed in terms of the velocity increment at the CBL top. Second, it suggests that they would most likely apply to sheared CBLs with Coriolis force and also to equivalent-barotropic CBLs, although a proof of concept is necessary to draw a definitive conclusion.

The Coriolis force takes the highest priority, even though we have already observed that main features of barotropic CBLs in the mid latitudes were reproduced by our idealized CBL. Retaining rotation effects and conducting few simulations that are formulated in terms of the Rossby number enable us to generalize the results of this dissertation. As an outcome of these simulations, one can determine the latitude up to which the rotation-free entrainment parameterizations are applicable and investigate the possible variation of the derived scaling laws. The Coriolis force induces an inertial oscillation of the horizontal velocity. Given that the amplitude of this oscillation depends on initial conditions (Stull, 1988), it sounds logical to prescribe the Coriolis force when the CBL is very shallow and the whole domain is in the geostrophic equilibrium. As the CBL grows and the surface friction decelerates the flow, the CBL gets out of the geostrophic equilibrium that leads to formation of an inertial oscillations. This approach enables us to study the quasi-geostrophic equilibrium and to perform a systematic analysis that is free from effects of initial conditions. In addition, this approach provides a reference case to systematically study influence of initial conditions on the oscillation. The time scale associated with the inertial oscillations is approximately 17 hours in the mid latitudes, meaning that a quarter of its cycle is of the same order as the time scale associated with entrainment. This implies that the inertial oscillation might affect the proposed entrainment parameterizations in this dissertation. Schröter (2018), however, found no specific influence of the inertial oscillation on the TKE budget, which indicates that our proposed characterization of entrainment in terms of $\Delta u/(N_0 z_{\mathrm{enc}})$ remains

approximately unchanged. A probable modification would be the replacement of Δu^2 with the modulus of the CBL-top velocity jump.

The next priority in the elimination of the limitations of this work is to study different boundary conditions. The important ones, in order of priority, are as following:

1. An aerodynamically rough surface: One might argue that the surface roughness for the CBL considered in this dissertation (with constant and homogeneous surface buoyancy flux) does not play a key role on entrainment, because we have learned that the surface wind shear is dissipated locally, and it only affects the entrainment indirectly by slowing the mixed-layer velocity (Pino & Vilà-Guerau De Arellano, 2008). In this regard, changing the surface roughness modifies the temporal evolution of the velocity jump at the CBL top, however, these changes are captured by $\Delta u/(N_0 z_{\mathrm{enc}})$, and therefore, the proposed characterization of entrainment should remain approximately valid.

2. A constant surface temperature: The characterization of wind-shear effects on the CBL with a constant surface temperature seems complicated due to the interplay between the growing CBL and the gradually decreasing surface buoyancy flux (see e.g. Van Heerwaarden & Mellado, 2016). Given that the surface wind shear modifies the evolution of the surface buoyancy flux, some large effects of wind shear even on the evolution of mixed-layer properties are expected. However, illustrating self-similar behavior, in spite of the unsteadiness, and providing the mathematical model for key properties of such a CBL in the shear-free limit in Van Heerwaarden & Mellado (2016) raises the hope to characterize wind-shear effects.

3. Heterogeneous heating at the surface: Wind-shear effects on the CBL with a heterogeneous surface heating also sounds appealing. The reason is that, in reality, the shear-free limit is very rare and the surface heating is often heterogeneous, for instance, because of variations in land cover, topography, and soil moisture. The main aim of this study would be to address how wind shear modifies the main phenomena observed in a shear-free CBL with a heterogeneous surface heating. These phenomena include first, the optimal heterogeneity state, which is defined as the state when a peak in the vertically integrated kinetic energy, and accordingly the strongest secondary circulation, is formed and second, the transition from the mesoscale towards the microscale regimes (Van Heerwaarden et al., 2014). The interaction of the surface wind shear and heterogeneity might be significant in accelerating the onset of the optimal heterogeneity state, as the surface wind shear intensifies merging process of the plumes near the surface (see the figure on the front page of this dissertation).

Another limitation of this dissertation is the studied range of the parameter space. Although one can keep increasing the Froude number to determine the critical $\Delta u/(N z_{\mathrm{enc}})$ up to which the derived scaling laws remain valid, it sounds more practical to study sheared CBLs from the limit of the purely shear-driven boundary layer and then gradually adding convection to the system. Jonker et al. (2013) have shown than for the purely shear-driven boundary layer growing into a linearly stratified free atmosphere, not a very flat profile is observed for the mean velocity. As outcome of studying sheared CBLs from the limit opposite to what we have discussed

in this dissertation, first, one can show how much convection is needed to get the vertical profile of mean velocity flat within the boundary-layer interior (Moeng & Sullivan, 1994), and second, one can determine the maximum value of $\Delta u/(Nz_{\mathrm{enc}})$ under which the derived scaling laws hold valid.

Apart from the limitations of this project, one can address other relevant problems in sheared CBLs using the available data. The following topics sound promising in this respect. First, conditional analysis can be employed to study the turbulent and non-turbulent regions at the CBL top to provide characteristic scales, and accordingly scaling laws, for other properties such as variances that are important, for instance, for cloud formation. Second, one can investigate large-scale circulation within the mixed layer, in particular, the formation of the convective rolls and their possible interaction with Kelvin-Helmholtz-like billows in the entrainment zone and near-surface dynamics (Salesky et al., 2017). Third, from fluid-dynamics perspective, despite the fact that our preliminary analysis of the simulations with $Re_0 = 25$ showed non-negligible effects of the moderate Reynolds number on surface-layer properties, one can use the data for $Re_0 = 25$ and $Re_0 = 42$ to study the Monin-Obukhov similarity theory over an aerodynamically smooth surface and to investigate the convergence of gradient-flux relations towards the available functional relationships in the literature (Maronga, 2014), supporting Reynolds-number similarity theory.

BIBLIOGRAPHY

Angevine, W. M. (1999). "Entrainment results including advection and case studies from the Flatland boundary layer experiments." In: *J. Geophys. Res.* 104, pp. 947–963.

Angevine, W. M., H. K. Baltink & F. C. Bosveld (2001). "Observations Of The Morning Transition Of The Convective Boundary Layer." In: *Boundary-Layer Meteorology* 101.2, pp. 209–227.

Ansorge, C. & J. P. Mellado (2014). "Global Intermittency and Collapsing Turbulence in the Stratified Planetary Boundary Layer." In: *Bound.-Layer Meteor.* 153.1, pp. 89–116.

Ayotte, K. W. et al. (1996). "An evaluation of neutral and convective planetary boundary-layer parameterizations relative to large eddy simulations." In: *Bound.-Layer Meteor.* 79.1, pp. 131–175.

Baklanov, Alexander A., Branko Grisogono, Robert Bornstein, Larry Mahrt, Sergej S. Zilitinkevich, Peter Taylor, Søren E. Larsen, Mathias W. Rotach & H. J. S. Fernando (2011). "The Nature, Theory, and Modeling of Atmospheric Planetary Boundary Layers." In: *Bulletin of the American Meteorological Society* 92.2, pp. 123–128.

Barlow, Janet F. (2014). "Progress in observing and modelling the urban boundary layer." In: *Urban Climate* 10. ICUC8: The 8th International Conference on Urban Climate and the 10th Symposium on the Urban Environment, pp. 216–240.

Batchvarova, E. & S.-E. Gryning (1994). "An applied model for the height of the daytime mixed layer and the entrainment zone." In: *Bound.-Layer Meteor.* 71.3, pp. 311–323.

Bernardini, M., S. Pirozzoli & P. Orlandi (2014). "Velocity statistics in turbulent channel flow up to Re=4000." In: *J. Fluid Mech.* 742, pp. 171–191.

Betts, A. K. (1974). "Reply to comment on the paper 'Non-precipitating cumulus convection and its parameterization'." In: *Quart. J. Roy. Meteor. Soc.* 100, pp. 469–471.

Betts, Alan K. & J. H. Ball (1994). "Budget analysis of FIFE 1987 sonde data." In: *Journal of Geophysical Research: Atmospheres* 99.D2, pp. 3655–3666.

Boer, A. van de, A. F. Moene, A. Graf, D. Schüttemeyer & C. Simmer (2014). "Detection of Entrainment Influences on Surface-Layer Measurements and Extension of Monin–Obukhov Similarity Theory." In: *Bound.-Layer Meteor.* 152.1, pp. 19–44. ISSN: 1573-1472.

Boers, R., E. W. Eloranta & R. L. Coulter (1984). "Lidar Observations of Mixed Layer Dynamics: Tests of Parameterized Entrainment Models of Mixed Layer Growth Rate." In: *J. Appl. Meteor.* 23, pp. 247–266.

Brucker, K. A. & S. Sarkar (2007). "Evolution of an initially turbulent stratified shear layer." In: *Phys. Fluids* 19, p. 105105.

Burton, T., D. Sharpe, N. Jenkins & E. Bossanyi (2011). "Wind Energy Handbook." In: hinchester, West Sussex, England: Ellis Horwood.

Camillo, P. J., R. J. Gurney & T. J. Schmugge (1983). "A soil and atmospheric boundary layer model for evapotranspiration and soil moisture studies." In: *Water Resources Research* 19.2, pp. 371–380.

Carpenter, M. & C. A. Kennedy (1994). "Fourth-order 2N-storage Runge-Kutta schemes." In: *Technical Report NASA-TM-109112, NASA Langley Research Center*.

Carson, D. & F. Smith (1975). "Thermodynamic model for the development of a convectively unstable boundary layer." In: *Advances in Geophysics* 18, pp. 111–124.

Chung, D. & G. Matheou (2012). "Direct numerical simulation of stationary homogeneous stratified sheared turbulence." In: *J. Fluid Mech.* 696, pp. 434–467.

Conzemius, R. J. & E. Fedorovich (2006a). "Dynamics of sheared convective boundary layer entrainment. Part I: Methodological background and large eddy simulations." In: *J. Atmos. Sci.* 63, pp. 1151–1178.

– (2006b). "Dynamics of sheared convective boundary layer entrainment. Part II: Evaluation of bulk model predictions of entrainment flux." In: *J. Atmos. Sci.* 63, pp. 1179–1199.

– (2007). "Bulk models of the sheared convective boundary layer: evaluation through large eddy simulations." In: *J. Atmos. Sci.* 64, pp. 786–807.

Conzemius, R. & E. Fedorovich (2004). "Numerical models of entrainment into sheared convective boundary layers evaluated through large eddy simulations." In: *16th Symposium on Boundary Layers and Turbulence*.

De Roode, Stephan R., A. Pier Siebesma, Sara Dal Gesso, Harm J. J. Jonker, Jerôme Schalkwijk & Jasper Sival (2014). "A mixed-layer model study of the stratocumulus response to changes in large-scale conditions." In: *Journal of Advances in Modeling Earth Systems* 6.4, pp. 1256–1270.

Deardorff, J. W. (1970). "Preliminary results from numerical integration of the unstable boundary layer." In: *J. Atmos. Sci.* 27, pp. 1290–1211.

– (1972). "Theoretical expression for the countergradient vertical heat flux." In: *Journal of Geophysical Research* 77.30, pp. 5900–5904.

– (1974). "Three-dimensional numerical study of turbulence in an entraining mixed layer." In: *Bound.-Layer Meteor.* 7, pp. 199–226.

– (1979). "Prediction of Convective Mixed-Layer Entrainment for Realistic Capping Inversion Structure." In: *J. Atmos. Sci.* 36, pp. 424–436.

Deardorff, J. W., G. E. Willis & D. K. Lilly (1969). "Laboratory investigation of non-steady penetrative convection." In: *Journal of Fluid Mechanics* 35.1, pp. 7–31.

Deardorff, J. W., G. E. Willis & B. H. Stochton (1980). "Laboratory studies of the entrainment zone of a convectively mixed layer." In: *J. Fluid Mech.* 100, pp. 41–64.

Dimotakis, P. E. (2000). "The mixing transition in turbulent flows." In: *J. Fluid Mec* 409, pp. 69–98.

Dougherty, J. P. (1961). "The anisotropy of turbulence at the meteor level." In: *Journal of Atmospheric and Terrestrial Physics* 21, pp. 210–213.

Driedonks, A. G. M. (1982). "Models and observations of the growth of the atmospheric boundary layer." In: *Bound.-Layer Meteor.* 23, pp. 283–306.

Driedonks, A. G. M. & H. Tennekes (1984). "Entrainment effects in the well-mixed atmospheric boundary layer." In: *Boundary-Layer Meteorology* 30.1, pp. 75–105.

Fedorovich, E. (1995). "Modeling the Atmospheric Convective Boundary Layer within a Zero-Order Jump Approach: An Extended Theoretical Framework." In: *Journal of Applied Meteorology* 34.9, pp. 1916–1928.

Fedorovich, E. & R. J. Conzemius (2008). "Effects of wind shear on the atmospheric convective boundary layer structure and evolution." In: *Acta Geophysica* 56, pp. 114–141.

Fedorovich, E. & R. Kaiser (1998). "Wind Tunnel Model Study of Turbulence Regime in the Atmospheric Convective Boundary Layer." In: *Buoyant Convection in Geophysical Flows*. Ed. by E. J. Plate, E. E. Fedorovich, D. X. Viegas & J. C. Wyngaard. Dordrecht: Springer Netherlands, pp. 327–370.

Fedorovich, E. & J. Thäter (2001). "Vertical transport of heat and momentum across a sheared density interface at the top of a horizontally evolving convective boundary layer." In: *J. Turbul.* 2, N7.

Fedorovich, E., F. T. M. Nieuwstadt & R. Kaiser (2001a). "Numerical and Laboratory Study of Horizontally Evolving Convective Boundary Layer. Part II: Effects of Elevated Wind Shear and Surface Roughness." In: *Journal of the Atmospheric Sciences* 58.6, pp. 546–560.

– (2001b). "Numerical and Laboratory Study of a Horizontally Evolving Convective Boundary Layer. Part I: Transition Regimes and Development of the Mixed Layer." In: *Journal of the Atmospheric Sciences* 58.1, pp. 70–86.

Fedorovich, E., R. Conzemius & D. Mironov (2004a). "Convective entrainment into a shear-free linearly stratified atmosphere: Bulk models reevaluated through large-eddy simulation." In: *J. Atmos. Sci.* 61, pp. 281–295.

Fedorovich, E., R. J. Conzemius, I. Esau, F. K. Chow, D. Lewellen, C. H. Moeng, P. Sullivan, D. Pino & J. V. G. de Arellano (2004b). "Entrainment into sheared convective boundary layers as predicted by different large eddy simulation codes." In: ***In**: Preprints, 16th Symp. on Boundary Layers and Turbulence, 9-13 August, Amer. Meteor. Soc. Portland, ME,* CD–ROM, P4.7.

Fernando, H. J. S. (1991). "Turbulent mixing in stratified fluids." In: *Annu. Rev. Fluid. Mech.* 23, pp. 455–493.

Flamant, C., J. Pelon, B. Brashers & R. A. Brown (1999). "Evidence of a Mixed-Layer Dynamics Contribution to the Entrainment Process." In: *Bound.-Layer Meteor.* 93.1, pp. 47–73.

Flores, O., J. Jiménez & J. C. Del Álamo (2007). "Vorticity organization in the outer layer of turbulent channels with disturbed walls." In: *J. Fluid Mech.* 591, pp. 145–154.

Fritz, B.K. & W.C. Hoffmann (2008). "Atmospheric Effects on Fate of Aerially Applied Agricultural Sprays." In: *Agricultural Engineering International: the CIGR Ejournal* X.

Garcia, J. R. & J. P. Mellado (2014). "The two-layer structure of the entrainment zone in the convective boundary layer." In: *J. Atmos. Sci.* 71, pp. 1935–1955.

Garratt, J. R. (1992). "The Atmospheric Boundary Layer." In: *Cambridge University Pres*.

Garratt, J. R., J. C. Wyngaard & R. J. Francey (1982). "Winds in the Atmospheric Boundary Layer-Prediction and Observation." In: *J. Atmos. Sci.* 39.6, pp. 1307–1316.

Garratt, J. R., G. D. Hess, W. L. Physick & P. Bougeault (1996). "The atmospheric boundary layer — advances in knowledge and application." In: *Boundary-Layer Meteorology* 78.1, pp. 9–37.

Garratt, J.R. (1994). "Review: the atmospheric boundary layer." In: *Earth-Science Reviews* 37.1, pp. 89–134.

Gohari, S. M. I. & S. Sarkar (2017). "Direct Numerical Simulation of Turbulence Collapse and Rebirth in Stably Stratified Ekman Flow." In: *Bound.-Layer Meteor.* 162.3, pp. 401–426.

Grant, A. L. M. & P. J. Mason (1990). "Observations of boundary-layer structure over complex terrain." In: *Quarterly Journal of the Royal Meteorological Society* 116, pp. 159–186.

Haghshenas, A. & J. P. Mellado (2019). "Characterization of wind-shear effects on entrainment in a convective boundary layer." In: *J. Fluid Mech.* 858, pp. 145–183.

Haltiner, G. J. & R. T. Williams (1980). "Numerical Prediction and Dynamic Meteorology." In: John Wiley and Sons, 477 pp.

Hebert, D. A. & S. M. de Bruyn Kops (2006). "Predicting turbulence in flows with strong stable stratification." In: *Phys. Fluids* 18.6, pp. 1–10.

Holt, Teddy & Sethu Raman (1988). "A review and comparative evaluation of multilevel boundary layer parameterizations for first-order and turbulent kinetic energy closure schemes." In: *Reviews of Geophysics* 26.4, pp. 761–780.

Holtslag, A. A. M. & B. A. Boville (1993). "Local Versus Nonlocal Boundary-Layer Diffusion in a Global Climate Model." In: *Journal of Climate* 6.10, pp. 1825–1842.

Howland, C. J., J. R. Taylor & C. P. Caulfield (2018). "Testing linear marginal stability in stratified shear layers." In: *J. Fluid Mech.* 839, R4.

Huang, J., X. Lee & E. G. Patton (2011). "Entrainment and budgets of heat, water vapor, and carbon dioxide in a convective boundary layer driven by time-varying forcing." In: *Journal of Geophysical Research: Atmospheres* 116.D6.

Hunt, J. C. R. & P. A. Durbin (1999). "Perturbed vortical layers and shear sheltering." In: *Fluid Dyn. Res.* 24.6, pp. 375–404.

Jonker, H. J. J., M. van Reeuwijk, P. Sullivan & G. Patton (2013). "On the scaling of shear driven entrainment: A dns study." In: *J. Fluid Mech* 732, pp. 150–165.

Kantha, L. H., O. M. Phillips & R. S. Azad (1977). "On turbulent entrainment at a stable density interface." In: *Journal of Fluid Mechanics* 79.4, pp. 753–768.

Kato, H. & O. M. Phillips (1969). "On the penetration of a turbulent layer into stratified fluid." In: *Journal of Fluid Mechanics* 37.4, pp. 643–655.

Kim, S. W., S. U. Park & C. H. Moeng (2003). "Entrainment processes in the convective boundary layer with varying wind shear." In: *Bound.-Layer Meteor.* 108, pp. 221–245.

Kim, S. W., S. Park, D. Pino & J. Vilà-Guerau De Arellano (2006). "Entrainment parameterization in a sheared convective boundary layer by using a first-order jump model." In: *Bound.-Layer Meteor.* 120, pp. 455–475.

LeMone, M. A. (1973). "The structure and dynamics of horizontal roll vortices in the planetary boundary layer." In: *J. Atmos. Sci.* 30, pp. 1077–1091.

Lele, S. (1992). "Compact finite difference schemes with spectral-like resolution." In: *J. Comput. Phys* 103, pp. 16–42.

Lenschow, D. H. (1970). "Airplane Measurements of Planetary Boundary Layer Structure." In: *Journal of Applied Meteorology* 9.6, pp. 874–884.

Lenschow, D. H., J. C. Wyngaard & W. T. Pennell (1980). "Mean-Field and Second-Moment Budgets in a Baroclinic, Convective Boundary Layer." In: *J. Atmos. Sci.* 37.6, pp. 1313–1326.

Lilly, D. K. (1968). "Models of cloud-topped mixed layers under a strong inversion." In: *Quart. J. Roy. Meteor. Soc.* 94, pp. 292–309.

Liu, P., J. Sun & L. Shen (2016). "Parameterization of sheared entrainment in a well-developed CBL. Part I: Evaluation of the scheme through large-eddy simulations." In: *Adv. Atmos. Sci.* 33, pp. 1171–1184.

Louis, Jean-François (1979). "A parametric model of vertical eddy fluxes in the atmosphere." In: *Boundary-Layer Meteorology* 17.2, pp. 187–202.

Mahrt, L. (1991). "Boundary-layer moisture regimes." In: *Quart. J. Roy. Meteor. Soc.* 117.497, pp. 151–176.

Mahrt, L. & D. H. Lenschow (1976). "Growth dynamics of the convective mixed layer." In: *J. Atmos. Sci.* 33, pp. 41–51.

Manabe, Syukuro & Robert F. Strickler (1964). "Thermal Equilibrium of the Atmosphere with a Convective Adjustment." In: *Journal of the Atmospheric Sciences* 21.4, pp. 361–385.

Margulis, Steven A. & Dara Entekhabi (2004). "Boundary-Layer Entrainment Estimation Through Assimilation of Radiosonde and Micrometeorological Data into a Mixed-Layer Model." In: *Boundary-Layer Meteorology* 110.3, pp. 405–433.

Maronga, Bjrn (2014). "MoninObukhov Similarity Functions for the Structure Parameters of Temperature and Humidity in the Unstable Surface Layer: Results from High-Resolution Large-Eddy Simulations." In: *Journal of the Atmospheric Sciences* 71.2, pp. 716–733.

Mashayek, A. & W. R. Peltier (2011). "Turbulence transition in stratified atmospheric and oceanic shear flows: Reynolds and Prandtl number controls upon the mechanism." In: *Geophys. Res. Lett.* 38.16. L16612.

Mason, P.J. & D.J. Thomson (2015). "Boundary layer (atmospheric) and air pollution | Overview." In: *Encyclopedia of Atmospheric Sciences (Second Edition)*. Ed. by Gerald R. North, John Pyle & Fuqing Zhang. Second Edition. Oxford: Academic Press, pp. 220 –226.

Mellado, J. P. (2012). "Direct numerical simulation of free convection over a heated plate." In: *J. Fluid Me* 712, pp. 418–450.

– (2017). "Cloud-Top Entrainment in Stratocumulus Clouds." In: *Annu. Rev. Fluid. Mech.* 49.1, pp. 145–169.

Mellado, J. P. & C. Ansorge (2012). "Factorization of the Fourier transform of the pressure-Poisson equation using finite differences in colocated grids." In: *Z. Angew. Math. Mech.* 92, pp. 380–392.

Mellado, J. P., C. C. van Heerwaarden & J. R. Garcia (2016). "Near-Surface Effects of Free Atmosphere Stratification in Free Convection." In: *Bound.-Layer Meteor.* 159.1, pp. 69–95.

Mellado, J. P., C. S. Bretherton, B. Stevens & M. C. Wyant (2018). "DNS and LES for Simulating Stratocumulus: Better Together." In: *Journal of Advances in Modeling Earth Systems* 10.7, pp. 1421–1438.

Mellado, J.P., M. Puche & C. C. van Heerwaarden (2017). "Moisture statistics in free convective boundary layers growing into linearly stratified atmospheres." In: *Quarterly Journal of the Royal Meteorological Society* 143.707, pp. 2403–2419.

Moeng, C. H. & P. P. Sullivan (1994). "A comparison of shear- and buoyancy-driven planetary boundary layer flows." In: *J. Atmos. Sci.* 51, pp. 999–1022.

Moin, P. & K. Mahesh (1998). "Direct numerical simulation: A tool in turbulence research." In: *Annu. Rev. Fluid Mech.* 30, pp. 539–578.

Naumann, Ann Kristin, Bjorn Stevens, Cathy Hohenegger & Juan Pedro Mellado (2017). "A Conceptual Model of a Shallow Circulation Induced by Prescribed Low-Level Radiative Cooling." In: *Journal of the Atmospheric Sciences* 74.10, pp. 3129–3144.

Nowotarski, Christopher J., Paul M. Markowski, Yvette P. Richardson & George H. Bryan (2014). "Properties of a Simulated Convective Boundary Layer in an Idealized Supercell Thunderstorm Environment." In: *Monthly Weather Review* 142.11, pp. 3955–3976.

Ozmidov, R. V. (1965). "On the turbulent exchange in a stably stratified ocean." In: *Izv., Atmospheric and Oceanic Physics Series* 1.8, pp. 853–860.

Pelly, J. L. & S. E. Belcher (2001). "A Mixed-Layer Model Of The Well-Mixed Stratocumulus Topped Boundary Layer." In: *Bound.-Layer Meteor.* 100.1, pp. 171–187.

Peltier, W. R. & C. P. Caulfield (2003). "Mixing efficiency in stratified shear flows." In: *Annu. Rev. of Fluid Mech.* 35.1, pp. 135–167.

Pennell, W. T. & M. A. LeMone (1974). "An Experimental Study of Turbulence Structure in the Fair-Weather Trade Wind Boundary Layer." In: *J. Atm. Sci* 31, pp. 1308–1323.

Pino, D. & J. Vilà-Guerau De Arellano (2008). "Effects of shear in the convective boundary layer: analysis of the turbulent kinetic energy budget." In: *Acta Geophysica* 56, pp. 167–193.

Pino, D., J. V. G. de Arellano & P. J. Duynkerke (2003). "The contribution of shear to the evolution of a convective boundary layer." In: *J. Atmos. Sci.* 60, pp. 1913–1926.

Pino, D., J. V. G. de Arellano & S. W. Kim (2006). "Representing sheared convective boundary layer by zeroth- and first-order-jump mixed-layer models: Large-eddy simulation verification." In: *J. Appl. Meteor. Clim.* 45, pp. 1224–1243.

Pirozzoli, S., M. Bernardini, R. Verzicco & P. Orlandi (2017). "Mixed convection in turbulent channels with unstable stratification." In: *J. Fluid Mech.* 821, pp. 482–516. ISSN: 0022-1120.

Portwood, G. D., S. M. de Bruyn Kops, J. R. Taylor, H. Salehipour & C. P. Caulfield (2016). "Robust identification of dynamically distinct regions in stratified turbulence." In: *J. Fluid Mech.* 807, R2.

Porté-Agel, F., H. Lu & Y. Wu (2014). "Interaction between Large Wind Farms and the Atmospheric Boundary Layer." In: *Procedia IUTAM* 10. Mechanics for the World: Proceedings of the 23rd International Congress of Theoretical and Applied Mechanics, ICTAM2012, pp. 307–318.

Reeuwijk, Maarten van, Dominik Krug & Markus Holzner (2018). "Small-scale entrainment in inclined gravity currents." In: *Environmental Fluid Mechanics* 18.1, pp. 225–239.

Salesky, S. T., M. Chamecki & E. Bou-Zeid (2017). "On the Nature of the Transition Between Roll and Cellular Organization in the Convective Boundary Layer." In: *Bound.-Layer Meteor.* 163, pp. 41–68.

Schröter, S. J. (2018). "Sheared convective boundary layers: turbulence kinetic energy and entrainment dynamics, (Doctoral dissertation)." In: *Wageningen University*, p. 256.

Sherman, F. S., J. Imberger & G. M. Corcos (1978). "Turbulence and mixing in stably stratified waters." In: *Annu. Rev. Fluid Mech.* 10, pp. 267–288.

Shishkina, O., R. J A M Stevens, S. Grossmann & D. Lohse (2010). "Boundary layer structure in turbulent thermal convection and its consequences for the required numerical resolution." In: *New J. Phys.* 12.7, p. 075022.

Smyth, W. D. & J. N. Moum (2000a). "Anisotropy of turbulence in stably stratified mixing layers." In: *Phys. Fluids* 12.6, pp. 1343–1362.

– (2000b). "Length scales of turbulence instably stratified mixing layers." In: *Phys. Fluids* 12, pp. 1327–1342.
Sorbjan, Z. (2005). "Statistics of scalar fields in the atmospheric boundary layer based on Large-eddy simulations. Part 1: Free convection." In: *Bound.-Layer Meteor.* 116, pp. 467–486.
– (2006). "Statistics of scalar fields in the atmospheric boundary layer based on Large-eddy simulations. Part II: Forced convection." In: *Bound.-Layer Meteor.* 119, pp. 57–79.
Spalart, P. R., G. N. Coleman & R. Johnstone (2008). "Direct numerical simulation of the Ekman layer: a step in Reynolds number, and cautious support for a log law with a shifted origin." In: *Phys. Fluids* 20.10.
Stewart, R. W. (1979). "The atmospheric boundary layer." In: *Interactive dynamics of convection and solidification*. World Meteorological Organization, 44 pp.
Strang, E. J. & H. J. S. Fernando (2001). "Entrainment and mixing in stratified shear flows." In: *J. Fluid Mech.* 428, pp. 349–386.
Stull, R. B. (1988). "An Introduction to Boundary Layer Meteorology." In: *Interactive dynamics of convection and solidification*. Kluwer Academic Press, pp. 113–138.
Suarez, Max J., Akio Arakawa & David A. Randall (1983). "The Parameterization Of the Planetary Boundary Layer in the UCLA General Circulation Model: Formulation and Results." In: *Monthly Weather Review* 111.11, pp. 2224–2243.
Sullivan, P., C. H. Moeng, B. Stevens, D. H. Lenschow & S. D. Mayor (1998). "Structure of the entrainment zone capping the convective atmospheric boundary layer." In: *J. Atmos. Sci.* 55, pp. 3042–3064.
Sun, J. & Q. Xu (2009). "Parameterization of Sheared Convective Entrainment in the First-Order Jump Model: Evaluation Through Large-Eddy Simulation." In: *Bound.-Layer Meteor.* 132.2, pp. 279–288.
Sun, R., S. K. Krueger, M. A. Jenkins, M. A. Zulauf & J. J. Charney (2009). "The importance of fire atmosphere coupling and boundary-layer turbulence to wildfire spread." In: *International Journal of Wildland Fire* 18.1, pp. 50–60.
Tennekes, H. (1973). "A Model for the Dynamics of the Inversion Above a Convective Boundary Layer." In: *J. Atmos. Sci.* 30, pp. 558–567.
Tennekes, H. & A. G. M. Driedonks (1981). "Basic entrainment equations for the atmospheric boundary layer." In: *Bound.-Layer Meteor.* 20.4, pp. 515–531.
Träumner, K., Ch. Kottmeier, U. Corsmeier & A. Wieser (2011). "Convective Boundary-Layer Entrainment: Short Review and Progress using Doppler Lidar." In: *Boundary-Layer Meteorology* 141.3, pp. 369–391.
Van Heerwaarden, Chiel C. & Juan Pedro Mellado (2016). "Growth and Decay of a Convective Boundary Layer over a Surface with a Constant Temperature." In: *Journal of the Atmospheric Sciences* 73.5, pp. 2165–2177.
Van Heerwaarden, Chiel C., Juan Pedro Mellado & Alberto De Lozar (2014). "Scaling Laws for the Heterogeneously Heated Free Convective Boundary Layer." In: *Journal of the Atmospheric Sciences* 71.11, pp. 3975–4000.
VanZanten, Margreet C. (2002). "Radiative and Evaporative Cooling in the Entrainment Zone of Stratocumulus – the Role of Longwave Radiative Cooling Above Cloud Top." In: *Boundary-Layer Meteorology* 102.2, pp. 253–280.

Waggy, S. B., S. Biringen & P. P. Sullivan (2013). "Direct numerical simulation of top-down and bottom-up diffusion in the convective boundary layer." In: *J. Fluid Mech.* 724, pp. 581–606.

Willis, G. E. & J. W. Deardorff (1974). "A Laboratory Model of the Unstable Planetary Boundary Layer." In: *Journal of the Atmospheric Sciences* 31.5, pp. 1297–1307.

Wood, Robert (2012). "Stratocumulus Clouds." In: *Monthly Weather Review* 140.8, pp. 2373–2423.

Wulfmeyer, Volker, Shravan Kumar Muppa, Andreas Behrendt, Eva Hammann, Florian Späth, Zbigniew Sorbjan, David D. Turner & R. Michael Hardesty (2016). "Determination of Convective Boundary Layer Entrainment Fluxes, Dissipation Rates, and the Molecular Destruction of Variances: Theoretical Description and a Strategy for Its Confirmation with a Novel Lidar System Synergy." In: *Journal of the Atmospheric Sciences* 73.2, pp. 667–692.

Yu, Miao, Yimin Liu, Yifeng Dai & Aqiang Yang (2013). "Impact of urbanization on boundary layer structure in Beijing." In: *Climatic Change* 120.1, pp. 123–136.

Zampieri, M., P. Malguzzi & A. Buzzi (2005). "Sensitivity of quantitative precipitation forecasts to boundary layer parameterization: a flash flood case study in the Western Mediterranean." In: *Natural Hazards and Earth System Sciences* 5, pp. 603–612.

Zanten, Margreet C. van, Peter G. Duynkerke & Joannes W. M. Cuijpers (1999). "Entrainment Parameterization in Convective Boundary Layers." In: *J. Atmos. Sci.* 56.6, pp. 813–828.

Zeman, O. & H. Tennekes (1977). "Parameterization of the turbulent energy budget at the top of the daytime atmospheric boundary layer." In: *J. Atmos. Sci.* 34, pp. 111–123.

Zilitinkevich, S. S. (1991). "Turbulent Penetrative Convection." In: Avebury Technical.

Part II

APPENDICES

A

CHARACTERIZATION OF WIND-SHEAR EFFECTS ON ENTRAINMENT IN A CONVECTIVE BOUNDARY LAYER

This appendix contains a paper, which has been published with minor modifications in the journal of fluid mechanics as

Haghshenas, A., Mellado, J.P., "Characterization of wind-shear effects on entrainment in a convective boundary layer", J. Fluid Mech., 858, 145-183 (2019).

The contribution of Armin Haghshenas (A.H.) and Juan Pedro Mellado (JP.M.) to this paper is as follows: JP.M. conceived and designed the original idea and had the supervision responsibility for the research. Both authors equally contributed to defining the problem formulation including the designed simplified configuration, the dimensional analysis, and setting up the simulations (section 2). A.H. carried out the numerical simulations and developed a numerical tool to perform the statistical analysis of the acquired data. As the cornerstones of the derivation of the scaling laws, A.H. conducted the structural analysis of the CBL and the integral analysis of the TKE budget equation (sections 4&5). These analyses have been regularly discussed with JP.M.. A.H. wrote the draft of the manuscript, and JP.M. contributed, from the mentorship perspective, to writing the final version of the manuscript. As the corresponding author, A.H. took the lead in response to the reviewers.

Characterization of wind-shear effects on entrainment in a convective boundary layer

Armin Haghshenas and Juan Pedro Mellado

Max Planck Institute for Meteorology, Bundesstrasse 53, 20146 Hamburg, Germany

(Received 14 February 2018; revised 20 September 2018; accepted 20 September 2018)

Direct numerical simulations are used to characterize wind-shear effects on entrainment in a barotropic convective boundary layer (CBL) that grows into a linearly stratified atmosphere. We consider weakly to strongly unstable conditions $-z_{enc}/L_{Ob} \gtrsim 4$, where z_{enc} is the encroachment CBL depth and L_{Ob} is the Obukhov length. Dimensional analysis allows us to characterize such a sheared CBL by a normalized CBL depth, a Froude number, and a Reynolds number. The first two non-dimensional quantities embed the dependence of the system on time, on the surface buoyancy flux, and on the buoyancy stratification and wind velocity in the free atmosphere. We show that the dependence of entrainment-zone properties on these two non-dimensional quantities can be expressed in terms of just one independent variable, the ratio between a shear scale $(\Delta z_i)_s \equiv \sqrt{1/3}\,\Delta u/N_0$ and a convective scale $(\Delta z_i)_c \equiv 0.25\,z_{enc}$, where Δu is the velocity increment across the entrainment zone, and N_0 is the buoyancy frequency of the free atmosphere. $(\Delta z_i)_s$ and $(\Delta z_i)_c$ represent the entrainment-zone thickness in the limits of weak convective instability (strong wind) and strong convective instability (weak wind), respectively. We derive scaling laws for the CBL depth, the entrainment-zone thickness, the mean entrainment velocity, and the entrainment-flux ratio as a function of $(\Delta z_i)_s/(\Delta z_i)_c$. These scaling laws can also be expressed as a function of only a Richardson number $(N_0 z_{enc}/\Delta u)^2$, but not in terms of only the stability parameter $-z_{enc}/L_{Ob}$.

Key words: atmospheric flows, stratified turbulence, turbulent convection

A.1 INTRODUCTION

Entrainment, the process by which air from the free atmosphere is incorporated and mixed into the boundary-layer interior, is crucial for the structure and evolution of planetary boundary layers. Entrainment is important for cloud formation and dessication at the boundary-layer top, for the evolution of mixed-layer properties in the interior, and for surface processes. However, characterizing entrainment remains a challenge despite continuing efforts. On one hand, it is difficult to obtain accurate data at the required small scales. On the other hand, entrainment often compounds turbulent mixing in a stably stratified environment with other complex phenomena such as clouds and wind shear (Stull, 1988; Garratt, 1992; Mellado, 2017). In this paper, we study the effect of wind shear on entrainment in a cloud-free convective boundary layer (CBL).

The effect of wind shear on entrainment in CBLs has been studied by means of atmospheric measurements, laboratory experiments, and numerical simulations (see review in Conzemius & Fedorovich, 2006a; Fedorovich & Conzemius, 2008, and

references therein). These studies have shown that wind shear generally enhances entrainment, which thickens the entrainment zone and increases the growth rate of the CBL. The entrainment zone is defined as the region of negative buoyancy flux at the boundary-layer top. The main cause for this enhancement is the shear-generated turbulence in the entrainment zone, and not the vertical transport of shear-generated turbulence in the surface layer. The shear in the surface layer affects entrainment mainly indirectly by slowing the flow in the CBL interior, which leads to the formation of a localized shear layer at the CBL top. This indirect effect is even found in the absence of convection, when turbulence is solely mechanically driven (Jonker et al., 2013). Consequently, local scales in the entrainment zone become more important in sheared CBLs than in shear-free CBLs, and the boundary-layer depth and the associated convective scales are insufficient to characterize the system (Kim et al., 2006; Conzemius & Fedorovich, 2006b, 2007). Nonetheless, the quantification of the shear enhancement of entrainment and of its dependence on the environmental conditions remains difficult. In the work here presented, we use a configuration of reduced complexity to better understand and characterize the vertical structure of the entrainment zone, and we use this new characterization to quantify the dependence of entrainment-zone properties on the surface and free-atmosphere conditions.

We consider a zero-pressure-gradient turbulent boundary layer that is forced by a constant surface buoyancy flux and that grows into a linearly stratified atmosphere. As we will show, such a configuration is representative of a barotropic CBL over land. Mixing and entrainment in a stably stratified environment has often been studied in idealized configurations where the turbulence is forced by a grid or by an imposed mean shear (e.g., Fernando, 1991; Strang & Fernando, 2001; Peltier & Caulfield, 2003; Chung & Matheou, 2012, and references therein). From these studies, we have learned about various mixing mechanisms and entrainment-rate laws depending on the stratification conditions. However, it remains difficult to extend these results to the entrainment zone of CBLs. For instance, these previous studies indicate that the buoyancy Reynolds number should be on the order of 100 for large patches of turbulence to be sustained (Smyth & Moum, 2000a; Portwood et al., 2016), whereas buoyancy Reynolds numbers on the order of 10 are sufficient in the entrainment zone of CBLs (Garcia & Mellado, 2014). The reason for this difference is that large-scale updraughts in the CBL continuously transport turbulence into the entrainment zone. Besides, turbulence in the CBL has its distinct properties, such as the large-scale organization of the flow in convective rolls and the possible interaction between entrainment and near-surface dynamics (LeMone, 1973; Moeng & Sullivan, 1994; Boer et al., 2014; Salesky et al., 2017). Configurations of intermediate complexity as the one considered here provide a closer representation of planetary boundary layers and can help to transfer results from studies of more idealized configurations, such as stratified shear layers and homogeneous stratified shear turbulence, to planetary boundary layers.

Because of the relevance of the local shear in the entrainment zone, understanding the vertical structure of the entrainment zone is crucial to understand shear effects on entrainment. In shear-free CBLs, Garcia & Mellado (2014) have introduced a two-layer structure to describe the entrainment zone. The lower sublayer is characterized by global scales, namely, by a length scale proportional to the CBL depth and by the convective scales that characterize the variances in the CBL interior. The upper

sublayer acts as a transition layer between the turbulent region below and the non-turbulent stably stratified region above, and is characterized by local scales. As the CBL broadens, the upper sublayer becomes thinner compared to the lower sublayer. This two-layer structure rationalizes the observation that the entrainment-zone thickness deviates from a constant fraction of the CBL depth as the CBL grows (Deardorff et al., 1980; Sullivan et al., 1998), and that the variance correlates with the local gradients and not with the convective scales that characterize the CBL interior (Deardorff, 1974; Sorbjan, 2005). This two-layer structure also helps explain the observed dependence on weak- and strong stratification regimes of the minimum buoyancy flux, and of the relationship between the mean entrainment velocity and the convective Richardson number. In this work, we show that the entrainment zone in sheared CBLs is also better described as a two-layer structure.

One last goal of the work here presented is to quantify the dependence of entrainment zone properties on environmental conditions, which is particularly important for sheared CBLs because, as indicated above, these properties partly define the evolution of global CBL properties. Previous studies have identified major sensitivities of entrainment-zone properties to changes in environmental conditions. For instance, Pino & Vilà-Guerau De Arellano (2008) showed that entrainment generally increases with the wind velocity in the free atmosphere. Conzemius & Fedorovich (2006a) found that increasing the free atmosphere stratification or decreasing the surface buoyancy flux enhances shear effects, because a slower CBL growth permits the accumulation of more shear in the entrainment zone. Mahrt & Lenschow (1976) and Kim et al. (2003) observed that gradient and flux Richardson numbers in the entrainment zone approach constant values in the range $0.25 - 0.3$ as shear increases, which indicates a balance between shear-production of turbulence kinetic energy (TKE), buoyancy destruction, and viscous dissipation. This condition is accompanied by patches of Kelvin-Helmholtz-like billows, which are induced by convective thermals impinging into the inversion and reducing locally the gradient Richardson number (Kim et al., 2003). The quantification of these sensitivities, however, remains elusive. In this paper, we provide explicit scaling laws in terms of the surface and free-atmosphere conditions. Based on these scaling laws, we identify the conditions for which shear effects become relevant, and for which shear effects become of order one. In contrast to previous work, the scaling laws proposed here do not have a singularity at a finite wind strength.

One curious aspect of wind-shear effects on entrainment is that, for weak shear conditions and during the early state of the CBL development, entrainment slightly decreases with respect to the shear-free CBL (Conzemius & Fedorovich, 2006a; Pino & Vilà-Guerau De Arellano, 2008). Such a reduction has been associated with the blockage of turbulence propagation near a turbulent/non-turbulent interface (Hunt & Durbin, 1999; Fedorovich & Thäter, 2001), and with the enhancement of the energy drain from the CBL top by gravity-wave radiation into the free atmosphere (Schröter, 2018). It remains unclear, however, how much this phenomenon depends on the initial conditions and on the different CBL regimes. Systematic studies of sheared CBLs can also help to clarify this aspect.

We note that one key to better quantify entrainment is to obtain accurate data at the required small scales, which are on the order of tens of meters. Typical grid spacings in large-eddy simulations are also on the order of ten meters or more, and

hence simulated properties can be strongly affected by the subgrid-scale models and numerical artefacts, as illustrated by the order-of-one intra-model variability of the minimum buoyancy flux in the inter-comparison study of Fedorovich et al. (2004b). To reduce this uncertainty, we use direct numerical simulation and assess the dependence of the results on the Reynolds number.

The structure of the paper is as follows. After defining the problem in §A.2, we discuss in §A.3 wind-shear effects on buoyancy and velocity properties, identifying the conditions at which these effects become significant. In §A.4, we characterize the two-layer structure of the entrainment zone. The local scales identified in this section are then used in §A.5 to provide scaling laws that express the dependence of entrainment-zone properties on the surface and free-atmosphere conditions, and on the state of development of the CBL. In §A.6, we use the results to define a convection-dominated regime, where shear effects are negligible, and a shear-dominated regime, where shear effects are on the order of one. We finally summarize these results and draw conclusions in §A.7.

A.2 PROBLEM DEFINITION

We consider a cloud-free CBL that develops over a flat, aerodynamically smooth wall and penetrates into a free atmosphere with constant buoyancy gradient, N_0^2, where N_0 is the Brunt-Väisälä frequency (see figure A.1). Convection is forced by a constant and homogeneous surface buoyancy flux, B_0. We consider barotropic conditions, i.e., the wind strength in the free atmosphere, U_0, is constant with height (Fedorovich & Conzemius, 2008; Pino & Vilà-Guerau De Arellano, 2008). This configuration is representative of midday conditions over land. In addition, we consider the limit of zero Coriolis parameter, which implies that the mean pressure gradient associated with the geostrophic balance is zero. Results show that our simulations reproduce main features of barotropic CBLs in middle latitudes, and the limit of zero Coriolis parameter provides a reference case to systematically study Coriolis effects. The resulting configuration is a temporally evolving zero-pressure-gradient boundary layer that is convectively forced at the surface. Because of the stable stratification in the free atmosphere, the boundary layer develops in a quasi-steady regime, in which CBL properties evolve on time scales much larger than the eddy turnover time of the large, energy-containing motions. We focus on this quasi-steady regime.

A.2.1 *Governing equations*

We solve the conservation equations for mass, momentum, and energy in the Boussinesq approximation

$$\boldsymbol{\nabla} \cdot \boldsymbol{u} = 0 \,, \tag{A.1a}$$

$$\frac{\partial \boldsymbol{u}}{\partial t} + \boldsymbol{\nabla}\cdot(\boldsymbol{u} \otimes \boldsymbol{u}) = -\boldsymbol{\nabla} p + \nu \nabla^2 \boldsymbol{u} + b\boldsymbol{k} \,, \tag{A.1b}$$

$$\frac{\partial b}{\partial t} + \boldsymbol{\nabla}\cdot(\boldsymbol{u} b) = \kappa_b \nabla^2 b \,, \tag{A.1c}$$

where $\boldsymbol{u}(\boldsymbol{x}, t)$ is the velocity vector with components (u, v, w), $\boldsymbol{x} = (x, y, z)$ is the position vector with x the streamwise coordinate, y the spanwise coordinate, and z

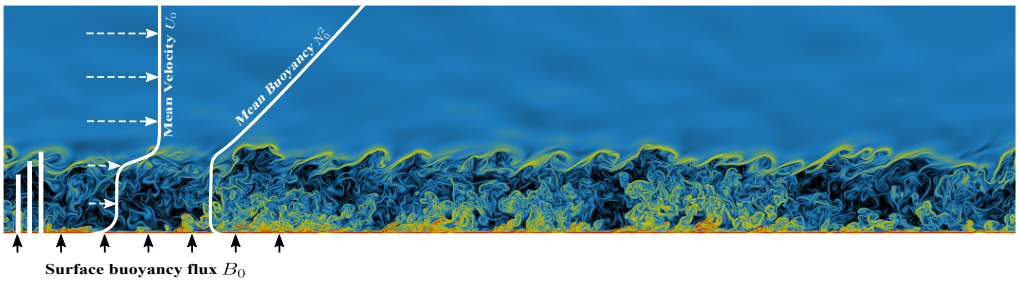

Figure A.1: Sketch of the barotropic CBL considered in this analysis. The vertical white bars indicate different definitions of the CBL depth, namely, from left to right, the encroachment length scale, z_{enc}, the flux-based height, $z_{\mathrm{i,f}}$, and the gradient-based height, $z_{\mathrm{i,g}}$. The background is a cross-section of the logarithm of the magnitude of the buoyancy gradient from case $Fr_0 = 20$ and $Re_0 = 25$ of table A.1 at $z_{\mathrm{enc}}/L_0 \simeq 15$. (The image only shows the lower 40% of the vertical domain.)

the vertical coordinate, t is the time, $\boldsymbol{k} = (0,0,1)$ is the unitary vector in the vertical direction, and p is the modified pressure divided by the constant reference density. The buoyancy b is linearly related to the virtual potential temperature θ_{v} by $b \simeq g(\theta_{\mathrm{v}} - \theta_{\mathrm{v},0})/\theta_{\mathrm{v},0}$, where $\theta_{\mathrm{v},0}$ is the constant reference value obtained by extrapolating the linear stratification of θ_{v} in the free atmosphere downwards to the surface. The parameters ν and κ_b are the kinematic viscosity and thermal diffusivity, respectively. Equation (A.1c) can be derived from the evolution equations of the energy variable (e.g., entropy or enthalpy) and the specific humidity assuming that the mass diffusivity of water vapour is equal to the thermal diffusivity, once b has been expressed as a linear combination of the energy variable and the specific humidity by linearising the equations of state.

Impermeable, no-slip and impermeable, free-slip boundary conditions are applied, respectively, at the bottom and at the top of the domain. Neumann boundary conditions are used for the buoyancy at the bottom, $\partial_z b = -B_0/\kappa_b$, and at the top, $\partial_z b = N_0^2$, to maintain fixed constant fluxes. Periodicity is applied at the lateral boundaries. A linear relaxation term acts on the velocity and buoyancy fields inside a sponge layer occupying the upper $15-20\%$ of the computational domain. The reference values of this relaxation term are the initial conditions. The proportionality coefficient of the relaxation term increases quadratically with the distance from the inner limit of the sponge layer, from zero at the inner limit to $N_0/(2\pi)$ at the outer limit (which coincides with the top of the computational domain).

The initial buoyancy field is defined as

$$b(\boldsymbol{x},0) = b_{\mathrm{ics}}\left[1 - \mathrm{erf}\left(\frac{\sqrt{\pi}}{2}\frac{z}{\delta_{\mathrm{ics}}}\right)\right] + N_0^2 z\,, \tag{A.2}$$

where $b_{\mathrm{ics}}(x_1,x_2) = (B_0/\kappa_b + N_0^2)\,\delta_{\mathrm{ics}}(x_1,x_2)$ is the surface buoyancy and δ_{ics} is the local gradient thickness (Mellado et al., 2016). A broadband field is constructed by specifying $\delta_{\mathrm{ics}}(x_1,x_2) = \delta_0[1+\xi(x_1,x_2)]$, the parameter δ_0 to be given. The random field $\xi(x_1,x_2)$ has a Gaussian power spectral density centred at a spatial frequency $\lambda_0^{-1} = (4\,\delta_0)^{-1}$ and with a standard deviation $(6\,\lambda_0)^{-1}$, so that there is practically no energy with spatial frequencies below $(2\,\lambda_0)^{-1}$. The phase of ξ is random, and its

mean value is zero and the root-mean-square (r.m.s.) is $\xi_{\text{rms}} = 0.1$. The initial velocity field is imposed as

$$\boldsymbol{u}(\boldsymbol{x}, 0) = U_0 \left[\text{erf}\left(\frac{\sqrt{\pi}}{2} \frac{z}{\delta_0} \right) \right] \boldsymbol{i} \,, \tag{A.3}$$

where $\boldsymbol{i} = (1, 0, 0)$. Such a function provides the no-slip boundary condition at the surface and a height-constant velocity in the streamwise direction in the bulk of the domain.

A finite difference method using Cartesian coordinates and a structured grid is employed to solve the governing equations. The discretization of the equations is carried out by sixth-order spectral-like compact schemes for the spatial derivatives (Lele, 1992) along with a low-storage fourth-order Runge-Kutta scheme to advance in time (Carpenter & Kennedy, 1994). For the compact schemes used in this study, about 4 points per wavelength provide 99% accuracy in the transfer function of the derivative operator. For comparison, second-order central schemes need about 8 points per wavelength to reach 90% accuracy, which is the motivation to employ compact schemes despite being computationally more demanding (Lele, 1992). The pressure-Poisson equation is solved using a Fourier decomposition along the horizontal directions, which results in a set of second-order differential equations along the vertical coordinate (Mellado & Ansorge, 2012).

A.2.2 *Dimensional analysis*

The sheared CBL described in the previous section is completely governed by the control parameters $\{\nu, \kappa_b, B_0, N_0, U_0\}$ once the turbulent flow has sufficiently forgotten the initial conditions. Hence, three non-dimensional parameters are sufficient to characterize the system. In this work, we take the shear-free limit $U_0 = 0$ as reference and study how entrainment-zone properties change as we gradually increase the wind velocity. Hence, we choose N_0 and B_0 to non-dimensionalize the problem, which yields N_0^{-1} as the reference time scale,

$$L_0 \equiv \left(\frac{B_0}{N_0^3} \right)^{1/2} \tag{A.4}$$

as the reference length scale, and $N_0 L_0 = (B_0/N_0)^{1/2}$ as the reference velocity scale. (Henceforth, the symbol $\equiv$ indicates a definition.) The characteristic length scale L_0 will be referred to as the reference Ozmidov length. This scale provides a reference value of the Ozmidov length

$$L_{\text{Oz}} \equiv \left(\frac{\varepsilon}{N^3} \right)^{1/2} \tag{A.5}$$

in the entrainment zone, since the viscous dissipation rate ε in shear-free CBLs is an order-of-one fraction of the surface buoyancy flux B_0 (Fedorovich et al., 2004a), and the mean buoyancy gradient N^2 is partly characterized by N_0^2 (Garcia & Mellado, 2014). The Ozmidov length represents the size of the largest motions unaffected by a background stratification N^2 in a turbulent field characterized by a viscous dissipation rate ε (Dougherty, 1961; Ozmidov, 1965). Garcia & Mellado (2014) and Mellado et al. (2017) have shown that, in shear-free CBLs, L_0 helps characterize main properties in the upper region of the entrainment zone, such as the mean gradients and variances

of temperature and specific humidity. We will show that L_0 is also a useful parameter to characterize the entrainment zone in the sheared CBLs considered in this study.

The shear-free limit is fully characterized by a reference buoyancy Reynolds number

$$Re_0 \equiv \frac{(N_0 L_0) L_0}{\nu} = \frac{B_0}{\nu N_0^2} \tag{A.6}$$

and the Prandtl number $Pr \equiv \nu/\kappa_b$. The parameter Re_0 provides a reference value of the buoyancy Reynolds number

$$Re_b \equiv \frac{\varepsilon}{\nu N^2} \tag{A.7}$$

in the lower part of the entrainment zone, since $\varepsilon \sim B_0$ and $N \sim N_0$ in shear-free CBLs, as explained before. A buoyancy Reynolds number is often used in the study of the interaction between turbulence and stable stratification (see, e.g., Smyth & Moum, 2000a; Hebert & Bruyn Kops, 2006; Chung & Matheou, 2012; Portwood et al., 2016). As explained in the introduction, the work here presented helps ascertain to what extent results from those previous studies apply to the entrainment zone of sheared CBLs.

To characterize wind-shear effects, we use the reference Froude number

$$Fr_0 \equiv \frac{U_0}{N_0 L_0} = \frac{U_0}{(B_0 L_0)^{1/3}} \tag{A.8}$$

as third non-dimensional parameter. The denominator is the velocity scale that stems from the buoyancy acceleration $N_0^2 L_0$ associated with a vertical displacement L_0 in an environment with a buoyancy stratification N_0^2. The last equality follows from the definition of L_0 and indicates that Fr_0 can be interpreted as the ratio between the wind velocity in the free atmosphere and the velocity scale associated with motions of size L_0 in a turbulent cascade characterized by an energy transfer rate B_0, as is the case is shear-free CBLs.

Due to statistical homogeneity in the horizontal directions, statistical properties are only functions of two independent variables, namely, height and time $\{z, t\}$. Following previous work in shear-free CBLs growing into linearly stratified atmospheres (Garcia & Mellado, 2014; Mellado et al., 2016; Van Heerwaarden & Mellado, 2016), we use the non-dimensionalized form of these variables $\{z/z_{\mathrm{enc}}, z_{\mathrm{enc}}/L_0\}$. The variable z_{enc} is the encroachment length scale defined as

$$z_{\mathrm{enc}} \equiv \left\{ 2 N_0^{-2} \int_0^{z_\infty} \left[\langle b \rangle (z,t) - N_0^2 z \right] \mathrm{d}z \right\}^{1/2}, \tag{A.9}$$

where z_∞ is located far enough into the non-turbulent free atmosphere for the integral to become approximately independent of z_∞. Angle brackets denote averaging along horizontal planes. The integral analysis of the buoyancy equation (A.1c) yields

$$\frac{z_{\mathrm{enc}}}{L_0} = \left[2 \left(1 + Re_0^{-1} \right) N_0 (t - t_0) \right]^{1/2}, \tag{A.10}$$

where t_0 is a constant of integration, so that z_{enc} can be easily calculated at any time. The reason to use z_{enc} instead of time as independent variable is that the encroachment length scale provides a measure of the shear-free CBL depth (Carson & Smith, 1975), and it can be calculated from the mean buoyancy profile according to Eq. (A.9), which

makes it convenient for the interpretation of results. We will show that z_{enc} also provides a relevant depth measure for the sheared CBLs considered in this study.

The sheared CBL can also be partly characterized by the stability parameter defined as the ratio between the CBL depth and the Obukhov length (Stull, 1988). The Obukhov length is defined as

$$L_{Ob} \equiv -\frac{u_*^3}{\kappa B_0} = -\left(\frac{u_*}{w_*}\right)^3 \frac{z_{enc}}{\kappa}, \tag{A.11}$$

where $\kappa \simeq 0.41$ is the von Karman constant,

$$u_* \equiv (\nu\, \partial_z \langle u \rangle)_{z=0}^{1/2} \tag{A.12}$$

is the friction velocity, and

$$w_* \equiv (B_0\, z_{enc})^{1/3} \tag{A.13}$$

is a convective velocity scale (Deardorff, 1970). Very large values of $-z_{enc}/L_{Ob}$ correspond to nearly shear-free CBLs, and very small values correspond to nearly neutral, shear-driven boundary layers. When studying entrainment-zone properties, however, the stability parameter alone is not sufficient as an independent variable, and alternative options have been proposed, such as a Richardson number (see Conzemius & Fedorovich, 2006b; Pino & Vilà-Guerau De Arellano, 2008, and references therein). We will discuss these alternative variables in §A.6.

A.2.3 *Parameter space and description of simulations*

For typical midday conditions $N_0 \simeq 0.6 - 1.8 \times 10^{-2}$ s^{-1}, $B_0 \simeq 0.3 - 1.0 \times 10^{-2}$ m^{2}s^{-3} and $z_{enc} \simeq 500 - 2000$ m, one finds $L_0 \simeq 20 - 200$ m and states of development in the range $z_{enc}/L_0 \simeq 5 - 50$. For these conditions and wind velocities in the interval $U_0 = 0 - 15$ ms^{-1}, the reference Froude number is in the range $Fr_0 \simeq 0 - 35$. Using $\kappa_b = 2.1 \times 10^{-5}$ m^{2}s^{-1} and $\nu = 1.5 \times 10^{-5}$ m^{2}s^{-1}, one further obtains $Re_0 \simeq 6 \times 10^5 - 2 \times 10^7$ and $Pr \simeq 0.7$.

In our simulations, we fix $Pr = 1$ and change the reference Froude number between zero (no wind condition) and 25 (strong wind condition) in intervals of 5. Table A.1 summarizes the configurations studied in this work. We reach $z_{enc}/L_0 \simeq 35$, covering in this way a large extent of the typical values observed in nature. The stability parameter $-z_{enc}/L_{Ob}$ is larger than 4. Hence, we cover the regime of weakly unstable conditions $0 < -z_{enc}/L_{Ob} \lesssim 15 - 20$, characterized by horizontal convective rolls aligned with the mean wind direction, as well as the regime of strongly unstable conditions, characterized by polygonal convective cells (LeMone, 1973; Moeng & Sullivan, 1994; Salesky et al., 2017). The reference Reynolds number that we achieve in our simulations, however, is much smaller than in the atmosphere. Nonetheless, the entrainment zone is largely occupied with turbulent patches, as shown in figure A.2. We use data from simulations with $Re_0 = 25$, $Re_0 = 42$ and $Re_0 = 117$. The main analysis is based on the simulations with $Re_0 = 25$ because these cases reach higher values of state of development z_{enc}/L_0, and, unless otherwise stated, the figures show data from these simulations. The cases with $Re_0 = 42$ are used to study the sensitivity of the results to the Reynolds number; for the shear-free cases, we also compare to case $Re_0 = 117$. Although this range of Reynolds number is small, the observed

Re_0	Fr_0	$\frac{z_{enc}}{L_0}$	Re_*	$(Re_t)_{max}$	$(Re_t)_{z_{i,f}}$	$(Re_b)_{z_{i,f}}$	$\frac{z_{enc}}{\eta_{min}}$	$\frac{z_{i,f}}{z_{enc}}$	$\frac{(\Delta z_i)_s}{(\Delta z_i)_c}$	$\frac{-z_{enc}}{L_{Ob}}$
25	0	35	2860	1400	410	4	575	$1.14 - 1.14$	0	∞
25	5	35	2860	1480	540	5	598	$1.14 - 1.14$	$0.27 - 0.16$	$57 - 241$
25	10	35	2860	1550	810	5	617	$1.16 - 1.15$	$0.58 - 0.34$	$17 - 78$
25	15	35	2860	1760	1090	6	643	$1.19 - 1.16$	$0.91 - 0.55$	$9 - 44$
25	20	35	2860	2300	1670	8	673	$1.24 - 1.18$	$1.21 - 0.78$	$6 - 28$
25	25	31	2410	1900	1770	9	597	$1.28 - 1.22$	$1.50 - 1.07$	$4 - 16$
42	0	33	4500	2540	940	10	850	$1.14 - 1.14$	0	∞
42	10	23	2680	1700	1040	8	610	$1.15 - 1.15$	$0.53 - 0.42$	$20 - 37$
42	15	21	2420	1710	1390	11	591	$1.19 - 1.18$	$0.84 - 0.71$	$10 - 17$
42	20	15	1610	1430	1080	14	466	$1.24 - 1.24$	$1.12 - 1.12$	$6 - 6$
117	0	22	6960	4050	1640	25	1240	$1.15 - 1.15$	0	∞

Table A.1: Simulation properties. Columns $3 - 8$ provide data at the final time of the simulations, and columns $9 - 11$ show the variation between $z_{enc}/L_0 = 15$ and the final time of the simulations: Re_0 is the reference buoyancy Reynolds number defined by Eq. (A.6), Fr_0 is the reference Froude number defined by Eq. (A.8), z_{enc} is the encroachment length defined by Eq. (A.9), and L_0 is the reference Ozmidov length defined by Eq. (A.4). The convective Reynolds number is defined as $Re_* \equiv z_{enc} w_* / \nu$, where w_* is the convective velocity scale defined by Eq. (A.13). The turbulent Reynolds number is defined as $Re_t \equiv e^2/\varepsilon\nu$, where e is the turbulence kinetic energy and ε its viscous dissipation rate. $(Re_t)_{max}$ is the maximum turbulent Reynolds number in the CBL, and $(Re_t)_{z_{i,f}}$ is the turbulent Reynolds number particularized at the height of the minimum buoyancy flux. $(Re_b)_{z_{i,f}}$ is the buoyancy Reynolds number defined by Eq. (A.7) particularized at the height of the minimum buoyancy flux. $\eta \equiv (\nu^3/\varepsilon)^{1/4}$ is the Kolmogorov scale. $(\Delta z_i)_c$ and $(\Delta z_i)_s$ are defined by Eq. (A.29) and Eq. (A.30), respectively, and are the convective and shear limits of the entrainment-zone scale, which is defined by Eq. (A.26). L_{Ob} is the Obukhov length defined by Eq. (A.11).

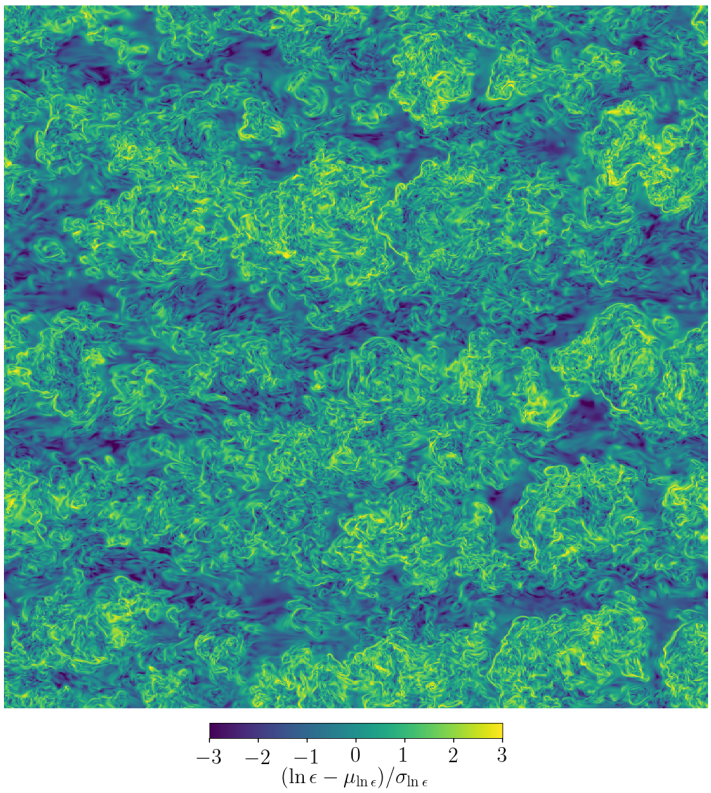

Figure A.2: Horizontal cross-section of the standardized natural logarithm of the viscous dissipation rate $\epsilon \equiv \nu(\partial_i u'_j + \partial_j u'_i)\partial_j u'_i$ at the height of the minimum buoyancy flux from case $Fr_0 = 20$ and $Re_0 = 42$ of table A.1 at $z_{\text{enc}}/L_0 \simeq 15$. Apostrophes indicate turbulent-fluctuation fields.

tendency towards Reynolds number similarity is consistent with that observed in previous work in similar configurations, and supports the use of DNS to study some aspects of the atmospheric boundary layer (Jonker et al., 2013; Waggy et al., 2013; Garcia & Mellado, 2014; Van Heerwaarden & Mellado, 2016; Mellado et al., 2018).

The domain size is $215\,L_0 \times 215\,L_0 \times 130\,L_0$ in all cases, and stopping the simulation at $z_{\text{enc}}/L_0 \simeq 35$ implies that the boundary layer occupies approximately 30% of the computational domain. Preliminary studies have shown that this ratio between the CBL depth and the depth of the computational domain is small enough for results to be independent of the depth of the computational domain. The aspect ratio of the horizontal domain size and the CBL depth varies between 12:1 at the beginning of the quasi-steady regime to around 5:1 at the final time considered in the analysis. The thickness δ_0 used in the initial conditions Eq. (A.2) and Eq. (A.3) is $\delta_0 \simeq 0.2\,L_0$, small compared to $z_{\text{enc}} \simeq 10\,L_0$, which is when the quasi-steady regime in shear-free CBLs starts. Preliminary studies considering additional perturbations in the velocity field over a similarly thin region have shown that results are independent to the details of the initial conditions.

Apart from the case $Fr_0 = 20$, the grid spacings are uniform and isotropic in all of the computational domain except near the surface and in the free atmosphere above the turbulent boundary layer (see table A.2). As we move towards the surface, the vertical grid spacing is smoothly refined according to a hyperbolic tangent profile to

Re_0	Fr_0	Grid	$(\Delta_z/\eta)_{\max}$	$(\Delta_x^+)_{\max}$	$(\Delta_y^+)_{\max}$	$\Delta_z^+\vert_{z=0}$
25	0	$1280 \times 1280 \times 512$	1.44	–	–	–
25	5	$1280 \times 1280 \times 512$	1.45	2.45	2.45	$0.80 - 0.66$
25	10	$1280 \times 1280 \times 512$	1.43	3.46	3.46	$1.19 - 0.96$
25	15	$1536 \times 1536 \times 576$	1.18	3.53	3.53	$1.24 - 0.96$
25	20	$1536 \times 2304 \times 576$	1.18	4.14	2.75	$1.46 - 1.12$
25	25	$2560 \times 2560 \times 896$	0.94	3.32	3.32	$1.14 - 0.89$
42	0	$2560 \times 2560 \times 896$	1.04	–	–	–
42	10	$2560 \times 2560 \times 896$	1.15	2.97	2.97	$1.09 - 1.01$
42	15	$3072 \times 3072 \times 1024$	0.84	2.71	2.71	$0.99 - 0.92$
42	20	$3072 \times 4608 \times 1024$	0.91	3.19	2.12	$1.17 - 1.17$
117	0	$5120 \times 5120 \times 1024$	1.16	–	–	–

Table A.2: Grid resolution. Here Δ_x, Δ_y, and Δ_z are the grid spacings in the streamwise, spanwise, and vertical directions, respectively. The maximum value of Δ_z/η occurs at the final time of the simulations, while the maximum values of Δ_x^+, Δ_y^+, and Δ_z^+ take place at the very beginning of the simulations, when the friction velocity is large. The last column shows the variation between $z_{\text{enc}}/L_0 = 15$ and the final time of the simulations.

provide the required higher resolution near the surface. The ratio between the vertical grid spacing in the bulk of the CBL and near the surface is 2.5, which is roughly the ratio between the Kolmogorov length scale in the bulk of the turbulent layer and near the surface in convection-dominated flows (Shishkina et al., 2010; Mellado, 2012). The grid stretching associated with this refinement concentrates between $z = 3\,L_0$ and $z = 15\,L_0$ and the stretching factor is less than 1.5%, which has been shown to be small enough to maintain the high accuracy of the compact schemes used in this work (Mellado & Ansorge, 2012). As we move upwards outside of the turbulent boundary layer and into the non-turbulent free atmosphere, the vertical grid spacing is smoothly coarsened according to a second hyperbolic tangent profile. The aim is to extend the vertical size of the computational domain and reduce the effect of the spurious reflection of gravity waves at the top of the computational domain without an excessive penalty in the required number of grid points. This coarsening starts beyond $z = 55\,L_0$, which is well above the turbulent boundary layer, and the corresponding stretching factor is less than 3.5%. We used preliminary studies to ascertain that the results were insensitive to the details of the grid.

The grid spacings are chosen according to the well established resolution requirements for shear-driven flows (Flores et al., 2007; Spalart et al., 2008; Bernardini et al., 2014) and convection-driven flows (Shishkina et al., 2010; Mellado, 2012; Waggy et al., 2013). The vertical grid spacing, Δ_z, satisfies always the relation $\Delta_z/\eta \lesssim 1.5$ (cf. table A.2), where $\eta \equiv (\nu^3/\varepsilon)^{1/4}$ is the Kolmogorov scale. This ratio is sufficient for the statistical properties of interest to depend less than 5% on the grid spacing, which is comparable to or less than the statistical convergence of the properties considered in the present work (Mellado, 2012; Garcia & Mellado, 2014). We also keep $\Delta_x^+ = \Delta_y^+ \lesssim 4.5$, where superscript $+$ denotes quantities normalized with the wall unit ν/u_* (Ansorge & Mellado, 2014; Pirozzoli et al., 2017; Gohari & Sarkar, 2017). Moreover, the viscous sublayer is resolved by $\simeq 10$ grid points in all simulations (Spalart et al., 2008; Gohari & Sarkar, 2017). The reason for the anisotropic grid in the horizontal directions in the cases with $Fr_0 = 20$ is that we could satisfy the aforementioned resolution constraints without the need to reduce the grid spacing in the streamwise direction with respect to the corresponding cases with $Fr_0 = 15$, which allowed us to save computational time.

To improve statistical convergence and thus the clarity of the results discussed below, horizontal averages are additionally averaged in time over an interval $\Delta z_{\mathrm{enc}}/L_0 = 2$, which means $\simeq 6$ large-eddy turnover times at $z_{\mathrm{enc}}/L_0 = 30$. This time interval is small compared to the time required for the mean properties to change significantly. When plotting the data, lines indicate this running average within an interval $\Delta z_{\mathrm{enc}}/L_0 = 2$, and shadow regions indicate the interval of two standard deviations around that average.

A.2.4 *Equilibrium (quasi-steady) entrainment regime*

Garcia & Mellado (2014) have shown that the equilibrium (quasi-steady) entrainment regime is reached beyond $z_{\mathrm{enc}}/L_0 \simeq 10$ in shear-free CBLs growing into linearly stratified atmospheres. In order to evaluate if the wind shear changes this critical

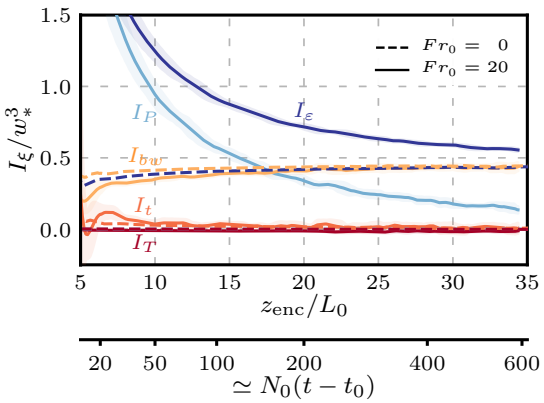

Figure A.3: Temporal evolution of the terms of the integral TKE budget equation (A.16) normalized with the convective velocity scale, defined in Eq. (A.13). Lines indicate the average within an interval $\Delta z_{\rm enc}/L_0 = 2$, and shadow regions indicate the interval of two standard deviations around that average.

value, following Fedorovich et al. (2004a), we perform an integral analysis of the TKE evolution equation

$$\partial_t e = P + \langle b'w' \rangle - \partial_z T - \varepsilon, \tag{A.14}$$

where $\partial_t e$ is the accumulation term, $P \equiv -\langle u'w' \rangle \partial_z \langle u \rangle$ is the shear-production rate, $\langle b'w' \rangle$ is the buoyancy production or destruction rate, $-\partial_z T$ is the turbulent transport, where $T \equiv \langle u_i' u_i' w'/2 + p'w' - u_i' \tau_{i3}' \rangle$, and $\varepsilon \equiv \langle \tau_{ij}' \partial_j u_i' \rangle$ is the viscous dissipation rate, $\tau_{ij} \equiv \nu(\partial_i u_j + \partial_j u_i)$ being the kinematic components of the viscous stress tensor. Apostrophes indicate turbulent-fluctuation fields, e.g., $b' \equiv b - \langle b \rangle$. Integrating Eq. (A.14) from the surface to a height z_∞ far into the non-turbulent free atmosphere yields

$$\int_0^{z_\infty} \partial_t e \, \mathrm{d}z = \int_0^{z_\infty} (P + \langle b'w' \rangle - \partial_z T - \varepsilon) \, \mathrm{d}z \, , \tag{A.15}$$

which for simplicity we write as

$$I_t = I_P + I_{bw} + I_T - I_\varepsilon \, . \tag{A.16}$$

The temporal evolution of each term normalized by w_*^3 is shown in figure A.3. (Curves in this figure correspond to the upper limit of integration $z_\infty = 2.5\, z_{\rm enc}$, but results remain similar when varying this limit between $1.5\, z_{\rm enc}$ and $2.5\, z_{\rm enc}$.) Similar to the shear-free case, the normalized integral of the transport term I_T is small, which implies that the energy drain due to the upward radiation of gravity waves is negligible. Moreover, the normalized integral of the temporal term I_t becomes negligible beyond $z_{\rm enc}/L_0 \simeq 10 - 15$, implying that there is a balance between shear production, buoyancy production, and viscous dissipation, i.e., $I_{bw} + I_P \simeq I_\varepsilon$. This balance corresponds to the equilibrium (quasi-steady) entrainment regime. In this work, we focus on this regime and study wind-shear effects beyond $z_{\rm enc}/L_0 \simeq 15$, and we will only consider the data in the quasi-steady regime to derive scaling laws. However, we will plot the data starting at $z_{\rm enc}/L_0 = 5$ to indicate how the statistics approach the quasi-steady regime.

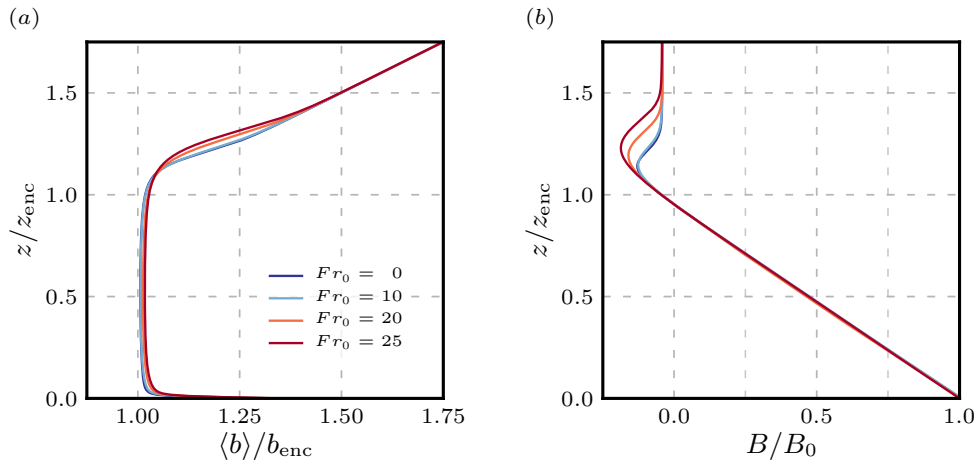

Figure A.4: Vertical profiles of (*a*) the mean buoyancy normalized by the encroachment buoyancy, defined by Eq. (A.17), and (*b*) the buoyancy flux, defined by Eq. (A.18), normalized by the surface buoyancy flux, for different Froude numbers at $z_{enc}/L_0 \simeq 30$. Data has been averaged within an interval $\Delta z_{enc}/L_0 = 2$.

A.3 WIND-SHEAR EFFECTS ON BUOYANCY AND VELOCITY

In this section, we discuss the dependence of buoyancy and velocity properties on Fr_0 and z_{enc}/L_0, obtaining the values of these quantities for which wind-shear effects become significant. Consistently with previous studies, some properties, like horizontal-velocity statistics, vary monotonically with the Froude number, some properties, like the buoyancy flux in the entrainment zone, change significantly only when $Fr_0 \gtrsim 10$, and some properties, like the buoyancy and vertical-velocity statistics in the mixed-layer, remain approximately unchanged and follow shear-free scaling laws for all conditions considered in this study. In the following sections, we will rationalize this behaviour.

A.3.1 *Effects on the buoyancy*

In the mixed layer, i.e., the well mixed region between $z \simeq 0.1\, z_{enc}$ and $z \simeq z_{enc}$, the mean buoyancy increases in time due to the surface buoyancy flux and the entrainment flux. In our study, the surface flux is constant and independent of the wind velocity, but the entrainment flux increases with the wind velocity, and therefore the mean buoyancy in the mixed layer is expected to increase with Fr_0. Previous studies have shown, however, that this increase is weak (e.g., Pino et al., 2003; Kim et al., 2003; Pino & Vilà-Guerau De Arellano, 2008), so that the encroachment buoyancy (Carson & Smith, 1975)

$$b_{enc} \equiv N_0^2 z_{enc} \tag{A.17}$$

characterizes the mean buoyancy in the mixed layer not only in shear-free conditions but also in sheared CBLs under weakly-to-strongly unstable conditions. Figure A.4(*a*) confirms this result up to wind velocities corresponding to $Fr_0 = 25$, for which the mean buoyancy is only $\simeq 2\%$ higher than in shear-free conditions. Wind-shear effects on the buoyancy flux

$$B \equiv \langle b' w' \rangle - \kappa_b \partial_z \langle b \rangle \tag{A.18}$$

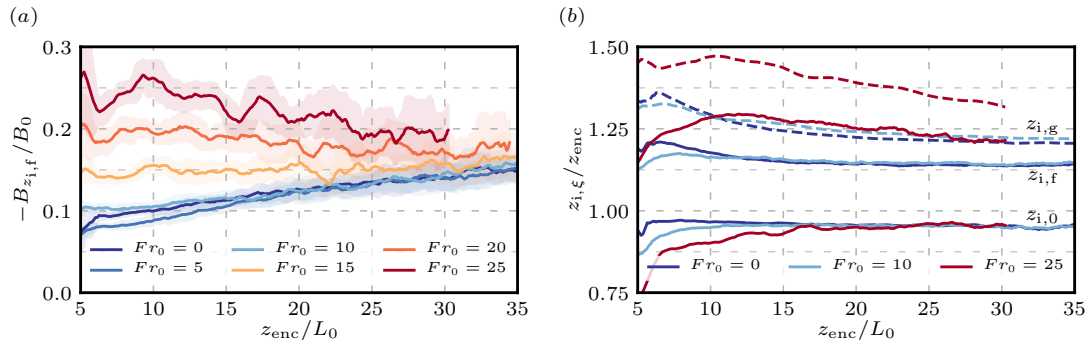

Figure A.5: Temporal evolution of (*a*) the minimum buoyancy flux normalized by the surface buoyancy flux, and (*b*) different definitions of the CBL depth normalized by the encroachment length scale. For clarity in the right panel, the height of the maximum buoyancy gradient, $z_{i,g}$, is indicated by dashed lines.

are also negligible in the mixed layer for all Froude numbers considered in this study (figure A.4*b*). In contrast, in the entrainment zone, the region of negative buoyancy flux above the mixed layer, wind-shear effects become significant for Froude numbers larger than 10. Hence, in agreement with the aforementioned previous studies where Coriolis effects are retained, wind-shear effects on buoyancy properties remain localized inside the entrainment zone for the idealized CBLs considered in this study.

To better quantify the effect of the wind shear on entrainment-zone properties, we plot the temporal evolution of the minimum buoyancy flux normalized by the surface buoyancy flux, $-B_{z_{i,f}}/B_0$, in figure A.5(*a*). (Henceforth, a subscript $z_{i,\cdot}$ indicates that the corresponding quantity is evaluated at $z_{i,\cdot}$, and $z_{i,f}$ is the height of the minimum buoyancy flux.) For $Fr_0 \lesssim 10$, this quantity approximately coincides with that of the shear-free case for $z_{enc}/L_0 \gtrsim 10-15$, which indicates a negligible effect of wind shear on the minimum buoyancy flux during the quasi-steady regime. The slight decrease for weak shear conditions $Fr_0 = 5$ at early states of development $z_{enc}/L_0 \lesssim 15$ has also been observed in Pino & Vilà-Guerau De Arellano (2008), and it might be a manifestation of the sheltering effect of shear on the propagation of turbulence near a turbulent/non-turbulent interface (Hunt & Durbin, 1999; Fedorovich & Thäter, 2001), or of the enhancement of the energy drain from the CBL top by gravity-wave radiation into the free atmosphere (Schröter, 2018). However, more analysis would be required to draw a definitive conclusion because the effect of the shear near the surface might still be significant in such a shallow CBL. For Froude numbers larger than 10, the ratio $-B_{z_{i,f}}/B_0$ increases. Visualizations show that Kelvin-Helmholtz-like instabilities inside the entrainment zone are associated with this increase (cf. figure A.1), in agreement with previous observations (Kim et al., 2003).

Another property that proves useful for the analysis of wind-shear effects on entrainment zone properties is the CBL depth. We consider the following definitions of the CBL depth (see, e.g., Garratt, 1992; Sullivan et al., 1998): (*i*) The zero-crossing height, $z_{i,0}$, where the buoyancy flux becomes zero, (*ii*) the flux-based height, $z_{i,f}$, where the buoyancy flux is minimum, and (*iii*) the gradient-based height, $z_{i,g}$, where the mean buoyancy gradient is maximum. The temporal evolution of these heights, shown in figure A.5(*b*), corroborates the features discussed before. First, the zero-

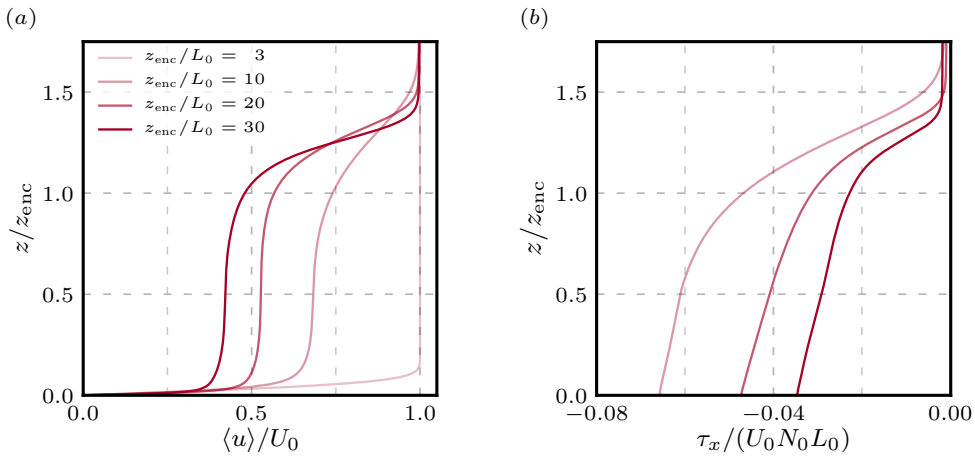

Figure A.6: Vertical profiles of (*a*) the mean streamwise velocity normalized by the wind velocity in the free atmosphere, U_0, (*b*) the momentum flux normalized with U_0 and the reference convection velocity $N_0 L_0$. Data corresponds to case $Fr_0 = 25$ at different z_{enc}/L_0.

crossing height $z_{i,0}$, which marks the bottom of the entrainment zone, is independent of the wind strength and it is well approximated by the encroachment length scale, z_{enc}. This result further indicates that wind-shear effects above the surface layer on the mean buoyancy concentrate in the entrainment zone (Fedorovich & Conzemius, 2008; Pino & Vilà-Guerau De Arellano, 2008). Second, the difference in $z_{i,f}$ and $z_{i,g}$ between cases $Fr_0 = 0$ and $Fr_0 = 10$ is small, which further indicates that entrainment-zone properties remain unchanged for such a weak wind condition. Third, for stronger wind conditions, wind-shear effects in the entrainment zone become considerable, and both $z_{i,f}$ and $z_{i,g}$ increase. We note that, although the change of these heights is small relative to the CBL depth, those changes are about 100% of the entrainment-zone thickness, and are relevant for the local analysis of the entrainment zone in §A.4.

Figure A.5(*a*, *b*) also shows that wind-shear effects diminish and eventually vanish as the CBL grows and thermals ascending from the mixed layer become more vigorous and dominate mixing in the entrainment zone (Mahrt & Lenschow, 1976; Pino & Vilà-Guerau De Arellano, 2008; Liu et al., 2016). Hence, shear effects depend not only on the Froude number Fr_0, or, equivalently, the wind velocity in the free atmosphere, but also on the normalized CBL depth z_{enc}/L_0. In §A.5, we find a non-dimensional variable that embeds the dependence on both Fr_0 and z_{enc}/L_0, which facilitates the characterization of wind-shear effects.

A.3.2 *Effects on the velocity*

As seen in figure A.6(*a*), when the CBL depth becomes an order of magnitude larger than L_0, the velocity profile varies rapidly across the CBL top, and becomes almost flat within the mixed-layer. Because of this flat shape, the vertically averaged mean velocity

$$u_{ml} \equiv \frac{1}{z_{i,f}} \int_0^{z_{i,f}} \langle u \rangle \, dz \tag{A.19}$$

provides an appropriate characteristic scale, and velocity profiles normalized by u_{ml} collapse on top of each other and exhibit self-similarity within the mixed layer. This

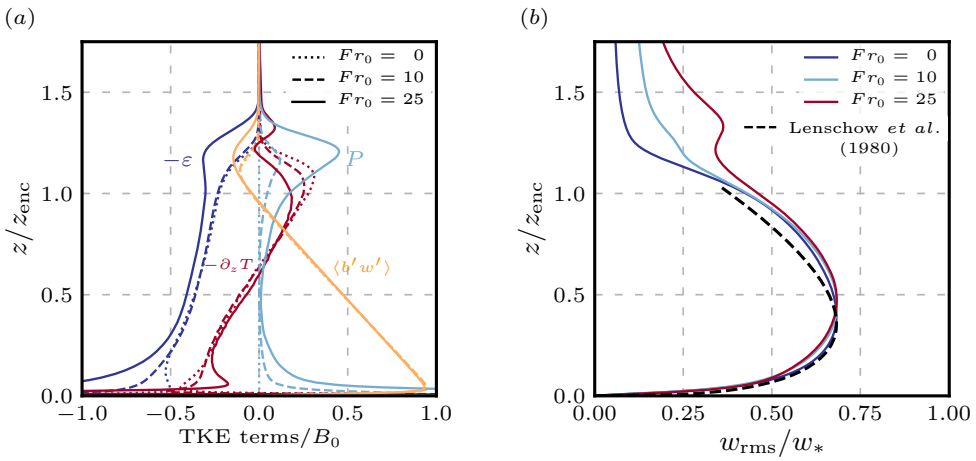

Figure A.7: Vertical profiles of (*a*) the TKE budget and (*b*) the root-mean-square of the vertical velocity at $z_{enc}/L_0 \simeq 30$. Data from case $Fr_0 = 10$ correspond to the transition from a convection-dominated regime in the entrainment zone to a shear-dominated regime, and data from case $Fr_0 = 25$ correspond to a shear-dominated regime [$(\Delta z_i)_s/(\Delta z_i)_c \approx 0.43$ and $(\Delta z_i)_s/(\Delta z_i)_c \approx 1.21$, respectively; see figure A.17 and table A.3].

vertical structure consisting of a well mixed velocity profile in the mixed layer and an elevated wind shear in the entrainment zone is characteristic of the weakly-to-strongly unstable conditions $-z_{enc}/L_{Ob} \gtrsim 4$ considered in this study (Kim et al., 2003; Sorbjan, 2006; Conzemius & Fedorovich, 2006a; Pino & Vilà-Guerau De Arellano, 2008). Hence, the idealized CBL considered in this study also reproduces this main feature of barotropic CBLs in middle latitudes, despite neglecting Coriolis effects.

The corresponding profiles of the kinematic momentum flux

$$\tau_x \equiv \langle u'w' \rangle - \nu \frac{\partial \langle u \rangle}{\partial z} \tag{A.20}$$

are shown in figure A.6(*b*). Horizontal momentum is entrained at the CBL top, transported down across the mixed layer, and finally removed by friction at the surface. The larger magnitude of the momentum flux at the surface compared to the entrainment zone causes the momentum inside the mixed layer to decrease in time (figure A.6*a*). However, the difference between the momentum flux at the surface and at the CBL top decreases in time, which implies a decrease in the time rate-of-change of the mean velocity in the mixed layer.

The TKE budget is shown in figure A.7(*a*). For $Fr_0 = 10$, the strong shear production of TKE near the surface changes the transport and dissipation terms, but those changes remain constrained to a depth below $\simeq 0.25\, z_{enc}$: compared to the shear-free case, the turbulent transport additionally removes energy from very near the surface, below $\simeq 0.05\, z_{enc}$, and deposits it in a thin layer above that region, between $\simeq 0.05\, z_{enc}$ and $\simeq 0.25\, z_{enc}$. The turbulent transport remains unchanged in the CBL interior, between $\simeq 0.25\, z_{enc}$ and $\simeq 0.9\, z_{enc}$. In the entrainment zone, the reduction of turbulent transport approximately compensates the shear production, while the buoyancy flux and viscous dissipation remain practically the same as in shear-free conditions.

For stronger shear conditions such as for $Fr_0 = 25$, the changes near the surface become larger but the turbulent transport still seems to redistribute TKE within a

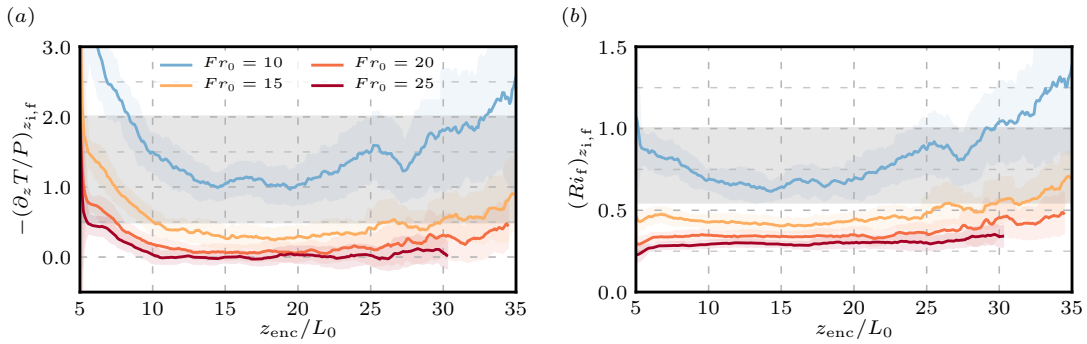

Figure A.8: Temporal evolution of (*a*) the ratio between turbulent transport and shear production of TKE, and (*b*) the flux Richardson number Eq. (A.21), both evaluated at the height of the minimum buoyancy flux. Grey areas indicate the interval where both shear and convection are important, as discussed in §A.6.

region below $\simeq 0.25\, z_{enc}$, which indicates that shear-generated turbulence near the surface is not responsible for the shear enhancement of entrainment (Conzemius & Fedorovich, 2006a; Fedorovich & Conzemius, 2008). In contrast, the changes in the entrainment zone are now more substantial. The turbulent transport develops a local minimum close to zero at the height of maximum shear production, and the magnitudes of the buoyancy flux and dissipation rate increase. We also observe a slight change in the turbulent transport in the CBL interior, a displacement of the curve towards the right. This change indicates that, with respect to the shear-free case, less TKE is being transported from the lower half of the CBL to the upper half, or that shear-generated TKE in the entrainment zone is actually being transported downwards towards the CBL interior. The magnitude of the dissipation rate in the CBL interior increases accordingly.

The variance of the vertical velocity, shown in figure A.7(*b*), further stresses the importance of shear across the entrainment zone compared to the shear near the surface, since the curves for different Froude numbers differ for $z \gtrsim z_{enc}$ but approximately collapse on top of each other for $z \lesssim z_{enc}$. In this region, the parametrisation for w_{rms} proposed by Lenschow et al. (1980) provides accurate estimates for the weakly-to-strongly unstable conditions $-z_{enc}/L_{Ob} \gtrsim 4$ considered here.

A.4 WIND-SHEAR EFFECTS ON THE ENTRAINMENT-ZONE VERTICAL STRUCTURE

We have seen in the previous section that wind-shear effects on entrainment-zone properties become significant when $Fr_0 \gtrsim 10$. This behaviour can be understood by examining the energetics in the entrainment zone. The ratio between the turbulent-transport term and the shear-production term decreases with Fr_0, as shown in figure A.8(*a*), and both terms become comparable at $Fr_0 \simeq 10$. Concomitantly, the flux Richardson number,

$$Ri_f \equiv -\frac{\langle b'w' \rangle}{P}\,, \tag{A.21}$$

becomes less than one and asymptotically approaches $\simeq 0.25 - 0.3$ (figure A.8*b*). This change in energetics with increasing shear has often been documented in previous studies (Pino et al., 2003; Conzemius & Fedorovich, 2006a; Fedorovich & Conzemius,

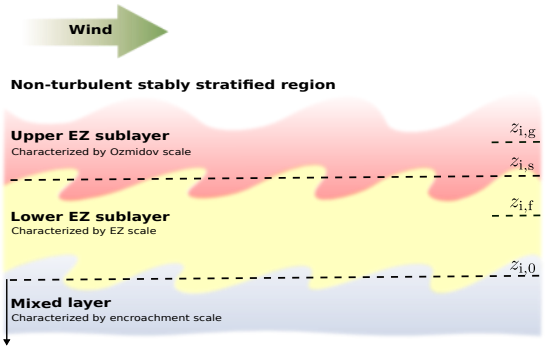

Figure A.9: Sketch of the vertical structure of the CBL-top region. $z_{i,0}$ is the zero-crossing height, $z_{i,f}$ is the height of the minimum buoyancy flux, $z_{i,s}$ marks the transition from the lower EZ sublayer to the upper EZ sublayer, and $z_{i,g}$ is the height of the maximum buoyancy gradient. Red indicates the upper EZ sublayer, yellow indicates the lower EZ sublayer, and blue indicates the mixed layer.

2008; Pino & Vilà-Guerau De Arellano, 2008). In this section, we further rationalize this change in energetics in terms of a change in characteristic length scales in the two-layer structure of the entrainment zone.

A.4.1 *The two-layer structure of the EZ in the shear-free CBL*

The analysis presented in this section is based on previous work on shear-free CBLs by Garcia & Mellado (2014), who described the entrainment zone as a composition of two sublayers (cf. figure A.9). The lower entrainment-zone (EZ) sublayer is located around $z_{i,f}$ and is characterized by a length scale proportional to the CBL depth and by the convective scales derived from the CBL depth and the surface buoyancy flux (Deardorff, 1970). The scaling law for $z_{i,f}$ in shear-free CBLs is (figure A.10*a*)

$$z_{i,f} - z_{enc} \simeq 0.14\, z_{enc}\ . \tag{A.22}$$

In the left-hand side, we measure distances with respect to z_{enc}, the encroachment length scale, because z_{enc} provides an analytical reference height for the position of the entrainment zone, and subtracting this order-of-one quantity allows us to emphasize the local structure. (By scaling law we mean functional relationships between dependent and independent variables that consistent with the dimensional analysis presented in §A.2.2.)

The upper EZ sublayer is centred around $z_{i,g}$, acts as a transition layer between the turbulent region below and the non-turbulent stably stratified region above, and is characterized by local scales. The local length scale is $(L_{Oz})_{z_{i,f}}$, the Ozmidov scale defined in Eq. (A.5) particularized at the height of the minimum buoyancy flux $z_{i,f}$. Since the upper EZ sublayer, which is characterized by $(L_{Oz})_{z_{i,f}}$, is on top of the lower EZ sublayer, which is characterized by z_{enc}, we seek for a scaling law for $z_{i,g}$ of the form

$$z_{i,g} - z_{enc} \simeq \alpha_c z_{enc} + \beta_c (L_{Oz})_{z_{i,f}}\ , \tag{A.23}$$

where α_c and β_c are constants to be determined. This ansatz is supported by figure A.10(*b*). A linear regression to the data for $z_{enc}/L_0 \gtrsim 15$ provides the values

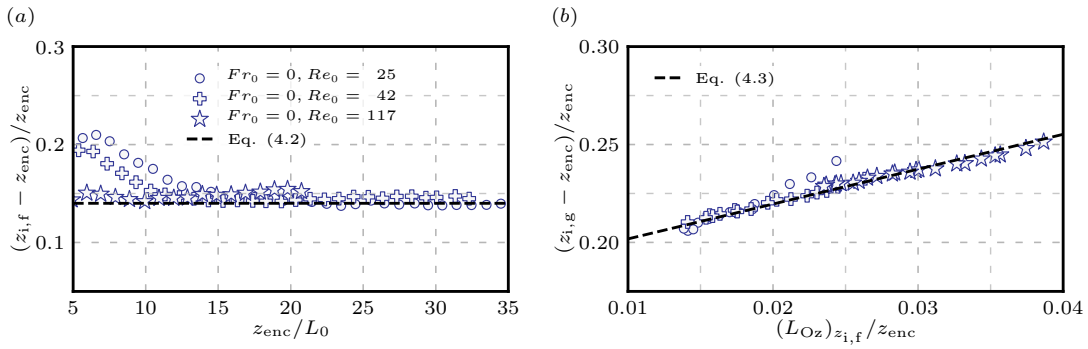

Figure A.10: Scaling of the flux-based and gradient-based CBL depths in the shear-free CBL in terms of the encroachment length, z_{enc}, and the Ozmidov length $(L_{Oz})_{z_{i,f}}$. Symbols indicate the average within an interval $\Delta z_{enc}/L_0 = 2$. In the right panel only data for $z_{enc}/L_0 \gtrsim 15$ is considered.

$\alpha_c = 0.184$ and $\beta_c = 1.78$. Equation (A.23) extends the result $z_{i,g} \propto z_{enc}$ proposed in Garcia & Mellado (2014) with a first-order correction proportional to $(L_{Oz})_{z_{i,f}}$.

We can define

$$z_{i,s} \equiv z_{i,g} - \beta_c (L_{Oz})_{z_{i,f}} \tag{A.24}$$

as a reference height that marks the transition from the lower EZ sublayer to the upper EZ sublayer, i.e., the transition from a region characterized by z_{enc} to a region characterized by $(L_{Oz})_{z_{i,f}}$. The upper boundary of the entrainment zone, and thus the upper boundary of the CBL, can be estimated as $z_{i,g} + 1.78\,(L_{Oz})_{z_{i,f}}$. The thickness of the upper EZ sublayer can be estimated as $2\,(z_{i,g} - z_{i,s}) \simeq 3.56\,(L_{Oz})_{z_{i,f}}$. As later discussed in §A.5, the length scale $(L_{Oz})_{z_{i,f}}$ varies only weakly in time and it is well approximated by $0.45\,L_0$, where L_0 is the reference Ozmidov length.

A.4.2 *The two-layer structure of the EZ in the sheared CBL*

How does the two-layer structure of the entrainment zone change with wind in the free atmosphere? As observed in §A.3, wind in the free atmosphere leads to the formation of a shear layer in the entrainment zone, i.e., a layer of marked variation of the mean velocity between two regions with homogeneous velocity. From the various idealized configurations often employed to study stably stratified sheared turbulence, the stably stratified shear layer seems appropriate to introduce the discussion on the interaction between shear and stratification in the entrainment zone of the CBL, given the coincidence of a localized shear layer with a localized stratified layer (see, e.g., Sherman et al., 1978; Peltier & Caulfield, 2003; Mashayek & Peltier, 2011). The minimum gradient Richardson number

$$Ri_g \equiv \frac{\partial_z \langle b \rangle}{(\partial_z \langle u \rangle)^2} \tag{A.25}$$

is a major variable characterizing the evolution of stably stratified shear layers. If the initial shear layer is thin enough for the Richardson number to be relatively small, Kelvin-Helmholtz-like instabilities will cause an overturning of the stably stratified fluid and a thickening of the shear layer. As the shear layer thickens, overturning the fluid becomes more difficult because the vertical displacement increases whereas

the available kinetic energy, proportional to the squared velocity jump across the shear layer, remains constant. Once the shear layer reaches a critical thickness, or equivalently a critical Richardson number, the available kinetic energy is insufficient to overturn the fluid and turbulence decays. Results show that this critical Richardson number is $1/3 \pm 15\%$, the uncertainty interval representing statistical convergence and the dependence on Prandtl number, Reynolds number, and initial conditions given that the flow is strongly transient (see, e.g., Smyth & Moum, 2000b; Brucker & Sarkar, 2007; Howland et al., 2018).

In the CBL, convection in the mixed layer underneath the entrainment zone is expected to introduce important differences with respect to the stably stratified shear layer. One difference is that turbulence is sustained for a gradient Richardson number significantly larger than $1/3$. This is shown in figure A.11(*a*), which plots Ri_g at the height of the minimum buoyancy flux, which approximately coincides with the height of the minimum Ri_g. The main reason is that convective motions in the CBL make the shear layer locally thinner, which leads to local subcritical Richardson numbers and hence local shear instabilities that maintain a turbulent state (Mahrt & Lenschow, 1976; Kim et al., 2003; Conzemius & Fedorovich, 2007). It is curious that the gradient Richardson number in the entrainment zone approaches the value $1/3$ as shear increases, which is the upper value observed in stably stratified shear layers, although there is a priori no strong argument to expect this agreement given the strong differences between the two cases.

To quantify how wind shear modifies the lower EZ sublayer, specifically, the scaling law Eq. (A.22) for $z_{i,f}$, we introduce the length scale

$$\Delta z_i \equiv \frac{\Delta u}{(\partial_z \langle u \rangle)_{z_{i,f}}} , \tag{A.26}$$

where

$$\Delta u \equiv U_0 - u_{ml} \tag{A.27}$$

is the velocity difference across the entrainment zone, the mixed-layer value u_{ml} being defined by Eq. (A.19). The length scale Δz_i is referred to as vorticity thickness in the literature of stably stratified shear layers. In this work we will refer to Δz_i as EZ scale, because, as shown in the remaining of this section and in §A.5, Δz_i characterizes the lower EZ sublayer (cf. figure A.9). Since the lower EZ sublayer is on top of the mixed layer, which is characterized by z_{enc}, we seek for a scaling law for $z_{i,f}$ that is a linear combination of Δz_i and z_{enc}. Figure A.12(*a*) supports this ansatz, and a linear regression to the data for $z_{enc}/L_0 \gtrsim 15$ yields

$$z_{i,f} - z_{enc} \simeq -0.06\, z_{enc} + 0.8\, \Delta z_i . \tag{A.28}$$

The largest deviation from this linear behaviour occurs for weak wind conditions, $Fr_0 \lesssim 10$, where the turbulent and buoyancy Reynolds numbers in the entrainment zone are smallest in our DNS (see table A.1). However, even in these cases the linear behaviour is approached as the CBL—and accordingly the Reynolds number—grows, the deviation becoming less than 20% for $z_{enc}/L_0 \gtrsim 25$. The data from the case $Fr_0 = 10$ and $Re_0 = 42$ further supports this argument, since the deviation of this data from Eq. (A.28) at $z_{enc}/L_0 = 15$ decreases by $\simeq 33\%$ with respect to the case $Fr_0 = 10$ and $Re_0 = 25$. To avoid this low-Reynolds-number effect from the weak

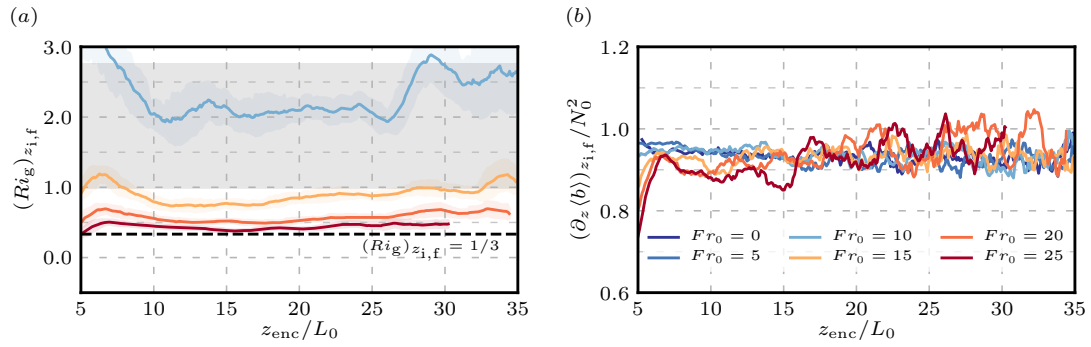

Figure A.11: Temporal evolution of (*a*) the gradient Richardson number Eq. (A.25), and (*b*) the normalized buoyancy gradient, both evaluated at the height of the minimum buoyancy flux. Grey area indicates the interval where both shear and convection are important, as discussed in §A.6.

shear cases, only the data from the cases $Fr_0 > 10$ is considered in the regression. Last, we also verified that the dependence of the regression coefficients on the threshold of z_{enc}/L_0 is small: the coefficients in $z_{i,f} \simeq 0.94\, z_{enc} + 0.8\, \Delta z_i$ vary by $\simeq 2\%$ and $\simeq 5\%$, respectively, as the threshold changes from 15 to 20.

We can easily find the limits of Δz_i for weak wind conditions and strong wind conditions. For a vanishingly small wind, Eq. (A.28) has to recover Eq. (A.22), which implies that we can define

$$(\Delta z_i)_c \equiv 0.25\, z_{enc} \tag{A.29}$$

as the asymptotic limit of Δz_i when Fr_0 tends towards zero. This limit is indicated in figure A.12(*a*) by the symbol "x". We will refer to $(\Delta z_i)_c$ as the convective limit of the EZ scale. To obtain the behaviour of Δz_i for a strong wind, we use Eq. (A.25) to rewrite Eq. (A.26) as $\Delta z_i \simeq \sqrt{(Ri_g)_{z_{i,f}}}\, \Delta u / N_0$, where we have used the result $(\partial_z \langle b \rangle)_{z_{i,f}} \simeq N_0^2$ shown in figure A.11(*b*). Hence, as the wind strength increases and the gradient Richardson number decreases towards $1/3$, Δz_i asymptotically approaches

$$(\Delta z_i)_s \equiv \sqrt{1/3}\, \frac{\Delta u}{N_0}\,. \tag{A.30}$$

We will refer to $(\Delta z_i)_s$ as the shear limit of the EZ scale. When convection dominates in the entrainment zone, $(\Delta z_i)_s$ is smaller than $(\Delta z_i)_c$, and the latter characterizes the lower EZ sublayer. As the wind intensity U_0 increases, $(\Delta z_i)_s$ increases and eventually becomes comparable to $(\Delta z_i)_c$, at which point $(\Delta z_i)_s$ starts to characterize the lower EZ sublayer. The weakly-to-strongly unstable conditions $-z_{enc}/L_{Ob} \gtrsim 4$ considered in this paper correspond to $(\Delta z_i)_s/(\Delta z_i)_c \lesssim 1.5$. We will further explore in §A.5 the capability of the ratio $(\Delta z_i)_s/(\Delta z_i)_c$ to characterize shear effects on entrainment-zone properties.

To characterize the upper EZ sublayer, we propose the following scaling law for the height of the maximum buoyancy gradient:

$$z_{i,g} - z_{i,f} \simeq \gamma_s \Delta z_i + \beta_s (L_{Oz})_{z_{i,f}}\,. \tag{A.31}$$

This ansatz is motivated by Eq. (A.23), which indicates that, for shear-free conditions, the position of the upper EZ sublayer with respect to the lower EZ sublayer can be

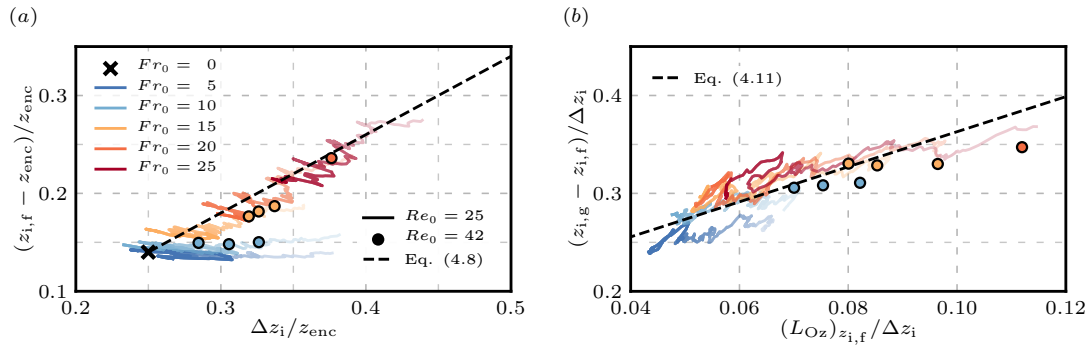

Figure A.12: Scaling of the flux-based and gradient-based CBL depths in the sheared CBL in terms of the encroachment length, z_{enc}, the EZ scale, Δz_i, and the Ozmidov length $(L_{Oz})_{z_{i,f}}$. Light colours indicate low values of z_{enc}/L_0, and dark colours indicate higher values of z_{enc}/L_0.

characterized by a linear combination of the scales characterizing the lower and upper sublayers. Figure A.12(b) supports this ansatz, providing the coefficients $\gamma_s \simeq 0.184$ and $\beta_s \simeq 1.78$. The linear behaviour is also supported by the data corresponding to higher Reynolds-number simulations ($Re_0 = 42$), although longer simulations would help to further validate Eq. (A.31). For vanishingly small Fr_0, substituting Δz_i by $(\Delta z_i)_c$ in equations Eq. (A.28) and Eq. (A.31) recovers the shear-free result Eq. (A.23), which indicates that changes in the upper EZ sublayer due to wind shear are captured by the changes in $(L_{Oz})_{z_{i,f}}$, the Ozmidov scale at $z_{i,f}$. This further supports this length as a characteristic scale of the upper EZ sublayer. As the turbulence intensity in the lower EZ sublayer increases with respect to shear-free conditions, the lower EZ sublayer broadens and so does the upper EZ sublayer.

In summary, the entrainment zone in sheared CBLs can also be described as a composition of two sublayers, the lower EZ sublayer around the height of the minimum buoyancy flux, and the upper EZ sublayer around the height of the maximum buoyancy gradient. The difference from the shear-free case is that wind introduces a local scale Δz_i in the characterization of the entrainment zone, in addition to the encroachment scale z_{enc} and the Ozmidov scale $(L_{Oz})_{z_{i,f}}$. The scaling laws for the reference heights are:

$$z_{i,f} \simeq 0.94\, z_{enc} + 0.8\, \Delta z_i \ , \tag{A.32a}$$

$$z_{i,s} \simeq 0.94\, z_{enc} + 1.0\, \Delta z_i \ , \tag{A.32b}$$

$$z_{i,g} \simeq 0.94\, z_{enc} + 1.0\, \Delta z_i + 1.78\, (L_{Oz})_{z_{i,f}} \ . \tag{A.32c}$$

These equations recover the shear-free results when Δz_i is substituted by $(\Delta z_i)_c$. The term $0.94\, z_{enc}$ can be identified with $z_{i,0}$, the height of zero-crossing of the buoyancy flux, which marks the base of the entrainment zone. Hence, the encroachment length scale provides a measure of the CBL depth, in particular the mixed-layer depth, which justifies referring to it as encroachment CBL depth. The height $z_{i,s}$ marks the transition from the lower EZ sublayer to the upper EZ sublayer, i.e., the transition from a region characterized by Δz_i to a region characterized by $(L_{Oz})_{z_{i,f}}$. The height $z_{i,g} + 1.78\, (L_{Oz})_{z_{i,f}}$ provides an upper boundary of the entrainment zone and of the whole CBL. Such an upper boundary is sometimes defined based on a threshold in the buoyancy-flux profile as the buoyancy flux increases from its minimum in

the entrainment zone towards zero in the free atmosphere. However, such a definition of an upper boundary is very sensitive to the threshold chosen, the statistical convergence, and the low-Reynolds-number effects (or the effect of subgrid-scale models and numerical artefacts in large-eddy simulation). For this reason, we follow Garcia & Mellado (2014) and define the upper boundary of the CBL as the upper boundary of the upper EZ sublayer $z_{i,g} + 1.78\,(L_{Oz})_{z_{i,f}}$. For the current study, this boundary approximately coincides with the height where the buoyancy flux is 15% of the minimum.

A.5 QUANTIFYING WIND-SHEAR EFFECTS ON ENTRAINMENT-ZONE PROPERTIES

Normalized entrainment-zone properties in the barotropic CBLs considered in this study depend on the Froude number Fr_0 and on the normalized CBL depth z_{enc}/L_0. The analysis of the entrainment-zone structure presented in §A.4, however, indicates that the variable $\Delta z_i/z_{enc}$ embeds both dependencies and fully describes key properties such as $z_{i,f}$. This reduction from two independent variables to one independent variable can help simplify the parametrisation of wind-shear effects in boundary-layer schemes of atmospheric models. Therefore, we further investigate in this section the capability of the EZ scale, Δz_i, to characterize entrainment-zone properties. Moreover, we will obtain a relationship between Δz_i and the velocity increment across the entrainment zone, Δu, so that the latter can be used as independent variable. The motivation for changing the variable Δz_i by the variable Δu is that Δz_i is locally defined in terms of a gradient [cf. Eq. (A.26)] whereas Δu is defined as the velocity difference between two regions of homogeneous velocity [cf. Eq. (A.27)], and thus Δu is less sensitive to measurements and numerical uncertainties.

A.5.1 *Scaling law for the EZ scale*

To derive a scaling law for Δz_i, we consider the integral analysis of the TKE balance equation discussed in §A.2.4 but restricted to the entrainment zone:

$$I_t^{EZ} = I_T^{EZ} + I_P^{EZ} + I_{bw}^{EZ} - I_\varepsilon^{EZ}\,. \tag{A.33}$$

Henceforth, the superscript EZ stands for entrainment zone and indicates that the corresponding integral is calculated in the interval $z_{i,0} < z < z_\infty$. To better quantify shear effects, we subtract the balance equation for the shear-free CBL from the balance equation for the sheared CBL, and we focus on the cases $Fr_0 \gtrsim 15$ because wind-shear effects on entrainment-zone properties are small for smaller Froude numbers.

The shear enhancement of the accumulation term in the left-hand side of Eq. (A.33) is less than $10-20\%$ of the shear-production term for $z_{enc}/L_0 \gtrsim 15$ (cf. figure A.13*a*) and hence negligible to leading order, which indicates a quasi-steady regime in the entrainment zone. The transport term can be written as

$$I_T^{EZ} = T_{z_{i,0}} - T_{z_\infty}\,, \tag{A.34}$$

i.e., the difference between the transport of kinetic energy from the mixed layer into the entrainment zone and the transport of kinetic energy from the entrainment zone into the free atmosphere. As seen in figure A.13(*b*), shear reduces the energy that is

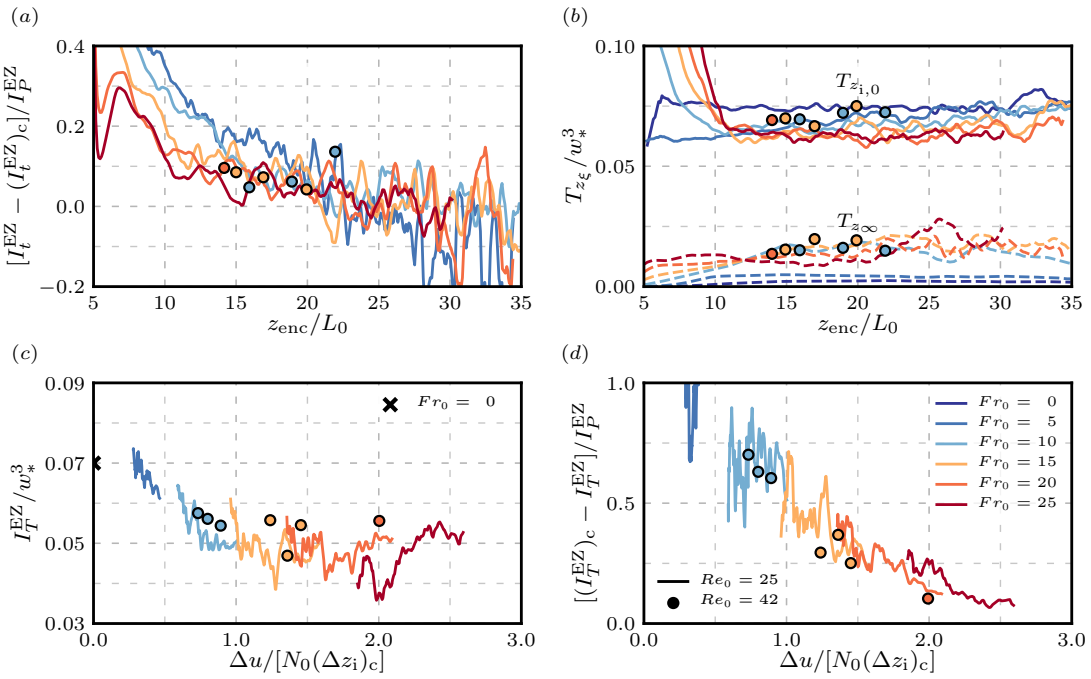

Figure A.13: Temporal evolution of the contributions from the accumulation term, I_t^{EZ}, and the turbulent-transport term, $I_T^{EZ} = T_{z_{i,0}} - T_{z_\infty}$, to the TKE budget equation (A.33). The subscript c indicates the convective limit $Fr_0 = 0$.

transported into the entrainment zone from the mixed layer and shear increases the energy that is radiated out into the free atmosphere by gravity waves, so that I_T^{EZ} decreases with increasing shear. For weak shear conditions $Fr_0 = 5$, the reduction of energy transported into the entrainment zone is larger than the enhancement of energy drained at the top (cf. figure A.13*b*), which suggests that shear sheltering (Hunt & Durbin, 1999) dominates over shear enhancement of gravity-wave radiation (Schröter, 2018). This effect on the transport term for weak shear conditions, however, is not observed in the entrainment flux and viscous dissipation rate, which remain practically unchanged for $Fr_0 \lesssim 10$ once the CBL is inside the quasi-steady regime (see also figure A.5*a* and A.7*a*). We also see that the shear reduction of I_T^{EZ} saturates and asymptotically approaches $\simeq 0.02\, w_*^3$ with increasing shear, where $w_*^3 = B_0 z_{enc}$. This saturation is more clearly shown in figure A.13(*c*), where we plot the flux difference across the entrainment zone as a function of the variable $\Delta u/[N_0(\Delta z_i)_c]$. (Using this independent variable is motivated by the results presented below.) Hence, as the shear production increases, the relative contribution of the turbulent transport in Eq. (A.33) decreases (cf. figure A.13*d*). For instance, the relative contribution is $\simeq 0.35\, I_P^{EZ}$ for $Fr_0 = 15$ and $\simeq 0.15\, I_P^{EZ}$ for $Fr_0 = 25$. We also observe that data from cases with $Re_0 = 42$ coincides with data from cases $Re_0 = 25$ within the statistical convergence reached in our simulations. Although the relative contribution of I_T^{EZ} is arguably non-negligible for $Fr_0 = 15$, the shear effect on entrainment-zone properties is still moderate for that Froude number, and therefore we neglect the turbulent transport terms in Eq. (A.33) as a first approximation; this approximation is validated below.

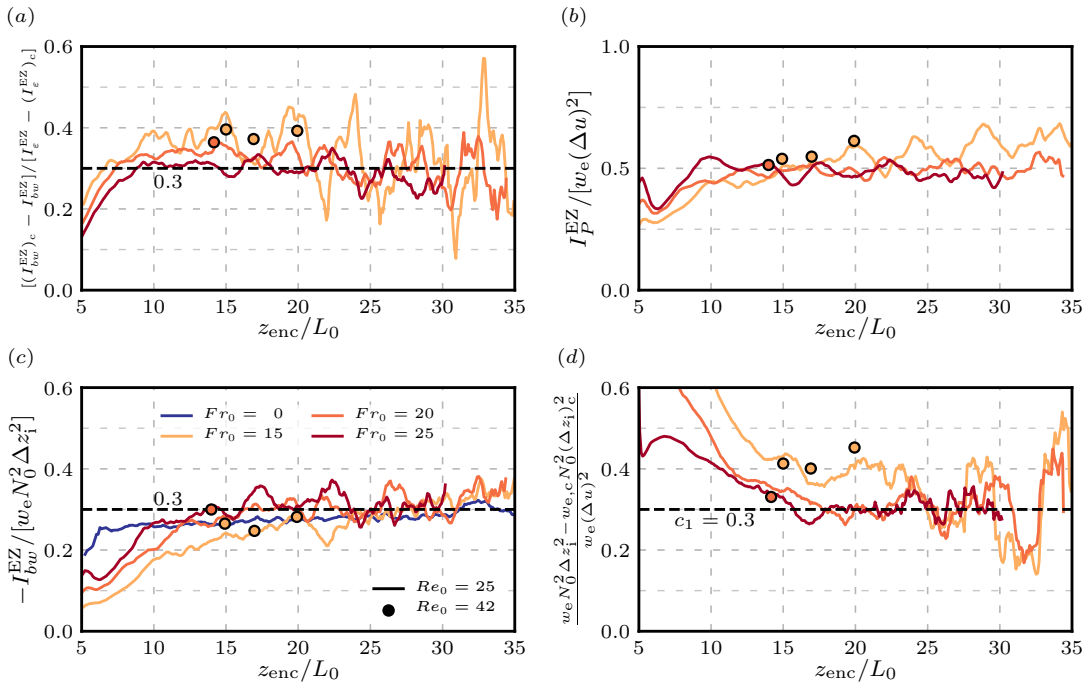

Figure A.14: Scaling laws for the dominant terms in the TKE budget equation (A.33) as a function of the mean entrainment velocity, w_e, the velocity jump across the entrainment zone, Δu, the buoyancy stratification of the free atmosphere, N_0^2, and the EZ scale, Δz_i.

Shear effects on the viscous dissipation rate and the buoyancy flux are negligible for $Fr_0 \lesssim 10$ once the CBL is inside the quasi-steady regime. For $Fr_0 > 10$, figure A.14(a) demonstrates that they are commensurate with each other,

$$-[I_{bw}^{EZ} - (I_{bw}^{EZ})_c] \sim I_\varepsilon^{EZ} - (I_\varepsilon^{EZ})_c \,, \tag{A.35}$$

which indicates that energy destruction by viscous dissipation and by conversion to potential energy increase in a constant ratio independently of the shear strength in the equilibrium entrainment regime of the sheared CBL. The subscript c indicates the convective limit $Fr_0 = 0$. All these considerations, namely, using Eq. (A.35) and neglecting the accumulation term and the turbulent transport term in Eq. (A.33), yield the relationship

$$(I_{bw}^{EZ})_c - I_{bw}^{EZ} \sim I_P^{EZ} \,. \tag{A.36}$$

This relationship implies that the entrainment enhancement in sheared CBLs is due to the additional turbulence kinetic energy generated by the wind shear in the entrainment zone.

Here, we proceed further and use the structure analysis presented in §A.4 to estimate the terms in Eq. (A.36) and thereby obtain a closed equation for the unknown Δz_i. First, neglecting the thickness of the upper EZ sublayer, the integration intervals in Eq. (A.36) are well approximated by Δz_i. Second, the velocity gradient can be scaled by its maximum value, $\Delta u/\Delta z_i$ [cf. Eq. (A.26)]. Last, to estimate the fluxes of buoyancy and momentum, we use the entrainment-rate equations, which are obtained by integrating the evolution equations for the mean buoyancy and mean velocity from

a height $z_{i,f}$ upwards (see appendix AA). The entrainment-rate equations provide the scalings $-\langle b'w'\rangle_{z_{i,f}} \sim w_e \Delta b$ and $-\langle u'w'\rangle_{z_{i,f}} \sim w_e \Delta u$. In these expressions,

$$w_e \equiv \frac{dz_{i,f}}{dt} \tag{A.37}$$

is the mean entrainment velocity, $\Delta b \equiv N_0^2 \Delta z_i$ is a measure of the buoyancy increment across the entrainment zone, and the velocity jump Δu is defined by Eq. (A.27). All these considerations indicate that the integrals on the left-hand side and right-hand side of Eq. (A.36) are scaled by $w_e \Delta b \Delta z_i$ and by $w_e (\Delta u)^2$, respectively, which is confirmed by figures A.14(b,c). Substituting these scaling laws into Eq. (A.36) yields

$$w_e N_0^2 (\Delta z_i)^2 - w_{e,c} N_0^2 (\Delta z_i)_c^2 \simeq c_1 w_e (\Delta u)^2 \,. \tag{A.38}$$

Figure A.14(d) supports this ansatz and shows that $c_1 \simeq 0.3$. This coefficient can be interpreted as a modified Richardson number where the shear enhancement of the buoyancy flux is considered instead of the total buoyancy flux as in Eq. (A.21). This interpretation indicates that the values $(Ri_f)_{z_{i,f}} \simeq 1$ observed when shear effects become relevant are significantly larger than the values $0.25 - 0.3$ reported in marginally stable stratified shear flows becasuse of the buoyancy flux caused by the turbulence in the CBL interior.

To use Eq. (A.38) to obtain a closed equation for the EZ scale, Δz_i, we need to consider the mean entrainment velocity, w_e. The shear enhancement of mean entrainment velocity, $w_e - w_{e,c}$, can be split into two contributions by factorizing $z_{i,f} - (z_{i,f})_c$ as the product of $[z_{i,f} - (z_{i,f})_c]/z_{enc}$ and z_{enc}, which yields

$$w_e - w_{e,c} = \left[\frac{z_{i,f} - (z_{i,f})_c}{z_{enc}} + z_{enc} \frac{d}{dz_{enc}} \frac{z_{i,f} - (z_{i,f})_c}{z_{enc}} \right] w_{enc} \,, \tag{A.39}$$

We have introduced the mean encroachment velocity $w_{enc} \equiv d_t z_{enc}$, which can be written as $w_{enc} \simeq N_0 L_0^2 / z_{enc}$ by using Eq. (A.10). The first contribution is positive and represents a quasi-steady contribution to the shear enhancement of the entrainment velocity due to penetrative convection of a CBL that is deeper than in shear-free conditions. The second contribution is negative and represents the unsteady contribution due to the reduction of shear effects in time as the CBL grows and approaches the shear-free limit. As inferred from table A.1, the ratio $[z_{i,f} - (z_{i,f})_c]/z_{enc}$ for $Fr_0 = 25$ changes less than 40% when z_{enc} changes by an order of one. Since $[z_{i,f} - (z_{i,f})_c]/z_{enc}$ is on the order of 0.15, neglecting the second term implies an error of $\simeq 5\%$ in the mean entrainment velocity w_e, which suggests to neglect this unsteady contribution as a first approximation. With this approximation, the mean entrainment velocity can be written as

$$w_e \simeq \frac{z_{i,f}}{z_{enc}} w_{enc} \,. \tag{A.40}$$

Substituting Eq. (A.40) into Eq. (A.38), using the relationship $w_{enc} \simeq N_0 L_0^2 / z_{enc}$, and using Eq. (A.32a) to express $z_{i,f}$ in terms of z_{enc} and Δz_i, we can derive a cubic equation for $\Delta z_i / z_{enc}$. This cubic equation, however, can be easily approximated by a simpler quadratic equation. To this aim, we rewrite Eq. (A.38) as

$$w_e \left[(\Delta z_i)^2 - (\Delta z_i)_c^2 \right] + (w_e - w_{e,c}) (\Delta z_i)_c^2 \simeq 0.3\, w_e N_0^{-2} (\Delta u)^2 \,. \tag{A.41}$$

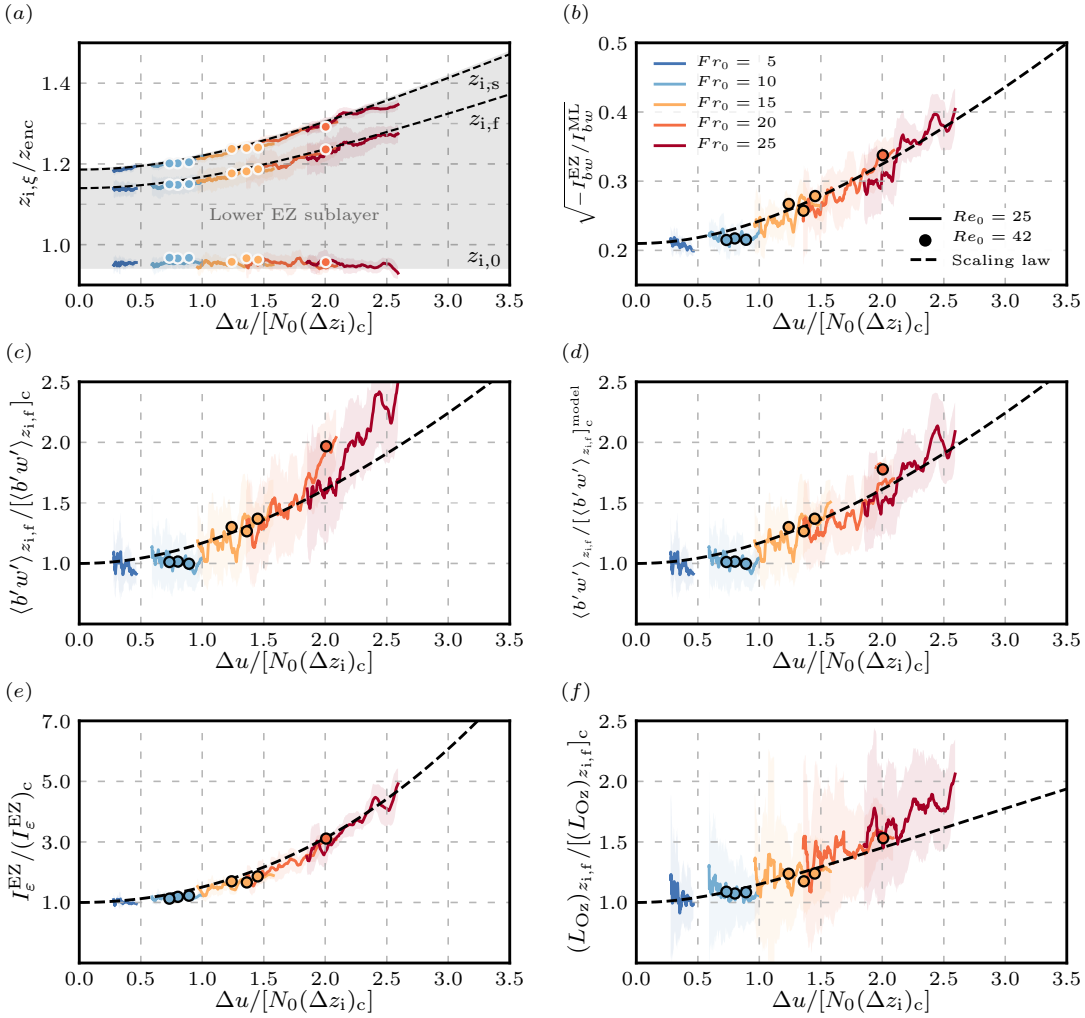

Figure A.15: Verification with DNS data (coloured lines) of the scaling laws for the entrainment-zone properties derived in §A.5 (dashed lines): (*a*) reference heights, (*b*, *c*, *d*) buoyancy-flux properties, (*e*) viscous dissipation rate, and (*f*) Ozmidov length.

Approximating w_e using Eq. (A.40), we can show that the ratio of the second to the first term satisfies

$$\frac{(w_e - w_{e,c})(\Delta z_i)_c^2}{w_e\,[(\Delta z_i)^2 - (\Delta z_i)_c^2]} \simeq \frac{0.8\,(\Delta z_i)_c^2}{[\Delta z_i + (\Delta z_i)_c]\,(0.94\,z_{enc} + 0.8\,\Delta z_i)} \lesssim 0.09\,, \tag{A.42}$$

where the upper bound is obtained by using the inequality $(\Delta z_i)_c < \Delta z_i$ and the definition $(\Delta z_i)_c \equiv 0.25\,z_{enc}$. This estimate is confirmed by the data, which shows that the ratio of the second to the first term in Eq. (A.41) is less than 0.04 (not shown). Hence, we can neglect the second term in Eq. (A.41), which leads to

$$\frac{\Delta z_i}{(\Delta z_i)_c} = \left[1 + 0.3\left(\frac{\Delta u}{N_0(\Delta z_i)_c}\right)^2\right]^{1/2} \tag{A.43}$$

as an explicit expression for the EZ scale in terms of the controlling parameters and the velocity increment across the entrainment zone. The proposed scaling law for Δz_i is supported in figure A.15(*a*), where the reference heights $z_{i,f}$ and $z_{i,s}$ calculated by Eq. (A.32a) and Eq. (A.32b) using Δz_i obtained from Eq. (A.43) agree with the DNS data. The small deviation between the scaling laws and the DNS data for $Fr_0 = 10$ and 15 in figure A.15(*a*) is due to the neglect of the turbulent flux of TKE in Eq. (A.33), but, as already indicated before, the shear effects in those cases are still relatively small. Comparing the data from cases $Re_0 = 25$ and cases $Re_0 = 42$ shows that the Reynolds-number dependence of these scaling laws is small, less than the achieved statistical convergence. Substituting the expression for $z_{i,f}$, Eq. (A.32a), into Eq. (A.40), we obtain

$$\frac{w_e}{w_{e,c}} \simeq 0.82 + 0.18\frac{\Delta z_i}{(\Delta z_i)_c} \tag{A.44}$$

as an explicit expression for the mean entrainment velocity in the barotropic CBLs considered in this study. The convective limits are $w_{e,c} \simeq 1.14\,N_0 L_0^2/z_{enc}$, from Eq. (A.37) and Eq. (A.32a), and $(\Delta z_i)_c \equiv 0.25\,z_{enc}$, from Eq. (A.29).

A.5.2 *Scaling law for buoyancy-flux properties*

Besides $z_{i,f}$ and Δz_i, other properties that are relevant to characterize the entrainment zone are the ratio between the minimum turbulent buoyancy flux and the surface buoyancy flux, $-\langle b'w'\rangle_{z_{i,f}}/B_0$, referred to as the entrainment-flux ratio (Pino et al., 2003; Conzemius & Fedorovich, 2006a; Pino et al., 2006), and the square root of the ratio between the negative and positive areas of the turbulent buoyancy flux, $(-I_{bw}^{EZ}/I_{bw}^{ML})^{1/2}$, where the superscript ML stands for the mixed layer and indicates that the corresponding integral is calculated in the interval $0 < z < z_{i,0}$ (Conzemius & Fedorovich, 2006a).

An estimate for $(-I_{bw}^{EZ}/I_{bw}^{ML})^{1/2}$ can be obtained as follows. From the relationship $-I_{bw}^{EZ} \sim w_e \Delta b \Delta z_i = w_e N_0^2 \Delta z_i^2$ used before, estimating the corresponding coefficient of proportionality as 0.3 according to figure A.14(*c*), and using the approximation $I_{bw}^{ML} \simeq 0.5\,B_0 z_{enc}$ based on the linear variation of the turbulent buoyancy flux between the surface and $z_{i,0}$ (see figure A.7*a*), the area ratio can be expressed as

$$\left[\frac{-I_{bw}^{EZ}}{I_{bw}^{ML}}\right]^{1/2} \simeq 0.21\frac{\Delta z_i}{(\Delta z_i)_c}\left[0.82 + 0.18\frac{\Delta z_i}{(\Delta z_i)_c}\right]^{1/2}, \tag{A.45}$$

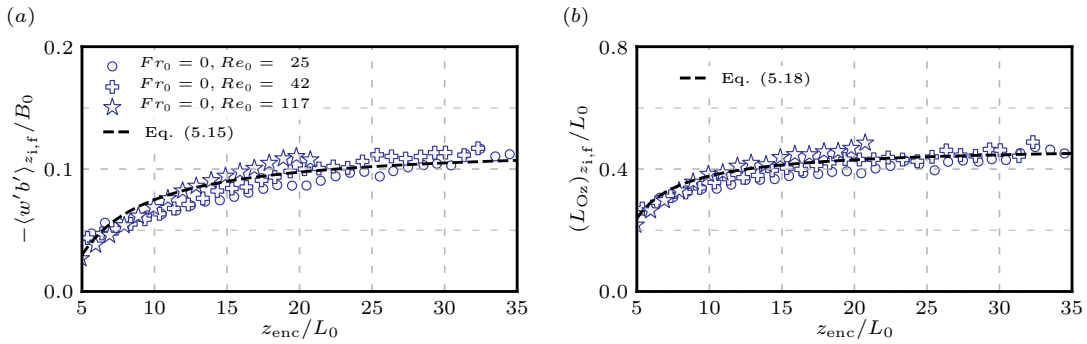

Figure A.16: Temporal evolution of (*a*) the entrainment-flux ratio, $\langle b'w'\rangle_{z_{i,f}}/B_0$; (*b*) the normalized Ozmidov length particularized at the height of the minimum buoyancy flux, $(L_{Oz})_{z_{i,f}}/L_0$, in the shear-free CBL. Symbols indicate the average within an interval $\Delta z_{enc}/L_0 = 2$.

where we have used Eq. (A.44) to express the result in terms of $\Delta z_i/(\Delta z_i)_c$. This scaling law is supported by the DNS data in figure A.15(*b*). Consistent with previous work, we obtain a value $\simeq 0.2$ in the shear-free limit (Conzemius & Fedorovich, 2006a).

An estimate for $-\langle b'w'\rangle_{z_{i,f}}/B_0$ can be obtained in a similar way. From the scaling law $-\langle b'w'\rangle_{z_{i,f}} \sim w_e\Delta b = w_e N_0^2 \Delta z_i$ employed before and using Eq. (A.44), we obtain

$$\frac{\langle b'w'\rangle_{z_{i,f}}}{[\langle b'w'\rangle_{z_{i,f}}]_c} \simeq \frac{\Delta z_i}{(\Delta z_i)_c}\frac{w_e}{w_{e,c}} \simeq \frac{\Delta z_i}{(\Delta z_i)_c}\left[0.82 + 0.18\frac{\Delta z_i}{(\Delta z_i)_c}\right]. \tag{A.46}$$

This scaling law is supported by the DNS data in figure A.15(*c*). The deviation of $\simeq 20\%$ for strong wind conditions is a Reynolds-number effect. For the cases with $Re_0 = 25$, the turbulent Reynolds number at $z = z_{i,f}$, $(Re_t)_{z_{i,f}}$, is approximately four times larger for cases $Fr_0 = 20$ and $Fr_0 = 25$ than for case $Fr_0 = 0$ (1600 compared to 400, as seen in table A.1). A similar variation in Re_t is observed between cases $Re_0 = 25$ and $Re_0 = 117$ in shear-free conditions, and the entrainment-flux ratio in shear-free conditions, which is used to normalize the entrainment-flux ratio in sheared conditions, varies about 30% over this interval of Reynolds number (see figure A.16*a*). Normalizing the minimum buoyancy flux for cases $Fr_0 = 20$ and $Fr_0 = 25$ with the approximation

$$-\frac{[\langle b'w'\rangle_{z_{i,f}}]_c^{\text{model}}}{B_0} \simeq 0.12 - 0.45\left(\frac{z_{enc}}{L_0}\right)^{-1}, \tag{A.47}$$

which is derived in Garcia & Mellado (2014) from data at $Re_t \simeq 1600$ and hence turbulent Reynolds numbers that are comparable to the ones here in the strong shear conditions, Eq. (A.46) represents better the DNS data, as shown in figure A.15(*d*).

The scaling laws Eq. (A.45) and Eq. (A.46) do not feature a reduction of entrainment flux for weak shear conditions. The slight decrease observed in figures A.15(*c*, *d*) for the case $Fr_0 = 5$ near $\Delta u/[N_0(\Delta z_i)_c] = 0.5$ is smaller than the statistical convergence of our data, as indicated in that figure by the shadow region. Besides, those values correspond to an early stage of the quasi-steady regime, and is not observed in the case $Fr_0 = 10$ near $\Delta u/[N_0(\Delta z_i)_c] = 0.5$, where the CBL is further into the quasi-steady regime and the local turbulent Reynolds number is six times larger. We recall that, for weak shear conditions, the analysis of the TKE budget equation presented in §A.5.2 indicates that the shear production of TKE is mostly used to modify the

transport of TKE in and out of the entrainment zone without significantly affecting the buoyancy flux and the dissipation rate, at least, to the accuracy achieved by our simulations.

A.5.3 *Scaling law for the Ozmidov length*

To reconstruct the complete entrainment-zone structure using Eq. (A.32) one needs a scaling law for the Ozmidov length $(L_{Oz})_{z_{i,f}}$ in addition to the scaling law Eq. (A.43) for the EZ scale Δz_i. From the definition of the Ozmidov length Eq. (A.5), this implies obtaining a scaling law for the viscous dissipation rate at the height of minimum buoyancy flux. Such scaling law can be obtained from the relationship Eq. (A.35), which states that changes in the dissipation rate relative to the shear-free limit are well scaled by the changes in the buoyancy flux, the constant of proportionality being $\simeq 0.3$, as observed in figure A.14(*a*). Hence, we can write

$$\frac{I_\varepsilon^{EZ}}{(I_\varepsilon^{EZ})_c} \simeq 1 + c_2 \left[\frac{I_{bw}^{EZ}}{(I_{bw}^{EZ})_c} - 1 \right] \simeq 1 + c_2 \left[\frac{\Delta z_i^2}{(\Delta z_i)_c^2} \frac{w_e}{w_{e,c}} - 1 \right] , \tag{A.48}$$

where the proportionality constant is $c_2 \equiv -(I_{bw}^{EZ})_c / [0.3\,(I_\varepsilon^{EZ})_c]$ and we have used the approximation $-I_{bw}^{EZ} \simeq 0.3\, w_e N_0^2 \Delta z_i^2$ employed before to derive Eq. (A.45). The ratio of mean entrainment velocities in the equation above is provided by Eq. (A.44). To evaluate the proportionality constant c_2, we know that $-(I_{bw}^{EZ})_c \simeq 0.022\, B_0 z_{enc}$ by substituting $\Delta z_i = (\Delta z_i)_c$ into Eq. (A.45), and we know that $(I_\varepsilon^{EZ})_c \simeq (I_T^{EZ} + I_{bw}^{EZ})_c$ from the TKE budget equation for shear-free conditions, which yields $(I_\varepsilon^{EZ})_c \simeq 0.048\, B_0 z_{enc}$ when we use the estimate $(I_T^{EZ})_c \simeq 0.07\, B_0 z_{enc}$ from figure A.13(*c*). The value that we obtain is $c_2 \simeq 1.53$ and the resulting scaling law Eq. (A.48) is validated with the DNS data in figure A.15(*e*).

To find the scaling law for the Ozmidov length at $z_{i,f}$, we define a characteristic scale for the dissipation rate in the entrainment zone as $I_\varepsilon^{EZ}/\Delta z_i$. From definition Eq. (A.5), we obtain the following ratio of the Ozmidov length between sheared conditions and shear-free conditions

$$\frac{(L_{Oz})_{z_{i,f}}}{[(L_{Oz})_{z_{i,f}}]_c} \simeq \left[\frac{(\Delta z_i)_c}{\Delta z_i} \frac{I_\varepsilon^{EZ}}{(I_\varepsilon^{EZ})_c} \right]^{1/2} \simeq \left\{ \frac{(\Delta z_i)_c}{\Delta z_i} \left[1.53 \frac{\Delta z_i^2}{(\Delta z_i)_c^2} \frac{w_e}{w_{e,c}} - 0.53 \right] \right\}^{1/2} , \tag{A.49}$$

where the ratio of mean entrainment velocities is given by Eq. (A.44) as a function $\Delta z_i/(\Delta z_i)_c$. This scaling law is supported in figure A.15(*f*). The deviation of $\simeq 20\%$ for strong wind conditions is a Reynolds-number effect, which, as explained in §A.5.2, arises because the Ozmidov length in sheared conditions is normalized by the shear-free value, and the latter varies about 15% within the interval of turbulent Reynolds numbers in the entrainment zone spanned between case $Fr_0 = 0$ and case $Fr_0 = 25$ (cf. figure A.16*b*). As a first approximation, one can consider

$$\frac{[(L_{Oz})_{z_{i,f}}]_c}{L_0} \simeq \left[0.23 - 0.85 \left(\frac{z_{enc}}{L_0} \right)^{-1} \right]^{1/2} , \tag{A.50}$$

which is obtained from definition Eq. (A.5), from Eq. (A.47), and from $(\partial_z \langle b \rangle)_{z_{i,f}} \simeq 0.9\, N_0^2$ (see figure A.11*b*) and the observation that $(-\varepsilon/\langle b'w' \rangle)_{z_{i,f}} \simeq 1.6$ according to figure A.7(*a*). Normalizing the Ozmidov scale in sheared CBLs with the shear-free limit provided by Eq. (A.50) represents better the DNS data (not shown).

A.6 DISCUSSION

The scaling laws Eq. (A.32) for the reference heights, Eq. (A.43) for the EZ scale, Eq. (A.49) for the Ozmidov length, and Eq. (A.46) for the entrainment-flux ratio help characterize the two-layer structure of the entrainment zone in the equilibrium (quasi-steady) entrainment regime of a barotropic CBL penetrating into a linearly stratified atmosphere. We still miss a relationship between the velocity increment Δu, the control parameter Fr_0, and the independent variable z_{enc}/L_0. This relationship could be obtained from the integral analysis of the momentum equation between $z = 0$ and $z = z_{i,f}$, but such analysis requires the study of the friction velocity and its dependence on surface properties, e.g., on the Reynolds number for an aerodynamically smooth wall or on the roughness properties for an aerodynamically rough wall, and such a study deserves its own paper. Nonetheless, the proposed characterization of entrainment-zone properties in terms of $\Delta u/(N_0 L_0)$ and z_{enc}/L_0 should remain approximately valid for different surface properties because, as reviewed in the introduction and shown in §A.3, the shear near the surface affects entrainment mainly indirectly through the change of Δu. Besides, scaling laws in terms of Δu are convenient because Δu might be more easily measured and simulated than local properties in the entrainment zone, such as Δz_i. The reason is that the mean velocity profile is approximately height-invariant inside the mixed layer and inside the free atmosphere, and hence Δu is insensitive to the exact location where those two velocity values are calculated.

The independent variable $\Delta u/[N_0(\Delta z_i)_c]$ can be interpreted in various ways. From Eq. (A.30), the definition of $(\Delta z_i)_s$, we can write $\Delta u/[N_0(\Delta z_i)_c] = \sqrt{3}\,(\Delta z_i)_s/(\Delta z_i)_c$ and use $(\Delta z_i)_s/(\Delta z_i)_c$ as the independent variable, which can be interpreted as the ratio between the shear limit and the convective limit of the EZ scale. Under strongly unstable conditions (weak wind), $(\Delta z_i)_s$ is smaller than $(\Delta z_i)_c$, and the latter characterizes the lower EZ sublayer. For weakly unstable conditions (strong wind), $(\Delta z_i)_s$ is comparable to $(\Delta z_i)_c$ and characterizes the lower EZ sublayer.

A second interpretation of $\Delta u/[N_0(\Delta z_i)_c]$ can be obtained by using Eq. (A.29), the definition of $(\Delta z_i)_c$, to write $\Delta u/[N_0(\Delta z_i)_c] = 4\,\Delta u/(N_0 z_{enc})$. We can then use

$$Ri_b \equiv N_0^2 z_{enc}^2/(\Delta u)^2 \tag{A.51}$$

as the independent variable, which can be interpreted as a bulk Richardson number that compares the energy necessary for a fluid particle to penetrate a distance z_{enc} into the free atmosphere, and the kinetic energy associated with the velocity difference across the entrainment zone.

This definition of a bulk Richardson number differs from the definition $\widetilde{Ri}_b \equiv \widetilde{\Delta b}\, z_{i,f}/\Delta u^2$ often used in previous analysis (Pino et al., 2003; Conzemius & Fedorovich, 2006b, 2007), where $\widetilde{\Delta b}$ represents a measure of the buoyancy increment across the entrainment zone and it is not necessarily equal to the definition $\Delta b \equiv N_0^2 \Delta z_i$ used here. These previous studies commonly result in an entrainment-flux ratio proportional to $(1 - a\,\widetilde{Ri}_b^{-1})^{-1}$, where $a \simeq 0.3 - 1.0$, which can become infinity and hence unphysical for strong wind conditions (Conzemius & Fedorovich, 2006b). Differently from these previous studies, we have used the EZ scale Δz_i instead of the CBL depth $z_{i,f}$ to estimate I_{bw}^{EZ} in the TKE budget analysis presented in §A.5. For small values of Δu, both scales z_{enc} and $z_{i,f}$ are proportional to each other, which implies

	$\frac{\Delta u}{N_0(\Delta z_i)_c}$	$\frac{(\Delta z_i)_s}{(\Delta z_i)_c}$	$\frac{\Delta z_i}{(\Delta z_i)_c}$	Ri_b	$(Ri_g)_{z_{i,f}}$	$(Ri_f)_{z_{i,f}}$	$-\frac{z_{enc}}{L_{Ob}}$	$\frac{\langle b'w'\rangle_{z_{i,f}}}{[\langle b'w'\rangle_{z_{i,f}}]_c}$
convection-dominated	0.6	0.35	1.05	44	2.75	1.0	60	1.06
shear-dominated	1.04	0.60	1.15	15	1.0	0.55	33	1.18

Table A.3: Critical values of various variables defining the boundary of the convection-dominated regime, where shear effects in the entrainment zone are negligible, and the boundary of the shear-dominated regime, where shear effects are of order one or larger.

$Ri_b \propto \widetilde{Ri}_b$. Besides, for small values of Δu, the Taylor expansion of Eq. (A.46) yields $\langle b'w'\rangle_{z_{i,f}}/[\langle b'w'\rangle_{z_{i,f}}]_c \simeq 1 + 2.8\, Ri_b^{-1}$, where the linear dependence on Ri_b^{-1} agrees with that obtained from the expansion $(1 - a\,\widetilde{Ri}_b^{-1})^{-1} \simeq 1 + a\,\widetilde{Ri}_b^{-1}$ for large values of $\widetilde{Ri}_b$. However, for larger values of Δu, the length scales z_{enc} and $z_{i,f}$ differ, Ri_b and $\widetilde{Ri}_b$ are not proportional to each other, and the scaling laws derived here remain finite for strong wind conditions.

We can use the scaling laws derived above to construct a partition of the parameter space depending on the relevance of shear in the entrainment zone. We choose to measure this relevance by the ratio between the shear-production rate and the turbulent-transport rate, since this variable is often used in the literature to discuss shear effects. We define the convective-dominated regime when $[P/(-\partial_z T)]_{z_{i,f}} \lesssim 0.5$ and the shear-dominated regime when $[P/(-\partial_z T)]_{z_{i,f}} \gtrsim 2$. These limits are indicated in figure A.8(*a*), the grey area in-between corresponding to conditions in which both shear and convection are important for entrainment-zone properties. These limits are also indicated in terms of the flux Richardson number in figure A.8(*b*). As observed previously in the literature (Conzemius & Fedorovich, 2006a; Pino & Vilà-Guerau De Arellano, 2008), we find that wind-shear effects appear at flux Richardson numbers of order one, which is significantly larger than the asymptotic value $\simeq 0.25 - 0.3$ characteristic of marginally stable stratified shear layers. As explained before with help of Eq. (A.38), the value $\simeq 0.25 - 0.3$ is recovered when we subtract the buoyancy flux in shear-free conditions from the buoyancy flux in sheared conditions.

Plotting $[P/(-\partial_z T)]_{z_{i,f}}$ as a function of $\Delta u/[N_0(\Delta z_i)_c]$ (not shown), we can express the thresholds that define the convective-dominated regime and the shear-dominated regime in terms of $\Delta u/[N_0(\Delta z_i)_c]$. We find that the upper threshold for the convection-dominated regime corresponds to

$$\frac{(\Delta u)_{conv}}{N_0(\Delta z_i)_c} \simeq 0.6 \tag{A.52}$$

and the lower threshold for the shear-dominated regime corresponds to

$$\frac{(\Delta u)_{shear}}{N_0(\Delta z_i)_c} \simeq 1.04\,. \tag{A.53}$$

The corresponding thresholds in terms of other independent variables are summarized in table A.3. The critical value of $\Delta u/[N_0(\Delta z_i)_c] = 0.6$ corresponds to $\simeq 5$ m s^{-1} wind velocity in the free atmosphere for typical midday conditions, which is often considered as a reference value for wind effects to become relevant in unstable conditions (Stull, 1988). We note, however, that even such a weak wind could significantly

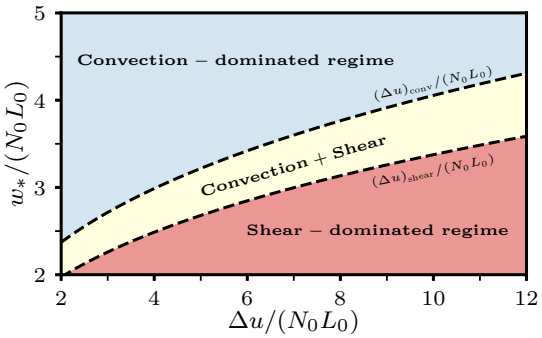

Figure A.17: Partition of the parameter space of a barotropic CBL penetrating into a linearly stratified atmosphere. The dashed lines mark the critical values separating the regimes as defined in Eq. (A.54) and Eq. (A.55).

affect the entrainment zone when the buoyancy forcing is weak, e.g., in the early morning or the late evening.

We can represent these various regimes in a parameter space spanned by the normalized velocity jump across the entrainment zone and the normalized convective velocity, as shown in figure A.17. Using the definition of the convective velocity scale Eq. (A.13), the boundaries between the various regions are

$$\frac{(\Delta u)_{\text{conv}}}{N_0 L_0} \simeq 0.15 \left(\frac{w_*}{N_0 L_0} \right)^3 , \tag{A.54}$$

and

$$\frac{(\Delta u)_{\text{shear}}}{N_0 L_0} \simeq 0.26 \left(\frac{w_*}{N_0 L_0} \right)^3 . \tag{A.55}$$

Hence, depending on the strength of Δu and w_*, the entrainment-zone dynamics in the equilibrium (quasi-steady) entrainment regime of a barotropic CBL penetrating into a linearly stratified atmosphere can be categorized in the following three regimes: the convection-dominated regime for $\Delta u < (\Delta u)_{\text{conv}}$, a regime in which shear and convective forcing are comparable for $(\Delta u)_{\text{conv}} < \Delta u < (\Delta u)_{\text{shear}}$, and the shear-dominated regime for $\Delta u > (\Delta u)_{\text{shear}}$.

We have also considered alternative variables that are often used in the literature to characterize shear effects, like the flux Richardson number. As observed in figure A.18(*a*), the flux Richardson number at the height of the minimum buoyancy flux captures wind-shear effects as well as the bulk Richardson number, since curves corresponding to different Froude numbers align into a single general curve. However, one disadvantage of using $(Ri_{\text{f}})_{z_{\text{i,f}}}$ instead of Ri_{b} to characterize wind-shear effects is that $(Ri_{\text{f}})_{z_{\text{i,f}}}$ asymptotes towards $\simeq 0.25 - 0.3$ for large Froude numbers (figure A.8*b*). Hence, properties become very sensitive with respect to $(Ri_{\text{f}})_{z_{\text{i,f}}}$ and small errors in determining $(Ri_{\text{f}})_{z_{\text{i,f}}}$ can lead to large errors in the diagnosed statistical properties. Another disadvantage of using $(Ri_{\text{f}})_{z_{\text{i,f}}}$ to characterize wind-shear effects is that, from a practical point of view, measuring the flux Richardson number at the height of the minimum buoyancy flux requires calculating gradients and covariances, which can be challenging, whereas estimating Δu, the velocity difference between the free atmosphere and the mixed layer, can be easier.

Another variable that we have studied as an alternative independent variable is the stability parameter $-z_{\text{enc}}/L_{\text{Ob}}$, since this variable is often used to characterize

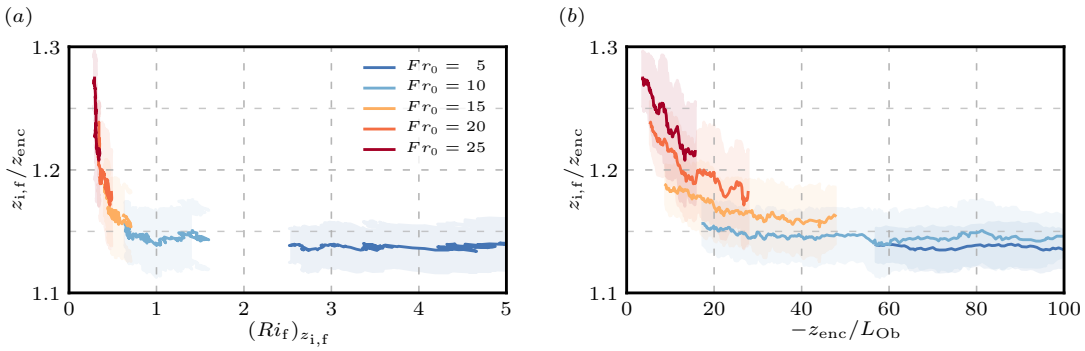

Figure A.18: Temporal evolution of the normalized flux-based CBL depth as a function of (*a*) the flux Richardson number $(Ri_f)_{z_{i,f}}$ and (*b*) the stability parameter $-z_{enc}/L_{Ob}$.

wind-shear effects on various properties of CBLs. We plot in figure A.18(*b*) the evolution of the height of the minimum buoyancy flux normalized by the encroachment length scale versus $-z_{enc}/L_{Ob}$. Curves corresponding to different Froude numbers do not align into a single general curve, and the dependence of the entrainment-zone thickness on Fr_0 is on the order of one for $-z_{enc}/L_{Ob} < 20$. Hence, the stability parameter $-z_{enc}/L_{Ob}$ is insufficient to characterize wind-shear effects on entrainment-zone properties.

One last aspect that is worth discussing is to what extent DNS studies as the ones presented here might be representative of the atmospheric CBL, given the disparity of Reynolds numbers between the DNS and the atmospheric CBL. There are properties that might certainly be poorly represented with the Reynolds number that we reach in our simulations. For instance, inertial-range and dissipative-range properties in the entrainment zone are likely poorly represented, since the ratio between the Ozmidov scale and the Kolmogorov scale, quantified by $(Re_b)^{3/4}$, is less than 10. However, the entrainment-zone properties addressed in this work, such as second-order moments and the TKE budget equation, show less than $10-20\%$ sensitivity to the larger Reynolds numbers reached in our simulations—the mean properties and the corresponding layered vertical structure show even less sensitivity. The reason is that much of those properties is determined by the interaction between convection in the mixed layer, which is dominated by large scales, and the mean velocity profile in the entrainment zone, which is also well represented. Hence, even if some of the coefficients in the scaling laws derived in this work might still vary on the order of $10-20\%$ as the Reynolds number in the DNS is further increased, the functional relationships in those scaling laws are likely robust, and therefore DNS can provide relevant information about the atmospheric CBL. A similar convergence towards Reynolds number similarity has also been reported in cloud-topped boundary layers, and it is associated with the capability to resolve the Ozmidov scale at the CBL top, and hence resolve wave-like motions, which are very poorly represented by standard down-gradient mixing models (Mellado et al., 2018). A more challenging aspect, we believe, is how to transfer the results obtained from idealized studies to the atmospheric context, given the complex interaction of various processes often occurring in the atmospheric CBL.

A.7 SUMMARY AND CONCLUSIONS

A systematic analysis of wind-shear effects on barotropic convective boundary layers growing into linearly stratified atmospheres has been carried out by means of dimensional analysis and direct numerical simulation. Dimensional analysis allows us to characterize the system by a normalized CBL depth, z_{enc}/L_0, a Froude number $Fr_0 \equiv U_0/(N_0 L_0)$, a reference buoyancy Reynolds number, $Re_0 \equiv N_0 L_0^2/\nu$, and the Prandtl number. The first two non-dimensional quantities embed the dependence of the system on time, on the surface buoyancy flux, B_0, and on the wind velocity and the buoyancy stratification in the free atmosphere, U_0 and N_0^2, respectively. The encroachment length scale z_{enc} is a measure of the shear-free CBL depth, and $L_0 = (B_0/N_0^3)^{1/2}$ is the reference Ozmidov length. L_0 and Re_0 characterize the turbulence in the upper sublayer of the entrainment zone, a strongly stratified region that serves as a transition between the CBL and the free atmosphere. The ratio z_{enc}/L_0 increases as the CBL grows into the linearly stratified atmosphere, and we have focused on the equilibrium (quasi-steady) entrainment regime, when CBL properties evolve on time scales much larger than the eddy turnover time of the large, energy-containing motions. In particular, we have studied the intervals $15 \lesssim z_{enc}/L_0 \lesssim 35$ and $0 \leq Fr_0 \leq 25$, which represents typical midday atmospheric conditions over land with wind velocities of up to $U_0 \simeq 15$ m s^{-1}. The Prandtl number has been set to 1. We have thoroughly studied the case $Re_0 = 25$ and compared the main results with data from $Re_0 = 42$. The observed degree of Reynolds-number similarity indicates that the results found in this study can be informative for atmospheric conditions.

We have found that the dependence of mixed-layer and entrainment-zone properties on the normalized CBL depth z_{enc}/L_0 and the Froude number Fr_0 can be expressed in terms of one single independent variable, $(\Delta z_i)_s/(\Delta z_i)_c$, where $(\Delta z_i)_s = \sqrt{1/3}\,\Delta u/N_0$ is the entrainment-zone scale in weakly unstable conditions (strong wind), $\Delta u \equiv U_0 - u_{ml}$ being the velocity difference between the free atmosphere and the mixed layer, and $(\Delta z_i)_c = 0.25\, z_{enc}$ is the entrainment-zone scale in strongly unstable conditions (weak wind). The ratio $(\Delta z_i)_s/(\Delta z_i)_c$ increases as the wind velocity increases and in this study we have considered the range $0 \leq (\Delta z_i)_s/(\Delta z_i)_c \lesssim 1.5$, which corresponds to the weakly-to-strongly unstable conditions $-z_{enc}/L_{Ob} \gtrsim 4$. The mean buoyancy and the mean buoyancy flux in the mixed layer follow shear-free scaling laws for all those conditions. For $(\Delta z_i)_s/(\Delta z_i)_c < 0.35$, convection dominates the entrainment-zone dynamics and wind-shear effects on entrainment-zone properties are negligible. Wind-shear effects on entrainment appear when $(\Delta z_i)_s/(\Delta z_i)_c \simeq 0.35$, which corresponds to $\simeq 5$ m s^{-1} for typical midday conditions, and become of order one when $(\Delta z_i)_s/(\Delta z_i)_c \simeq 0.6$. The corresponding critical values of Δu are provided in Eq. (A.54) and Eq. (A.55) in terms of the encroachment CBL depth, the surface buoyancy flux, and the stratification in the free atmosphere.

We have rationalized the relevance of the variable $(\Delta z_i)_s/(\Delta z_i)_c$ and the validity of shear-free scaling laws below $(\Delta z_i)_s/(\Delta z_i)_c \simeq 0.35$ by analysing the two-layer vertical structure of the entrainment zone. In particular, we have obtained the entrainment-zone scale Δz_i that characterizes the lower entrainment-zone sublayer. The limit of Δz_i for vanishingly weak wind is $(\Delta z_i)_c$, and the limit of Δz_i for strong wind is $(\Delta z_i)_s$. The variable $(\Delta z_i)_s$ can be interpreted as the asymptotic thickness of a stably stratified shear layer that would form in the limit of strong wind. Hence, as wind shear

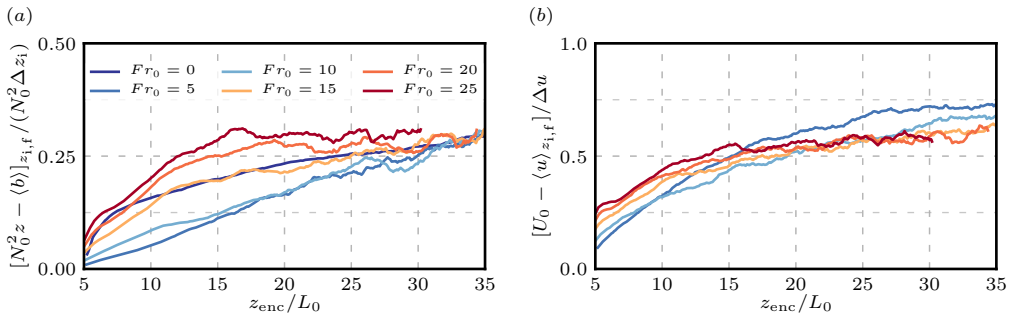

Figure A.19: Temporal evolution of the normalized buoyancy difference and velocity difference at the height of minimum buoyancy flux in the entrainment-rate equations for the buoyancy (A.58) and for the velocity (A.59).

increases and the variable $(\Delta z_i)_s/(\Delta z_i)_c$ increases, the value $\simeq 0.35$ can be interpreted as the condition at which the characteristic length scale in the lower entrainment-zone sublayer Δz_i changes from the convective limit $(\Delta z_i)_c$ towards the shear limit $(\Delta z_i)_s$. Consistently, the analysis of the budget of the turbulence kinetic energy shows that, at this condition, shear production becomes comparable to turbulent transport as a source of turbulence kinetic energy in the entrainment zone. The corresponding flux Richardson number $Ri_f \equiv -\langle b'w' \rangle / P$ particularized at $z_{i,f}$ at this state is $\simeq 1$, instead of the value $\simeq 0.25 - 0.3$ characteristic of marginally stable stratified shear layers: the value $\simeq 0.25 - 0.3$ is recovered when we substract the buoyancy flux of the shear-free limit from the numerator. The upper entrainment-zone sublayer is characterized by the Ozmidov scale evaluated at the height of the minimum buoyancy flux. As the turbulence intensity in the lower entrainment-zone sublayer increases with respect to shear-free conditions, the lower entrainment-zone sublayer broadens and so does the upper entrainment-zone sublayer.

The reduction of the number of independent variables from two to one can help simplify the parametrisation of mixed-layer and entrainment-zone properties in atmospheric models. To this aim, we have provided scaling laws for the reference heights in Eq. (A.32), for the entrainment-zone scale in Eq. (A.43), for the Ozmidov length in Eq. (A.49), and for the entrainment-flux ratio in Eq. (A.46), in terms of B_0, N_0, Δu, and time. Such a reduction from two independent variables to one can also be expressed in terms of the bulk Richardson number $Ri_b \equiv N_0^2 z_{enc}^2/(\Delta u)^2$, but not in terms of the stability parameter $-z_{enc}/L_{Ob}$.

Acknowledgements

The authors gratefully acknowledge the Gauss Centre for Supercomputing (GCS) for providing computing time through the John von Neumann Institute for Computing (NIC) on the GCS share of the supercomputer JUQUEEN at Jülich Supercomputing Centre (JSC). Funding was provided by the Max Planck Society through its Max Planck Research Groups program. Primary data and scripts used in the analysis and other supporting information that may be useful in reproducing the author's work are archived by the Max Planck Institute for Meteorology and can be obtained by contacting publications@mpimet.mpg.de.

APPENDIX AA

Entrainment-rate equation

To derive the entrainment-rate equation based on the mean buoyancy, we integrate the evolution equation of the mean buoyancy relative to the reference background profile

$$\partial_t(\langle b\rangle - N_0^2 z) = -\partial_z\left[\langle b'w'\rangle - \kappa_b\partial_z\langle b\rangle\right] \tag{A.56}$$

from $z_{i,f}$ upwards. Applying the Leibniz rule yields

$$\mathrm{d}_t\int_{z_{i,f}}^{z_\infty}(\langle b\rangle - N_0^2 z)\,\mathrm{d}z + \left[\langle b\rangle - N_0^2 z\right]_{z_{i,f}}\mathrm{d}_t z_{i,f} = -\int_{z_{i,f}}^{z_\infty}\partial_z\left[\langle b'w'\rangle - \kappa_b\partial_z\langle b\rangle\right]\mathrm{d}z\ , \tag{A.57}$$

which can be rearranged to obtain the entrainment rate equation

$$\left[N_0^2 z - \langle b\rangle\right]_{z_{i,f}}\mathrm{d}_t z_{i,f} = -\left[\langle b'w'\rangle - \kappa_b\partial_z\langle b\rangle\right]_{z_{i,f}} - Re_0^{-1}B_0 - \mathrm{d}_t\int_{z_{i,f}}^{z_\infty}(N_0^2 z - \langle b\rangle)\,\mathrm{d}z\ . \tag{A.58}$$

Garcia & Mellado (2014) have shown that the distortion term (the integral term in A.58) is relatively small. Therefore, for Reynolds numbers that are large enough to neglect the molecular-flux terms, the turbulent buoyancy flux at $z_{i,f}$ is approximately equal to $[N_0^2 z - \langle b\rangle]_{z_{i,f}}\mathrm{d}_t z_{i,f}$. Concomitantly, figure A.19(*a*) shows that $[N_0^2 z - \langle b\rangle]_{z_{i,f}}$, which is the local deviation of the mean profile with respect to the background profile b_0 at the height $z_{i,f}$, is well scaled by $N_0^2\Delta z_i$. As a result, the entrainment-rate equation based on the mean buoyancy provides the scaling law $-\langle b'w'\rangle_{z_{i,f}} \sim w_e N_0^2\Delta z_i$, where $w_e \equiv \mathrm{d}_t z_{i,f}$.

The same analysis is carried out to derive the entrainment-rate equation based on the mean velocity

$$\left[U_0 - \langle u\rangle\right]_{z_{i,f}}\mathrm{d}_t z_{i,f} = -\left[\langle u'w'\rangle - \nu\partial_z\langle u\rangle\right]_{z_{i,f}} - \mathrm{d}_t\int_{z_{i,f}}^{z_\infty}(U_0 - \langle u\rangle)\,\mathrm{d}z\ . \tag{A.59}$$

The contribution of the distortion term compared to the contribution of the kinematic momentum flux at $z_{i,f}$ is small, which implies that $-\langle u'w'\rangle_{z_{i,f}}$ is approximately equal to $[U_0 - \langle u\rangle]_{z_{i,f}}\,\mathrm{d}_t z_{i,f}$ for a large enough Re_0. Figure A.19(*b*) shows that $[U_0 - \langle u\rangle]_{z_{i,f}}$ is well scaled by Δu, the velocity increment across the entrainment zone defined by (A.27). Therefore, the entrainment-rate equation based on the mean velocity provides the scaling law $-\langle u'w'\rangle_{z_{i,f}} \sim w_e\Delta u$.

The entrainment-rate equations derived above recover the jump relations used in mixed-layer-models when the mixed-layer-model approximations to the actual solutions are substituted into them (Fedorovich et al., 2004a). With this mixed-layer approximation, the increments $[N_0^2 z - \langle b\rangle]_{z_{i,f}}$ and $[U_0 - \langle u\rangle]_{z_{i,f}}$ coincide with the jumps of buoyancy and velocity across the CBL top. However, when the entrainment-rate equations are applied to the actual solutions of the governing equations (A.1), those increments are not the difference between two arbitrary heights at the CBL top, but have a very specific definition, namely, the difference between the reference background profiles and the mean values at the particular height chosen to track the CBL top, in this case, the height of minimum buoyancy flux.

BIBLIOGRAPHY

Ansorge, C. & J. P. Mellado (2014). "Global Intermittency and Collapsing Turbulence in the Stratified Planetary Boundary Layer." In: *Bound.-Layer Meteor.* 153.1, pp. 89–116.

Bernardini, M., S. Pirozzoli & P. Orlandi (2014). "Velocity statistics in turbulent channel flow up to Re=4000." In: *J. Fluid Mech.* 742, pp. 171–191.

Boer, A. van de, A. F. Moene, A. Graf, D. Schüttemeyer & C. Simmer (2014). "Detection of Entrainment Influences on Surface-Layer Measurements and Extension of Monin–Obukhov Similarity Theory." In: *Bound.-Layer Meteor.* 152.1, pp. 19–44. ISSN: 1573-1472.

Brucker, K. A. & S. Sarkar (2007). "Evolution of an initially turbulent stratified shear layer." In: *Phys. Fluids* 19, p. 105105.

Carpenter, M. & C. A. Kennedy (1994). "Fourth-order 2N-storage Runge-Kutta schemes." In: *Technical Report NASA-TM-109112, NASA Langley Research Center*.

Carson, D. & F. Smith (1975). "Thermodynamic model for the development of a convectively unstable boundary layer." In: *Advances in Geophysics* 18, pp. 111–124.

Chung, D. & G. Matheou (2012). "Direct numerical simulation of stationary homogeneous stratified sheared turbulence." In: *J. Fluid Mech.* 696, pp. 434–467.

Conzemius, R. J. & E. Fedorovich (2006a). "Dynamics of sheared convective boundary layer entrainment. Part I: Methodological background and large eddy simulations." In: *J. Atmos. Sci.* 63, pp. 1151–1178.

– (2006b). "Dynamics of sheared convective boundary layer entrainment. Part II: Evaluation of bulk model predictions of entrainment flux." In: *J. Atmos. Sci.* 63, pp. 1179–1199.

– (2007). "Bulk models of the sheared convective boundary layer: evaluation through large eddy simulations." In: *J. Atmos. Sci.* 64, pp. 786–807.

Deardorff, J. W. (1970). "Preliminary results from numerical integration of the unstable boundary layer." In: *J. Atmos. Sci.* 27, pp. 1290–1211.

– (1974). "Three-dimensional numerical study of turbulence in an entraining mixed layer." In: *Bound.-Layer Meteor.* 7, pp. 199–226.

Deardorff, J. W., G. E. Willis & B. H. Stochton (1980). "Laboratory studies of the entrainment zone of a convectively mixed layer." In: *J. Fluid Mech.* 100, pp. 41–64.

Dougherty, J. P. (1961). "The anisotropy of turbulence at the meteor level." In: *Journal of Atmospheric and Terrestrial Physics* 21, pp. 210–213.

Fedorovich, E. & R. J. Conzemius (2008). "Effects of wind shear on the atmospheric convective boundary layer structure and evolution." In: *Acta Geophysica* 56, pp. 114–141.

Fedorovich, E. & J. Thäter (2001). "Vertical transport of heat and momentum across a sheared density interface at the top of a horizontally evolving convective boundary layer." In: *J. Turbul.* 2, N7.

Fedorovich, E., R. Conzemius & D. Mironov (2004a). "Convective entrainment into a shear-free linearly stratified atmosphere: Bulk models reevaluated through large-eddy simulation." In: *J. Atmos. Sci.* 61, pp. 281–295.

Fedorovich, E., R. J. Conzemius, I. Esau, F. K. Chow, D. Lewellen, C. H. Moeng, P. Sullivan, D. Pino & J. V. G. de Arellano (2004b). "Entrainment into sheared convective boundary layers as predicted by different large eddy simulation codes." In: ***In**: Preprints, 16th Symp. on Boundary Layers and Turbulence, 9-13 August, Amer. Meteor. Soc. Portland, ME*, CD–ROM, P4.7.

Fernando, H. J. S. (1991). "Turbulent mixing in stratified fluids." In: *Annu. Rev. Fluid. Mech.* 23, pp. 455–493.

Flores, O., J. Jiménez & J. C. Del Álamo (2007). "Vorticity organization in the outer layer of turbulent channels with disturbed walls." In: *J. Fluid Mech.* 591, pp. 145–154.

Garcia, J. R. & J. P. Mellado (2014). "The two-layer structure of the entrainment zone in the convective boundary layer." In: *J. Atmos. Sci.* 71, pp. 1935–1955.

Garratt, J. R. (1992). "The Atmospheric Boundary Layer." In: *Cambridge University Pres*.

Gohari, S. M. I. & S. Sarkar (2017). "Direct Numerical Simulation of Turbulence Collapse and Rebirth in Stably Stratified Ekman Flow." In: *Bound.-Layer Meteor.* 162.3, pp. 401–426.

Hebert, D. A. & S. M. de Bruyn Kops (2006). "Predicting turbulence in flows with strong stable stratification." In: *Phys. Fluids* 18.6, pp. 1–10.

Howland, C. J., J. R. Taylor & C. P. Caulfield (2018). "Testing linear marginal stability in stratified shear layers." In: *J. Fluid Mech.* 839, R4.

Hunt, J. C. R. & P. A. Durbin (1999). "Perturbed vortical layers and shear sheltering." In: *Fluid Dyn. Res.* 24.6, pp. 375–404.

Jonker, H. J. J., M. van Reeuwijk, P. Sullivan & G. Patton (2013). "On the scaling of shear driven entrainment: A dns study." In: *J. Fluid Mech* 732, pp. 150–165.

Kim, S. W., S. U. Park & C. H. Moeng (2003). "Entrainment processes in the convective boundary layer with varying wind shear." In: *Bound.-Layer Meteor.* 108, pp. 221–245.

Kim, S. W., S. Park, D. Pino & J. Vilà-Guerau De Arellano (2006). "Entrainment parameterization in a sheared convective boundary layer by using a first-order jump model." In: *Bound.-Layer Meteor.* 120, pp. 455–475.

LeMone, M. A. (1973). "The structure and dynamics of horizontal roll vortices in the planetary boundary layer." In: *J. Atmos. Sci.* 30, pp. 1077–1091.

Lele, S. (1992). "Compact finite difference schemes with spectral-like resolution." In: *J. Comput. Phys* 103, pp. 16–42.

Lenschow, D. H., J. C. Wyngaard & W. T. Pennell (1980). "Mean-Field and Second-Moment Budgets in a Baroclinic, Convective Boundary Layer." In: *J. Atmos. Sci.* 37.6, pp. 1313–1326.

Liu, P., J. Sun & L. Shen (2016). "Parameterization of sheared entrainment in a well-developed CBL. Part I: Evaluation of the scheme through large-eddy simulations." In: *Adv. Atmos. Sci.* 33, pp. 1171–1184.

Mahrt, L. & D. H. Lenschow (1976). "Growth dynamics of the convective mixed layer." In: *J. Atmos. Sci.* 33, pp. 41–51.

Mashayek, A. & W. R. Peltier (2011). "Turbulence transition in stratified atmospheric and oceanic shear flows: Reynolds and Prandtl number controls upon the mechanism." In: *Geophys. Res. Lett.* 38.16. L16612.

Mellado, J. P. (2012). "Direct numerical simulation of free convection over a heated plate." In: *J. Fluid Me* 712, pp. 418–450.

– (2017). "Cloud-Top Entrainment in Stratocumulus Clouds." In: *Annu. Rev. Fluid. Mech.* 49.1, pp. 145–169.

Mellado, J. P. & C. Ansorge (2012). "Factorization of the Fourier transform of the pressure-Poisson equation using finite differences in colocated grids." In: *Z. Angew. Math. Mech.* 92, pp. 380–392.

Mellado, J. P., C. C. van Heerwaarden & J. R. Garcia (2016). "Near-Surface Effects of Free Atmosphere Stratification in Free Convection." In: *Bound.-Layer Meteor.* 159.1, pp. 69–95.

Mellado, J. P., C. S. Bretherton, B. Stevens & M. C. Wyant (2018). "DNS and LES for Simulating Stratocumulus: Better Together." In: *Journal of Advances in Modeling Earth Systems* 10.7, pp. 1421–1438.

Mellado, J.P., M. Puche & C. C. van Heerwaarden (2017). "Moisture statistics in free convective boundary layers growing into linearly stratified atmospheres." In: *Quarterly Journal of the Royal Meteorological Society* 143.707, pp. 2403–2419.

Moeng, C. H. & P. P. Sullivan (1994). "A comparison of shear- and buoyancy-driven planetary boundary layer flows." In: *J. Atmos. Sci.* 51, pp. 999–1022.

Ozmidov, R. V. (1965). "On the turbulent exchange in a stably stratified ocean." In: *Izv., Atmospheric and Oceanic Physics Series* 1.8, pp. 853–860.

Peltier, W. R. & C. P. Caulfield (2003). "Mixing efficiency in stratified shear flows." In: *Annu. Rev. of Fluid Mech.* 35.1, pp. 135–167.

Pino, D. & J. Vilà-Guerau De Arellano (2008). "Effects of shear in the convective boundary layer: analysis of the turbulent kinetic energy budget." In: *Acta Geophysica* 56, pp. 167–193.

Pino, D., J. V. G. de Arellano & P. J. Duynkerke (2003). "The contribution of shear to the evolution of a convective boundary layer." In: *J. Atmos. Sci.* 60, pp. 1913–1926.

Pino, D., J. V. G. de Arellano & S. W. Kim (2006). "Representing sheared convective boundary layer by zeroth- and first-order-jump mixed-layer models: Large-eddy simulation verification." In: *J. Appl. Meteor. Clim.* 45, pp. 1224–1243.

Pirozzoli, S., M. Bernardini, R. Verzicco & P. Orlandi (2017). "Mixed convection in turbulent channels with unstable stratification." In: *J. Fluid Mech.* 821, pp. 482–516. ISSN: 0022-1120.

Portwood, G. D., S. M. de Bruyn Kops, J. R. Taylor, H. Salehipour & C. P. Caulfield (2016). "Robust identification of dynamically distinct regions in stratified turbulence." In: *J. Fluid Mech.* 807, R2.

Salesky, S. T., M. Chamecki & E. Bou-Zeid (2017). "On the Nature of the Transition Between Roll and Cellular Organization in the Convective Boundary Layer." In: *Bound.-Layer Meteor.* 163, pp. 41–68.

Schröter, S. J. (2018). "Sheared convective boundary layers: turbulence kinetic energy and entrainment dynamics, (Doctoral dissertation)." In: *Wageningen University*, p. 256.

Sherman, F. S., J. Imberger & G. M. Corcos (1978). "Turbulence and mixing in stably stratified waters." In: *Annu. Rev. Fluid Mech.* 10, pp. 267–288.

Shishkina, O., R. J A M Stevens, S. Grossmann & D. Lohse (2010). "Boundary layer structure in turbulent thermal convection and its consequences for the required numerical resolution." In: *New J. Phys.* 12.7, p. 075022.

Smyth, W. D. & J. N. Moum (2000a). "Anisotropy of turbulence in stably stratified mixing layers." In: *Phys. Fluids* 12.6, pp. 1343–1362.

Smyth, W. D. & J. N. Moum (2000b). "Length scales of turbulence instably stratified mixing layers." In: *Phys. Fluids* 12, pp. 1327–1342.

Sorbjan, Z. (2005). "Statistics of scalar fields in the atmospheric boundary layer based on Large-eddy simulations. Part 1: Free convection." In: *Bound.-Layer Meteor.* 116, pp. 467–486.

– (2006). "Statistics of scalar fields in the atmospheric boundary layer based on Large-eddy simulations. Part II: Forced convection." In: *Bound.-Layer Meteor.* 119, pp. 57–79.

Spalart, P. R., G. N. Coleman & R. Johnstone (2008). "Direct numerical simulation of the Ekman layer: a step in Reynolds number, and cautious support for a log law with a shifted origin." In: *Phys. Fluids* 20.10.

Strang, E. J. & H. J. S. Fernando (2001). "Entrainment and mixing in stratified shear flows." In: *J. Fluid Mech.* 428, pp. 349–386.

Stull, R. B. (1988). "An Introduction to Boundary Layer Meteorology." In: *Interactive dynamics of convection and solidification*. Kluwer Academic Press, pp. 113–138.

Sullivan, P., C. H. Moeng, B. Stevens, D. H. Lenschow & S. D. Mayor (1998). "Structure of the entrainment zone capping the convective atmospheric boundary layer." In: *J. Atmos. Sci.* 55, pp. 3042–3064.

Van Heerwaarden, Chiel C. & Juan Pedro Mellado (2016). "Growth and Decay of a Convective Boundary Layer over a Surface with a Constant Temperature." In: *Journal of the Atmospheric Sciences* 73.5, pp. 2165–2177.

Waggy, S. B., S. Biringen & P. P. Sullivan (2013). "Direct numerical simulation of top-down and bottom-up diffusion in the convective boundary layer." In: *J. Fluid Mech.* 724, pp. 581–606.

B

NON-SINGULAR ZERO-ORDER BULK MODELS OF SHEARED CONVECTIVE BOUNDARY LAYERS

This appendix contains a paper, which has been submitted to the journal of the atmospheric sciences.

Haghshenas, A., Mellado, J.P., and Hartmann, M., "Non-singular zero-order bulk models of sheared convective boundary layers", J. Atmos. Sci., in review (2019).

The contribution of Armin Haghshenas (A.H.), Juan Pedro Mellado (JP.M.), and Moritz Hartmann (M.H.) to this paper is as follows: A.H. and JP.M. devised the idea of providing the bulk models together. A.H. shaped the research independently and developed the analytical formulation and the geometric- and energetics-based closures and a brief review of previous bulk models (sections 2,3&4). A.H. wrote the numerical code to solve the set of equations and was in general responsible for the evaluation analysis and the interpretation of the results (sections 5&6). The findings of the research have been regularly discussed with JP.M.. The contribution of M.H. was to verify the evaluation analysis by developing a different numerical code and to aid in interpreting the results corresponding to moisture. A.H. took the lead in writing the manuscript, and JP.M. and M.H. provided some feedback on it.

Non-singular zero-order bulk models of sheared convective boundary layers

Armin Haghshenas, Juan Pedro Mellado and Moritz Hartmann

Max Planck Institute for Meteorology, Bundesstrasse 53, 20146 Hamburg, Germany

Two zero-order bulk models (ZOM) are developed for the velocity, buoyancy, and moisture of a cloud-free barotropic convective boundary layer (CBL) that grows into a linearly stratified atmosphere. The models differ in the entrainment-closure assumption: in the first one, termed "energetics-based model", the negative and positive areas of the buoyancy flux are assumed to match between the model and the actual CBL; in the second one, termed "geometric-based model", the modeled CBL depth is assumed to match different definitions of the actual CBL height. Parameterizations for these properties derived from direct numerical simulation are employed as the entrainment-closure equations. These parameterizations, and hence the resulting models, are free from the potential singularity at finite wind strength that has been a major limitation in previous models. A good agreement is observed in the temporal evolution of CBL bulk properties predicted by the energetics-based model and previous ZOMs that appropriately estimate the contribution of entrainment-zone shear in their entrainment closure. Predictions of the geometric-based model suggest that the CBL depths obtained from the energetics-based model and previous ZOMs correspond better to the height that marks the transition from the lower to the upper entrainment-zone sublayer; this reference height is few hundred meters above the height of the minimum buoyancy flux. We also argue that ZOMs, despite their simplicity compared to higher-order models, can accurately represent CBL bulk properties when the relevant features of the actual entrainment zone are considered in the entrainment closures.

B.1 INTRODUCTION

Bulk, or integral, models of a convective boundary layer (CBL) have been developed over the last decades to parametrize bulk properties such as the CBL depth, the inversion strength, and the entrainment fluxes in atmospheric models whose grid spacings are much larger than the dynamically relevant scales of CBLs (Haltiner & Williams, 1980; Suarez et al., 1983; Ayotte et al., 1996). Equally important, bulk models have broadly been used to investigate the sensitivity of the evolution of CBLs to changes in environmental conditions (Pelly & Belcher, 2001; De Roode et al., 2014), and even to study process interaction (Naumann et al., 2017). Nonetheless, uncertainties still remain in some key aspects associated with the surface and entrainment closures. The work presented here focuses on the entrainment closure and is motivated by challenges identified in previous work, namely, the lack of agreement on the minimum complexity of the bulk model that is necessary to accurately represent sheared CBLs (Pino et al., 2006; Liu et al., 2016), the large uncertainties in the empirical constants of the entrainment closure (see review in Conzemius & Fedorovich, 2006b, and references

therein), and a singularity in the entrainment closure that can appear at finite wind strength (Driedonks, 1982; Conzemius & Fedorovich, 2004). In this work, we address these three issues.

Bulk models are classified based on their degree of complexity in the representation of the transition layer between the mixed layer and the free atmosphere. The simplest is the zero-order model (ZOM) (Lilly, 1968) in which the transition layer is considered as an infinitesimally thin layer with discontinuous variations of velocity, buoyancy, and moisture. Alternatively, the first-order model (FOM) (Betts, 1974) and higher-order models (Deardorff, 1979) have been proposed, arguing that the transition layer between the mixed layer and the free atmosphere plays a key role in the dynamics of the CBL, and therefore, a better representation of the transition layer is required to accurately reproduce CBL bulk properties (Mahrt & Lenschow, 1976; Sullivan et al., 1998; Zanten et al., 1999; Kim et al., 2003). These models consider the transition layer as a layer of finite thickness with, respectively, linear and high-order polynomial variations of velocity, buoyancy, and moisture. Although the dependence of entrainment-zone properties on the entrainment-zone Richardson number, already shown by Mahrt & Lenschow (1976), might suggest that one needs at least the FOM representation of the CBL to adequately capture the entrainment process in sheared CBLs, some recent work has found no substantial differences between the overall ability of the ZOM and FOM to predict sheared CBL bulk properties (Pino et al., 2006; Conzemius & Fedorovich, 2007). However, Conzemius & Fedorovich (2007) found that the FOM largely mitigates—though not completely removes—the singularity of the ZOM at finite wind strength. Because of this advantage, they argued that the FOM is superior to the ZOM. Following this line of argumentation, most recent work made the effort to further develop a FOM (Sun & Xu, 2009; Huang et al., 2011; Liu et al., 2016). In this paper, we show that the infinitesimal transition-layer representation of the ZOM is sufficient to precisely reproduce bulk properties in the cloud-free sheared CBL, as long as the entrainment closure appropriately represents the local effects of wind shear on entrainment.

A parameterization for the entrainment-flux ratio, defined as the ratio of a buoyancy flux at the CBL top to the surface buoyancy flux, is commonly used as the entrainment closure in the integral equations. This parameterization, also referred to as the entrainment parameterization or the entrainment equation, is developed by analyzing either the local turbulence kinetic energy (TKE) budget (Zeman & Tennekes, 1977; Tennekes & Driedonks, 1981; Driedonks, 1982) or the integrated TKE budget (Boers et al., 1984; Batchvarova & Gryning, 1994; Conzemius & Fedorovich, 2006b). Even though there is a consensus regarding the processes that drive entrainment, the empirical constants associated with the contribution of each process to the entrainment flux vary widely. In particular, the contribution of the surface wind shear to the entrainment flux remains ambiguous, and the amount of the shear-generated TKE at the CBL top that is used for entrainment remains uncertain (see e.g. Conzemius & Fedorovich, 2006b).

More importantly, the previous entrainment parameterizations suffer from a potential singularity at finite wind strength, which is a major long-standing limitation of previous zero-order and first-order models (Driedonks, 1982; Conzemius & Fedorovich, 2004). Such a singularity arises when the CBL depth is used in the scaling arguments of different TKE terms in the entrainment zone (see e.g. Tennekes &

Driedonks, 1981; Boers et al., 1984). This is physically inconsistent with the observation that, under strong wind-shear conditions, the entrainment zone, defined as the region of negative buoyancy flux at the boundary-layer top, is characterized by a local length scale that is different from the CBL depth (Zeman & Tennekes, 1977; Kim et al., 2003; Pino & Vilà-Guerau De Arellano, 2008; Haghshenas & Mellado, 2019). Applying this local length scale in the integral analysis of the TKE budget, Haghshenas & Mellado (2019) derived non-singular parameterizations (or scaling laws) for different CBL properties. In the present work, we exploit these parameterizations to develop non-singular zero-order bulk models for the velocity, buoyancy, and moisture.

We structure the paper as follows. After describing the formulation in section B.2, we summarize the derivation of the set of equations in the zero-order bulk model and briefly discuss the closures used in previous work in section B.3. In section B.4, we introduce two new entrainment-closure equations and develop two ZOMs based on them. Evaluation of the proposed models is done in section B.5 by comparing their predictions with those of previous work. In section B.6, the potential singularity observed in the previous entrainment parameterization is investigated numerically and analytically. One of the developed models is then used to address the dependence of the sheared CBL on environmental conditions. We finally summarize these results and draw conclusions in section B.7.

B.2 FORMULATION

We consider a cloud-free convective boundary layer over an aerodynamically rough surface that grows into a linearly stratified atmosphere (Fig. B.1). The background profiles of buoyancy and specific humidity are, respectively,

$$b_{\mathrm{bg}} \equiv N_0^2 z \,, \tag{B.1a}$$

$$q_{\mathrm{bg}} \equiv q_{\mathrm{bg},0} - \gamma_q \, z \,, \tag{B.1b}$$

where $-N_0^2$ and γ_q are the lapse rates, N_0 is the Brunt-Väisälä frequency, and z is the vertical distance from the surface. The subscript "bg" denotes background, and $q_{\mathrm{bg},0}$ is the background specific humidity at the surface obtained by extrapolating the linear variation of q in the free atmosphere downwards to the surface. The surface roughness, z_0, and the surface kinematic fluxes of buoyancy and specific humidity, respectively B_0 and $F_{q,0}$, are constant and horizontally homogeneous. We assume $F_{q,0} \geq 0$ and $\gamma_q \geq 0$, which correspond to a moist surface and a dry free atmosphere. In addition, we consider a barotropic case in the limit of zero Coriolis parameter, which indicates that the wind strength in the free atmosphere, U_0, is constant with height. (Henceforth, the symbol $\equiv$ indicates a definition.)

B.2.1 *Governing equations*

The set of governing equations comprises the conservation equations for mass, momentum, energy, and moisture in the Boussinesq approximation. Under the assumptions of statistical homogeneity in the horizontal directions, no subsidence, and neglecting condensation and radiation, and in the limit of zero Coriolis parameter, the

horizontally-averaged equations for streamwise kinematic momentum, u, buoyancy, b, and specific humidity, q, read

$$\frac{\partial \langle u \rangle}{\partial t} = -\frac{\partial \tau_x}{\partial z} , \tag{B.2a}$$

$$\frac{\partial \langle b \rangle}{\partial t} = -\frac{\partial B}{\partial z} , \tag{B.2b}$$

$$\frac{\partial \langle q \rangle}{\partial t} = -\frac{\partial F_q}{\partial z} . \tag{B.2c}$$

We have chosen the streamwise coordinate x aligned with the wind in the free atmosphere, so that the mean wind in the spanwise direction is zero. The buoyancy is linearly related to the virtual potential temperature θ_v by $b \simeq g(\theta_v - \theta_{v,0})/\theta_{v,0}$, where $\theta_{v,0}$ is the constant reference value obtained by extrapolating the linear stratification of θ_v in the free atmosphere downwards to the surface. The variables τ_x, B, and F_q are, respectively, the fluxes of kinematic momentum, buoyancy, and specific humidity. Angle brackets denote averaging along horizontal planes. Mathematically, the moisture becomes a passive scalar once the equation of state is linearized and the system is formulated in terms of buoyancy and moisture instead of temperature and moisture. This means that changing moisture without changing buoyancy does not alter the CBL dynamics, which facilitates the study of how moisture properties vary with changes in environmental conditions (Mellado et al., 2017). The energy variable (e.g. potential temperature or static energy) can be recovered from the buoyancy, the specific humidity, and the linearized equation of state.

B.2.2 *Dimensional analysis*

In the limit of high Reynolds number and once the initial conditions have been sufficiently forgotten, the dynamics of the sheared CBL is completely governed by the control parameters $\{B_0, N_0, U_0, z_0\}$ and the independent variables $\{z, t\}$, where t represents the time. We focus on the quasi-steady (equilibrium) entrainment regime under which CBL properties evolve on time scales much larger than the large-eddy turnover time, and the profiles of various properties, when appropriately normalized, behave approximately self-similarly (Fedorovich et al., 2004a). Hereafter, we will use the term "quasi-steady regime" for simplicity.

The system in the quasi-steady regime, hence, depends on two non-dimensional parameters: a reference Froude number

$$Fr_0 \equiv \frac{U_0}{N_0 L_0} \tag{B.3}$$

and a normalized surface roughness, z_0/L_0. Here L_0 is the reference Ozmidov length defined as

$$L_0 \equiv \left(\frac{B_0}{N_0^3} \right)^{1/2} , \tag{B.4}$$

which provides a relevant measure for the thickness of the upper region of the entrainment zone in the shear-free and sheared CBL (Garcia & Mellado, 2014; Haghshenas & Mellado, 2019).

Statistical properties of the specific humidity depend on $\{F_{q,0}, \gamma_q, q_{\mathrm{bg},0}\}$ in addition to the aforementioned non-dimensional parameters. Mellado et al. (2017) have

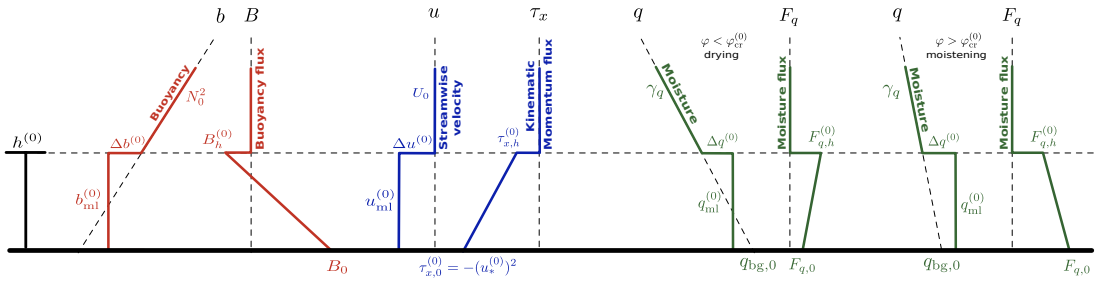

Figure B.1: Vertical profiles of different properties in the conceptual framework of the zero-order bulk model. The parameters defining the problem are the kinematic surface fluxes B_0 and $F_{q,0}$, the lapse rates in the free atmosphere $-N_0^2$ and γ_q, the wind velocity in the free atmosphere U_0, and the background specific humidity at the surface $q_{bg,0}$. The sketch depicts two different moisture regimes: entrainment-drying regime ($\varphi < \varphi_{cr}^{(0)}$) and surface-moistening regime ($\varphi > \varphi_{cr}^{(0)}$), where φ is the flux-ratio parameter defined in Eq. (B.5), and $\varphi_{cr}^{(0)}$ is its critical value whose analytical relationship is provided in Eq. (B.24).

shown that moisture statistics can be conveniently analyzed by the non-dimensional parameter

$$\varphi \equiv \frac{2\,F_{q,0}}{F_{q,0} + F_{q,1}}\,. \tag{B.5}$$

The parameter $F_{q,1}$ is a reference scale for the entrainment flux of the specific humidity and is defined as

$$F_{q,1} \equiv \gamma_q\, B_0 N_0^{-2} = (\gamma_q\, L_0)(N_0 L_0)\,, \tag{B.6}$$

which can be interpreted as the product of a moisture variation $\gamma_q\, L_0$ and a velocity scale $N_0 L_0$ both in the upper region of the entrainment zone. The quantity φ is a flux-ratio parameter that varies, by definition, between 0 and 2. These limits correspond to the pure-drying regime and the pure-moistening regime, respectively. The condition $\varphi \approx 1$ corresponds to $F_{q,0} \approx F_{q,1}$, i.e. an entrainment flux comparable with the surface flux, which marks the transition from the drying regime to the moistening regime (Mahrt, 1991).

We express the dependence of statistical properties on time in terms of the non-dimensional variable z_{enc}/L_0. The variable z_{enc} is the encroachment length scale (Lilly, 1968; Carson & Smith, 1975) defined as

$$z_{enc}(t) \equiv \left\{ 2\,N_0^{-2} \int_0^{z_\infty} \left[\langle b \rangle (z,t) - N_0^2 z \right] \mathrm{d}z \right\}^{1/2}\,, \tag{B.7}$$

where z_∞ is located far enough into the non-turbulent stably stratified region for the integral to become approximately independent of z_∞. The integral analysis of the buoyancy equation in the limit of high Reynolds number yields

$$z_{enc}/L_0 = \left[2\,N_0\,(t - t_0) \right]^{1/2}\,, \tag{B.8}$$

where t_0 is a constant of integration, which quantifies the dependence on the initial buoyancy profile.

The logic behind using z_{enc}/L_0 instead of tN_0 to represent the state of the CBL development is that it facilitates the comparison between atmospheric measurements and results from numerical simulations conducted with different initial conditions.

Notice that the encroachment length scale provides a measure for the depth of the mixed layer in shear-free and sheared CBLs growing into linearly stratified atmosphere (Van Heerwaarden & Mellado, 2016; Mellado et al., 2016; Haghshenas & Mellado, 2019), and it can be calculated from the mean buoyancy profile, obtained from atmospheric measurements or numerical simulations, according to Eq. (B.7).

For typical midday conditions of the sheared CBL over land, one finds $N_0 \simeq 0.006 - 0.018$ s^{-1}, $B_0 \simeq 0.001 - 0.01$ m^{2}s^{-3}, $U_0 \simeq 0 - 20$ ms^{-1}, $z_0 \simeq 0.01 - 0.1$ m, $\gamma_q \simeq 0 - 0.002$ g kg^{-1}m^{-1}, $F_{q,0} \simeq 0.03 - 0.1$ g kg^{-1}ms^{-1}, and $z_{\mathrm{enc}} \simeq 500 - 2000$ m, which yields the parameter space $Fr_0 \simeq 0 - 85$, $z_0/L_0 \simeq (0.05 - 5) \times 10^{-3}$ and $z_{\mathrm{enc}}/L_0 \simeq 5 - 50$. The parameter φ can change between its theoretical limits, 0 and 2.

B.3 ZERO-ORDER BULK MODEL

In this section, we summarize the derivation of ZOM equations for a barotropic CBL without the Coriolis force, and we discuss the basic form of previous surface and entrainment closures and their corresponding limitation and uncertainty. Further details of the derivation of the equation set and closures can be found, e.g., in Conzemius & Fedorovich (2006b).

The CBL in the conceptual framework of the zero-order model is represented by a single layer of height-constant buoyancy, kinematic momentum, and specific humidity, which is accompanied by zero-order discontinuities in these quantities at the top (see Fig. B.1). These profiles concomitantly result in a linear variation of the fluxes of buoyancy, kinematic momentum, and specific humidity within the CBL with zero-order discontinuities at the top. The superscript "(0)" indicates the zero-order bulk model, and we use a prefix "zero-order" to distinguish quantities in the model from those in the actual CBL. The variable $h^{(0)}$ is the zero-order CBL depth, $\Delta b^{(0)}$, $\Delta u^{(0)}$, and $\Delta q^{(0)}$ are, respectively, the zero-order buoyancy, kinematic momentum, and specific-humidity increments at the CBL top, $u_*^{(0)} = (-\tau_{x,0}^{(0)})^{1/2}$ is the zero-order friction velocity, and $B_h^{(0)}$, $\tau_{x,h}^{(0)}$, and $F_{q,h}^{(0)}$ are the zero-order fluxes of buoyancy, kinematic momentum, and specific humidity at the CBL top, respectively.

B.3.1 *Derivation of zero-order model equations*

The full set of zero-order model equations is derived by approximating the actual properties with the ZOM properties, by vertically integrating Eqs. (B.2) from the surface $z = 0$ up to a height that is slightly above the CBL depth $z = h^{(0)} + \epsilon$ and taking the limit $\epsilon \to 0$ after the integration, and by evoking basic assumptions of the zero-order representation of the CBL vertical structure (see e.g. Fedorovich, 1995). This analysis yields

$$\frac{\mathrm{d}}{\mathrm{d}\,t}\left[\Delta u^{(0)} h^{(0)}\right] = (u_*^{(0)})^2 \,, \tag{B.9a}$$

$$\frac{\mathrm{d}}{\mathrm{d}\,t}\left[\frac{N_0^2 (h^{(0)})^2}{2} - \Delta b^{(0)} h^{(0)}\right] = B_0 \,, \tag{B.9b}$$

$$\frac{\mathrm{d}}{\mathrm{d}\,t}\left[\frac{\gamma_q\,(h^{(0)})^2}{2} - \Delta q^{(0)} h^{(0)}\right] = -F_{q,0} \,. \tag{B.9c}$$

The zero-order fluxes of buoyancy, kinematic momentum, and specific humidity at the CBL top are related to the zero-order increment of these properties at the CBL top and the growth rate of the CBL depth as

$$-B_h^{(0)} = \Delta b^{(0)} \frac{\mathrm{d}\, h^{(0)}}{\mathrm{d}\, t} \,, \tag{B.10a}$$

$$-\tau_{x,h}^{(0)} = \Delta u^{(0)} \frac{\mathrm{d}\, h^{(0)}}{\mathrm{d}\, t} \,, \tag{B.10b}$$

$$F_{q,h}^{(0)} = \Delta q^{(0)} \frac{\mathrm{d}\, h^{(0)}}{\mathrm{d}\, t} \,. \tag{B.10c}$$

These equations are derived by vertically integrating Eqs. (B.2) over the height from $z = h^{(0)} - \epsilon$ up to $z = h^{(0)} + \epsilon$ and taking the limit $\epsilon \to 0$ after the integration. In addition to the three fluxes introduced above, the unknown variables are $h^{(0)}$, $u_*^{(0)}$, $\Delta u^{(0)}$ (or alternatively the mixed-layer velocity $u_{\mathrm{ml}}^{(0)} = U_0 - \Delta u^{(0)}$), $\Delta b^{(0)}$ (or alternatively the mixed-layer buoyancy $b_{\mathrm{ml}}^{(0)} = N_0^2 h^{(0)} - \Delta b^{(0)}$), and $\Delta q^{(0)}$ (or alternatively the mixed-layer specific humidity $q_{\mathrm{ml}}^{(0)} = q_{\mathrm{bg},0} - \gamma_q\, h^{(0)} + \Delta q^{(0)}$). Therefore, two more equations are required to close the system of equations.

B.3.2 *Surface-closure equation*

Previous work has often considered the surface-drag relation

$$(u_*^{(0)})^2 = C_D\, (u_{\mathrm{ml}}^{(0)})^2 \,, \tag{B.11}$$

as the surface-closure equation (see e.g. Boers et al., 1984; Garratt, 1992). The parameter C_D is the surface-drag coefficient, which is derived from the Monin-Obukhov similarity theory as a function of the surface roughness, Obukhov length, and surface-layer depth (see Garratt et al., 1982, for a review). A constant value is, however, usually taken for simplification (Flamant et al., 1999; Kim et al., 2006; Conzemius & Fedorovich, 2007). Hence, the dependence of CBL properties on the normalized surface roughness, z_0/L_0 (cf. section B.2.2), is translated to a dependence on the surface-drag coefficient, C_D.

B.3.3 *Entrainment-closure equation*

Previous work has often developed a parameterization for the entrainment-flux ratio as the entrainment-closure equation. The basic form of this parameterization in previous work reads

$$-\frac{B_h^{(0)}}{B_0} = \left[1 + A \left(\frac{u_*^{(0)}}{w_*^{(0)}}\right)^3\right] \frac{C_1}{1 + C_T Ri_t^{-1} - C_P Ri_{\mathrm{GS}}^{-1}} \,, \tag{B.12}$$

which is derived by either a local analysis of the TKE budget (Zeman & Tennekes, 1977; Tennekes & Driedonks, 1981; Driedonks, 1982) or an integral analysis of the TKE budget (Boers et al., 1984; Batchvarova & Gryning, 1994; Conzemius & Fedorovich, 2006b), assuming that, respectively, the local or bulk energetics in the model and the actual CBL match. The local TKE approach, however, has proven more challenging

Author	C_1	C_T	C_P	A
Tennekes (1973)	0.2	0	0.0	12.5
Driedonks (1982)	0.2	0	0.0	25.0
Pino et al. (2003)	0.2	4	0.7	8.0
Conzemius & Fedorovich (2006b)	0.2	0	0.4	0.0
Pino et al. (2006)	0.2	0	0.72	1.3
Sun & Xu (2009)	0.2	0	0.3	1.3
Liu et al. (2016)	0.21	0	0.43	$0.05\,C_D^{-1/2}$

Table B.1: Values of empirical constants in the entrainment parameterization, Eq. (B.12), in some previous work.

due to difficulties in the accurate quantification of the TKE budget at a single level (Kim et al., 2006). The variable $w_*^{(0)} \equiv (B_0 h^{(0)})^{1/3}$ is the convective velocity scale (Deardorff, 1970), and the variables

$$Ri_t \equiv \frac{\Delta b^{(0)} h^{(0)}}{(w_*^{(0)})^2 + A(u_*^{(0)})^2} \tag{B.13}$$

and

$$Ri_{\mathrm{GS}} \equiv \frac{\Delta b^{(0)} h^{(0)}}{(\Delta u^{(0)})^2 + (\Delta v^{(0)})^2} \tag{B.14}$$

are the bulk Richardson numbers associated, respectively, with the accumulation term and the entrainment-zone wind shear.

The parameters A, C_1, C_T, and C_P are empirical constants, which were obtained by different approaches in previous literature. One approach is to consider separately the different mechanisms of the TKE production, namely, the surface buoyancy flux and the surface and entrainment-zone wind shear. Early studies (e.g., Tennekes, 1973; Tennekes & Driedonks, 1981; Driedonks, 1982) followed this approach using results from laboratory experiments of shear-free CBLs (Deardorff et al., 1969; Willis & Deardorff, 1974) and of purely shear-driven boundary layers (Kato & Phillips, 1969; Kantha et al., 1977). More recently, Conzemius & Fedorovich (2006a) followed the same approach but using results from numerical simulations instead of laboratory experiments. Another approach taken in previous work is applying a regression analysis to bulk properties obtained from numerical simulations and obtaining the empirical constants directly (Kim et al., 2006; Liu et al., 2016).

The main differences among entrainment parameterizations in previous work lie in the values of the empirical constants (see Table B.1). It is important to point out that Sun & Xu (2009) and Liu et al. (2016) have derived the entrainment parameterization in the FOM framework, but we obtain their corresponding parameterization in the ZOM framework by setting to zero the variable that represents the thickness of the transition layer between the mixed layer and the free atmosphere, as done in Pino et al. (2006) and Conzemius & Fedorovich (2007).

The constant C_1 corresponds to the zero-order entrainment-flux ratio in the shear-free limit and its most commonly used value is 0.2. The constant C_T corresponds to

the contribution of the accumulation term, which is negligibly small with respect to the other terms in the TKE budget equation once the quasi-steady regime is reached. The main controversy stems from the constants associated to wind-shear effects on entrainment, namely, C_P and A, which correspond to the contribution from the entrainment-zone and surface wind shear to the entrainment flux, respectively.

Aside from the large uncertainty in the empirical constants, the main limitation of the previous entrainment parameterization is the potential singularity at finite wind strength. The contribution of the entrainment-zone shear to the entrainment flux represented by a negative sign term in the denominator of Eq. (B.12) could cause the denominator to become zero and the entrainment-flux ratio to become unbounded. Such a singularity occurs not only under very strong shear-conditions characterized by large Froude numbers, but also under moderate shear-conditions with initial conditions that are far from the quasi-steady regime (Driedonks, 1982; Conzemius & Fedorovich, 2004; Conzemius & Fedorovich, 2007).

This singularity arises when the entrainment parameterization is derived in the idealized framework of the bulk models. In the ZOM framework, the CBL depth—as the only length scale defined in this framework—is used in the scaling of the shear production at the CBL top in the local TKE approach (see e.g. Tennekes & Driedonks, 1981), and is used in the scaling of the integral of the negative buoyancy flux in the integral TKE approach (see e.g. Boers et al., 1984). This is physically contradictory to the observation that the entrainment zone under strong wind-shear conditions is characterized by a local length scale that is different from the CBL depth (Zeman & Tennekes, 1977; Kim et al., 2003; Pino & Vilà-Guerau De Arellano, 2008; Haghshenas & Mellado, 2019). Increasing the complexity of the bulk model to the first-order or higher-order models does not help tackle the singularity issue as long as the CBL depth is deemed as a characteristic length scale in the scaling arguments of different TKE terms in the entrainment zone.

B.4 NON-SINGULAR ENTRAINMENT-CLOSURE SCHEMES

The work presented here focuses on the entrainment closure and, following previous work, uses the surface-drag relation as the surface-closure equation [cf. Eq. (B.11)]. As entrainment closure, we introduce two new non-singular equations by making two different closure assumptions and by employing the non-singular parameterizations for different CBL properties derived in Haghshenas & Mellado (2019). In contrast to previous work, these authors have considered the actual CBL structure instead of the bulk-model structure, and have used the local length scale to characterize the entrainment zone, which led to non-singular parameterizations.

B.4.1 *Energetics-based closure*

As the first option for the entrainment closure, we assume that the negative and positive areas of the buoyancy flux in the model equal the ones in the actual CBL. This assumption is similar to that used in previous work, where the bulk or local energetics between the model and the actual CBL were assumed to be equal (cf. section B.3.3).

Mathematically, the zero-order entrainment-flux ratio can be written in terms of the energetics as (Conzemius & Fedorovich, 2006a)

$$-\frac{B_h^{(0)}}{B_0} = \left[\frac{A_N^{(0)}}{A_P^{(0)}}\right]^{1/2}, \tag{B.15}$$

evoking basic assumptions of the zero-order representation of the CBL vertical structure (cf. Fig. B.1). Here $A_N^{(0)}$ and $A_P^{(0)}$ are, respectively, the negative and positive areas of the buoyancy flux in the zero-order model framework.

A parameterization for the ratio of the negative and positive buoyancy flux in the actual CBL is obtained in appendix A using the results of Haghshenas & Mellado (2019). This parameterization, Eq. (B.36), along with Eq. (B.15) and the closure assumption that the negative and positive areas of the buoyancy flux in the actual CBL equal the ones in the model yields

$$-\frac{B_h^{(0)}}{B_0} \simeq 0.21\left[1+4.5\,\frac{\mathrm{d}\,h^{(0)}}{\mathrm{d}\,t}\frac{(\Delta u^{(0)})^2}{B_0 z_{\mathrm{enc}}}\right]^{1/2}. \tag{B.16}$$

We will refer to this entrainment closure as energetics-based closure and to the model that uses this closure as energetics-based model.

We obtain $-B_h^{(0)}/B_0 \simeq 0.21$ in the shear-free limit, which is consistent with Liu et al. (2016) and is slightly larger than the value 0.2 that is commonly used in previous work (cf. Table B.1). The energetics-based closure indicates that the shear-free entrainment flux of buoyancy is solely characterized by the surface buoyancy flux as the only source of turbulence in this case, and that the entrainment flux of buoyancy in the sheared CBL increases due to extra turbulence generated by the entrainment-zone shear. Explicitly representing the extra shear-generated turbulence, which is a relevant feature of the dynamics of actual sheared CBLs (see review in Fedorovich & Conzemius, 2008), raises the expectation that the energetics-based ZOM, despite the simplification in the CBL structure, should be able to faithfully represent the CBL bulk properties.

B.4.2 *Geometric-based closure*

The CBL depth predicted by the energetics-based model and by models in previous work cannot be *a priori* associated to any actual CBL height, such as the height of the minimum buoyancy flux or the height of the maximum buoyancy gradient. These heights differ by approximately 100 m for typical midday atmospheric conditions over land in the shear-free limit, and might increase to 200 m under strong-shear conditions in the barotropic CBL. This uncertainty about the CBL depth might be relevant for the parameterization of other processes in the CBL, for instance, for cloud formation. To address this issue, we propose a new model in which the zero-order CBL is assumed to equal different definitions of the actual CBL height, and then we compare the results of this model with those of the energetics-based model and models in previous work.

Several definitions of the actual CBL height might be associated with the zero-order CBL depth. Two common choices are the height of the minimum buoyancy flux

(Fedorovich et al., 2004a; Pino et al., 2003, 2006) and the height of the maximum mean gradient of buoyancy (Sullivan et al., 1998). These heights mark, respectively, the lower and upper entrainment-zone sublayers (Garcia & Mellado, 2014; Haghshenas & Mellado, 2019). Hence, as a third option, we consider the height that marks the transition between these two sublayers. Using Eqs. (4.12) and (5.11) in Haghshenas & Mellado (2019) as parameterizations for these heights, we obtain

$$\frac{h^{(0)}}{z_{\mathrm{enc}}} \simeq 0.94 + 0.25\,\alpha \left[1 + 4.8 \left(\frac{\Delta u^{(0)}}{N_0 z_{\mathrm{enc}}}\right)^2\right]^{1/2}, \tag{B.17}$$

where $\alpha \simeq 0.8$ corresponds to the height of the minimum buoyancy flux, and $\alpha \simeq 1.0$ corresponds to the height that marks the transition from the lower to upper entrainment-zone sublayer. The parameterization for the height of the maximum buoyancy gradient has an additional contribution from the upper entrainment-zone sublayer, and it is discussed in appendix B but not in the main text, for conciseness. We will refer to Eq. (B.17) as geometric-based closure and to the model that uses this closure as geometric-based model.

The geometric-based closure indicates that the zero-order shear-free CBL depth can be interpreted as a buoyancy-driven single-layer entity, since the right hand side of Eq. (B.17) reduces to a constant in the limit of zero wind velocity. For a non-zero wind velocity, this closure indicates that the zero-order CBL depth can be interpreted as a two-layer entity, namely, a buoyancy-driven layer that represents the actual mixed layer, and a buoyancy- and shear-driven layer that represents part of the actual entrainment zone. This is important because, as mentioned before, the finite thickness of the entrainment zone is a relevant feature of actual sheared CBLs (Mahrt & Lenschow, 1976; Zanten et al., 1999; Kim et al., 2003), and explicitly representing this feature in the ZOM raises the expectation that this model should faithfully represent the CBL bulk properties.

B.4.3 *Closed set of zero-order model equations*

The closed set of ZOM equations in non-dimensional form for the buoyancy and velocity are derived from Eqs. (B.9a) and (B.9b) as follows:

$$\frac{\mathrm{d}}{\mathrm{d}\,z_{\mathrm{enc}}}\left[\frac{\Delta u^{(0)}}{N_0 L_0} h^{(0)}\right] = C_D \left[Fr_0 - \frac{\Delta u^{(0)}}{N_0 L_0}\right]^2 \frac{z_{\mathrm{enc}}}{L_0}, \tag{B.18a}$$

$$\frac{\Delta b^{(0)}}{N_0^2 z_{\mathrm{enc}}} = \frac{h^{(0)}}{2\,z_{\mathrm{enc}}} - \frac{z_{\mathrm{enc}}}{2\,h^{(0)}} \tag{B.18b}$$

plus either the energetics-based closure, Eq. (B.16),

$$\frac{\Delta b^{(0)}}{N_0^2 z_{\mathrm{enc}}} \frac{\mathrm{d}\,h^{(0)}}{\mathrm{d}\,z_{\mathrm{enc}}} = 0.21 \left[1 + 4.5 \frac{\mathrm{d}\,h^{(0)}}{\mathrm{d}\,z_{\mathrm{enc}}} \left(\frac{\Delta u^{(0)}}{N z_{\mathrm{enc}}}\right)^2\right]^{1/2}, \tag{B.19}$$

or the geometric-based closure, Eq. (B.17). We have already substituted Eq. (B.11) and Eq. (B.10a), respectively, in Eq. (B.18a) and Eq. (B.19). We have also taken the integral

in Eq. (B.9b) and changed the variable from t to z_{enc}, where $\mathrm{d}/\mathrm{d}\,t = N_0 L_0^2\, z_{\mathrm{enc}}^{-1} \times \mathrm{d}/\mathrm{d}\,z_{\mathrm{enc}}$ [cf. Eq. (B.8)]. Recall that Fr_0 and C_D are the non-dimensional control parameters.

The ZOM equation for the moisture reads

$$\frac{\Delta q^{(0)}}{q_{\mathrm{ref}}} = \frac{h^{(0)}}{L_0}\left\{1 + \frac{\varphi}{2}\left[\left(\frac{z_{\mathrm{enc}}}{h^{(0)}}\right)^2 - 1\right]\right\}\,, \tag{B.20}$$

which is obtained by integrating Eq. (B.9c). Here φ is the flux-ratio parameter that characterizes the moisture, and q_{ref} is the reference moisture scale

$$q_{\mathrm{ref}} \equiv \frac{F_{q,0} + F_{q,1}}{2\,N_0 L_0}\,, \tag{B.21}$$

which is defined as a linear combination of $F_{q,0}$ and $F_{q,1}$ normalized by a velocity scale $N_0 L_0$ (Mellado et al., 2017). Normalization of $\Delta q^{(0)}$ with q_{ref} instead of $F_{q,0}/(N_0 L_0)$ or $F_{q,1}/(N_0 L_0)$ allows us to study the whole theoretical range of the flux-ratio parameter, since q_{ref} remains non-zero for both limits of $\varphi = 0$ (associated with $F_{q,0} = 0$) and $\varphi = 2$ (associated with $F_{q,1} = 0$).

A key property to characterize the moisture is the critical zero-order flux-ratio parameter $\varphi_{\mathrm{cr}}^{(0)}$. This parameter marks the transition between drying and moistening regimes. A functional relationship for $\varphi_{\mathrm{cr}}^{(0)}$ can be readily determined from the condition $\mathrm{d}\,q_{\mathrm{ml}}^{(0)}/\mathrm{d}\,\mathrm{t} = 0$, which, by definition [obtained from Eq. (B.9c)], corresponds to

$$F_{q,h}^{(0)} = F_{q,0}\,. \tag{B.22}$$

Substituting $F_{q,h}^{(0)}$ from Eq. (B.10c) in the equation above, and using Eq. (B.10a) to rewrite $\mathrm{d}\,h^{(0)}/\mathrm{d}\,t$ in the resulting equation in terms of $\Delta b^{(0)}$ and $B_h^{(0)}$ yields

$$\frac{\Delta q^{(0)}}{\Delta b^{(0)}} = -\frac{F_{q,0}}{B_h^{(0)}}\,, \tag{B.23}$$

as the condition that marks the transition between drying and moistening regimes. Provided that the LHS of Eq. (B.23) is larger than the RHS, the entrainment flux of drying air is dominant and the CBL is in the drying regime. When the LHS is smaller than the RHS, the surface flux of moisture dominates and the CBL is in the moistening regime. When the LHS equals the RHS, the mean moisture, $q_{\mathrm{ml}}^{(0)}$, remains constant in time and the water vapor introduced at the surface is used to moisten the entrained dry air towards the mixed-layer value.

The critical zero-order flux-ratio parameter, $\varphi_{\mathrm{cr}}^{(0)}$, can be written in terms of the CBL depth and the entrainment rate as

$$\varphi_{\mathrm{cr}}^{(0)} = \frac{\left(\frac{\mathrm{d}\,h^{(0)}}{\mathrm{d}\,z_{\mathrm{enc}}}\frac{h^{(0)}}{z_{\mathrm{enc}}}\right)}{1 + \frac{1}{2}\left(\frac{\mathrm{d}\,h^{(0)}}{\mathrm{d}\,z_{\mathrm{enc}}}\right)\left(\frac{h^{(0)}}{z_{\mathrm{enc}}} - \frac{z_{\mathrm{enc}}}{h^{(0)}}\right)}\,, \tag{B.24}$$

by substituting $B_h^{(0)}$, $\Delta b^{(0)}$, and $\Delta q^{(0)}$ from Eqs. (B.10a), (B.18b), and (B.20) in Eq. (B.23) and by solving the resulting equation for φ. The idea behind providing this functional

relationship is that it allows us to determine whether the CBL is in the drying or in the moistening regime. The CBL is in the moistening regime when the flux-ratio parameter, calculated from Eq. (B.5), is larger than the critical value, determined from Eq. (B.24), and the CBL is in the drying regime when the flux-ratio parameter is smaller than the critical value.

The critical flux-ratio parameter is constant in time for the shear-free limit, when $h^{(0)} \propto z_{\text{enc}}$, but varies in time for the sheared CBL, according to Eq. (B.24). The reason is that the entrainment enhancement due to the wind shear—causing the critical flux-ratio parameter to increase with respect to the shear-free limit—diminishes as the CBL grows. Therefore, the critical flux-ratio parameter decreases with time and asymptotes towards the corresponding shear-free value. We further discuss this behaviour in section B.6.

B.5 EVALUATION OF ZOM PREDICTIONS

Although the entrainment-closure equations and thus the ZOMs proposed in this work have been validated in Haghshenas & Mellado (2019) and appendix A, in this section we compare the resulting ZOMs with previous work. Such an analysis enables us to further examine the capability and accuracy of the new models proposed in this work.

B.5.1 *The shear-free CBL*

The set of equations for the shear-free limit has an analytical solution of the following form (see Fedorovich et al., 2004a, for a review)

$$\begin{aligned} -B_h^{(0)} &= C_1\, B_0\,, \\ h^{(0)} &= C_2\, z_{\text{enc}}\,, \\ \Delta b^{(0)} &= C_3\, N_0^2 z_{\text{enc}}\,, \end{aligned} \tag{B.25}$$

where the model coefficients satisfy the following relationships

$$C_2 = \left(2\,C_1 + 1\right)^{1/2} \quad \text{and} \quad C_3 = C_1\, C_2^{-1}\,. \tag{B.26}$$

One of the three model coefficients $\{C_1, C_2, C_3\}$ remains free and has to be prescribed to close the system.

In the energetics-based model, we prescribe $C_1 = 0.21$ according to Eq. (B.16) and obtain $C_2 \simeq 1.19$ and $C_3 \simeq 0.18$. These coefficients coincide with those of Liu et al. (2016)'s model, but are slightly larger than the predictions of models in previous work with $C_1 = 0.2$, where one obtains $C_2 \simeq 1.18$ and $C_3 \simeq 0.17$.

In the geometric-based model with $\alpha = 1.0$, we prescribe $C_2 \simeq 1.19$ according to Eq. (B.17) and obtain $C_1 \simeq 0.21$ and $C_3 \simeq 0.18$. These coefficients agree with those of the energetics-based model presented in the previous paragraph, suggesting that the zero-order CBL depth in the energetics-based model and also models in previous work corresponds approximately to the reference height that marks the transition from the lower to upper entrainment-zone sublayer. The geometric-based model with $\alpha = 0.8$ that matches the zero-order CBL depth to the height of the minimum buoyancy flux

prescribes $C_2 \simeq 1.14$ according to Eq. (B.17) and yields $C_1 \simeq 0.15$ and $C_3 \simeq 0.13$. These coefficients are different than those of the energetics-based model. This difference helps explain the controversy in C_1 in some previous work. Fedorovich et al. (2004a) and Mellado et al. (2017) estimated $C_1 \simeq 0.17$ and $C_1 \simeq 0.16 \pm 0.01$ assuming that the zero-order CBL depth matches the height of the minimum buoyancy flux in large-eddy simulations and direct-numerical simulation, respectively. These values are smaller than 0.2 simply as a result of the aforementioned assumption, and not because of statistical uncertainty.

Following the analytical solution of the set of equations for buoyancy-related properties, the moisture properties in the shear-free limit read

$$\begin{aligned} \Delta q^{(0)} &= C_4 \, q_{\mathrm{ref}} \, z_{\mathrm{enc}} / L_0 \, , \\ F_{q,h}^{(0)} &= C_5 \, q_{\mathrm{ref}} \, N_0 L_0 \, , \end{aligned} \tag{B.27}$$

where the model coefficients satisfy the following relationships

$$\begin{aligned} C_4 &= C_2 \left[1 + \varphi / 2 \, (C_2^{-2} - 1) \right] \, , \\ C_5 &= C_4 \, C_2 \, . \end{aligned} \tag{B.28}$$

We obtain $C_4 \simeq 1.19 - 0.17 \, \varphi$ and $C_5 \simeq 1.4 - 0.2 \, \varphi$ for the energetics-based model and the geometric-based model with $\alpha = 1$, and $C_4 \simeq 1.14 - 0.13 \, \varphi$ and $C_5 \simeq 1.3 - 0.15 \, \varphi$ for the geometric-based model with $\alpha = 0.8$. In the shear-free limit, one obtains $\varphi_{\mathrm{cr}}^{(0)} \simeq 1.17$ for the energetics-based and the geometric-based models with $\alpha = 1$, using Eqs. (B.24) and (B.25). One also obtains $\varphi_{\mathrm{cr}}^{(0)} \simeq 1.13$ for the geometric-based model with $\alpha = 0.8$, which coincides with that reported in Mellado et al. (2017).

B.5.2 *The sheared CBL*

As reference setup, we choose the strongest shear case investigated in Pino et al. (2006) and initialize the ZOMs using the values listed in Table 1 of that work (see Table B.2). The reason to select this case is twofold. First, the variation among the predictions of different models appears more clear for stronger shear conditions, since the main controversy in previous work stems from the contribution of the wind shear to the entrainment flux. Second, the ZOM variables and the vertical profiles of the mean buoyancy and buoyancy flux have been clearly reported in Pino et al. (2006) for a condition in which the quasi-steady regime has been reached. The reference Froude number and the reference Ozmidov length are, respectively, $Fr_0 \simeq 41$ and $L_0 \simeq 34$ m, according to Eqs. (B.3) and (B.4). We determine the encroachment length using Eq. (B.7) and integrating the vertical profile of the mean buoyancy presented in Fig. 2 of Pino et al. (2006), obtaining $z_{\mathrm{enc}} \simeq 510$ m. We also determine $t_0 \simeq -35$ s from Eq. (B.8), which is consistent with the fact that the corresponding numerical simulation has been started from a very shallow initial CBL.

For the model constants, we use those reported in Liu et al. (2016). The reason is that Liu et al. (2016) have provided high-quality data for a large number of simulated CBLs (twenty six cases) in terms of statistical convergence and of reaching the quasi-steady regime by running the simulations sufficiently long, such that they started to correct the second decimal in the empirical constants (cf. Table B.1).

Case		
$Q_s = 0.1$ Kms^{-1} $\partial\Theta_v/\partial z = 0.006$ Km^{-1} $U_0 = 20$ ms^{-1} $z_0 = 0.01$ m	$\Theta_{v,0} = 300$ K $\Longleftrightarrow$	$B_0 \simeq 0.0033$ ms^{-2} $N_0 \simeq 0.014$ s^{-1} $U_0 = 20$ ms^{-1} $C_D \simeq 0.002$
Initial Condition		
$t = 8000$ s $h^{(0)} = 704$ m $\Delta u^{(0)} = 5$ ms^{-1}	$z_{\text{enc}} \simeq 510$ m $\Longrightarrow$	$z_{\text{enc}}/L_0 \simeq 15$ $h^{(0)}/z_{\text{enc}} \simeq 1.4$ $\Delta u^{(0)}/(N_0 z_{\text{enc}}) \simeq 0.7$

Table B.2: The control parameters in the strongest shear case studied in Pino et al. (2006) and the corresponding initial conditions for ZOMs. Q_s is the surface heat flux.

We classify previous models into two groups based on how the contribution of the wind shear to entrainment is represented, facilitating in this way the comparison. Group I contains the previous models that take into account the entrainment-zone shear with or without the surface shear (Boers et al., 1984; Pino et al., 2003; Conzemius & Fedorovich, 2006b; Pino et al., 2006; Sun & Xu, 2009; Liu et al., 2016), and group II incorporates the ones that consider only the surface shear through their friction velocity term (Tennekes, 1973; Driedonks, 1982; Batchvarova & Gryning, 1994). We make the comparison with both groups for completeness, but we present the results for group II in appendix C because models in this group predict the CBL bulk properties poorly.

Figure B.2 illustrates that all considered ZOMs appropriately represent relevant features of sheared CBLs that have been documented in previous observational and numerical studies (Mahrt & Lenschow, 1976; Pino & Vilà-Guerau De Arellano, 2008; Haghshenas & Mellado, 2019). First, the CBL depth and the entrainment-flux ratio increase with respect to the shear-free limit. Second, as time goes by and the CBL depth grows, wind-shear effects diminish, and the CBL properties asymptote towards the shear-free values. Last but not least, wind-shear effects on buoyancy-related properties remain constrained to the CBL top. For instance, the entrainment-flux ratio grows substantially for strong wind conditions (by up to 100%, as shown in Fig. B.2*b*), while the CBL depth increases only slightly (by up to 10%, as shown in Fig. B.2*a*). Note, however, that this slight increase in the CBL depth implies an order-of-one change of the actual entrainment-zone thickness.

The variation in the entrainment-flux ratio predicted from different models is approximately $30 - 40\%$ (see Fig. B.2*b*). Pino et al. (2006) overestimate and Sun & Xu (2009) underestimate wind-shear effects with respect to Liu et al. (2016). Such a behaviour is explained by the different values of C_P used in these three models, since the contribution of the surface wind shear to the entrainment flux, represented by the empirical constant A in Eq. (B.12), is approximately the same in these models. This contribution is around 15% at $z_{\text{enc}}/L_0 \simeq 15$, but decreases to less than 5% at $z_{\text{enc}}/L_0 \simeq 25$ for the case studied here, to some extent supporting the conclusion in recent work that the surface wind shear affects entrainment mainly indirectly by

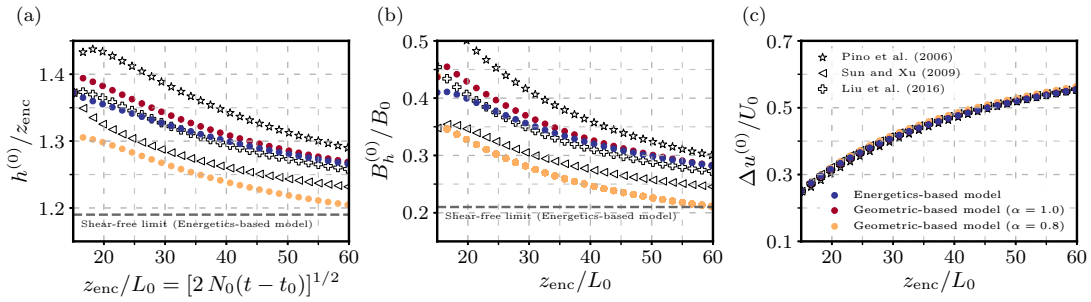

Figure B.2: Comparison of different properties of the sheared CBL characterized by $Fr_0 = 41$ and $C_D = 0.002$ obtained from ZOMs developed in the present and previous work classified as Group I.

changing the mean velocity in the mixed layer and thus the velocity jump at the CBL top (Fedorovich & Conzemius, 2008).

A very good match is observed between the results of both the energetics-based model and the geometric-based model with $\alpha = 1.0$ and those of Liu et al. (2016), with only $\simeq 5\%$ difference in the entrainment-flux ratio. This deviation is smaller than the achieved statistical convergence in direct numerical simulations from which the coefficients of proportionality in the closure equations were obtained (Haghshenas & Mellado, 2019). The coincidence of the results of the geometric-based model with $\alpha = 1.0$ with those of the energetics-based model indicates that also the sheared CBL depth predicted by the energetics-based model can be associated to the actual CBL height that marks the transition from the lower to upper entrainment-zone sublayer. The CBL depth predicted from the geometric-based model with $\alpha = 0.8$, which corresponds to the height of the minimum buoyancy flux, is $\simeq 5\%$ smaller than the one obtained from the energetics-based model (see Fig. B.2*a*). This finding helps explain the reported $\simeq 5\%$ deviation of the zero-order CBL depth from the height of the minimum buoyancy flux in Conzemius & Fedorovich (2007) (see Table 2 in that reference).

Figure B.2*c* demonstrates that, consistent with the actual sheared CBL (Liu et al., 2016; Haghshenas & Mellado, 2019), the velocity increment at the CBL top increases as the CBL grows. Moreover, all curves collapse on top of each other, because the corresponding closure, Eq. (B.11), is the same in all models, and the deviation in the CBL depth is small (approximately 10% or less).

B.6 DISCUSSION

In this section, we consider three relevant aspects of the ZOMs in some detail. First, we discuss the good agreement observed among predictions from different models despite differences in the entrainment closures and simulations setups. Second, we discuss the singularity at finite wind strength observed in previous work, which was one major limitation is those models. Third, we employ the energetics-based model to investigate and discuss the dependence on environmental conditions of sheared CBL bulk properties.

B.6.1 *Good agreement despite differences in closures*

We have shown that the energetics-based model and the geometric-based model with $\alpha = 1$ predict the CBL bulk properties similarly to previous work that appropriately estimate the contribution of the entrainment-zone wind shear to the entrainment flux. This agreement is remarkable because Liu et al. (2016) have simulated a variety of CBLs in middle latitudes including shear-free, barotropic sheared, and equivalent-barotropic sheared CBLs over an aerodynamically rough surface, while Haghshenas & Mellado (2019) have simulated only shear-free and barotropic sheared CBLs without the Coriolis force over an aerodynamically smooth surface.

The observed agreement is, hence, promising in two aspects: first, it confirms that the parameterizations derived in Haghshenas & Mellado (2019) are independent of the surface properties, as they are expressed in terms of the velocity increment at the CBL top. Second, it suggests that they would most likely apply to sheared CBLs with Coriolis force and also to equivalent-barotropic CBLs in which the velocity varies linearly with height in the free atmosphere, although a proof of concept is necessary to draw a definitive conclusion.

The observed agreement between the prediction of the present and previous models might also sound surprising because of the differences in entrainment closures, in particular, differences in the length scale used to estimate the various terms of the TKE budget equation in the entrainment zone. The reason for such an agreement is that under weak- and moderate-shear conditions, the CBL depth (applied in previous work) and the local length scale of the entrainment zone (applied in the present work) are approximately proportional to each other (Haghshenas & Mellado, 2019), which results in equally good predictions of the CBL bulk properties from the present and previous models for the moderate-shear conditions considered in section B.5. Under very strong-shear conditions, however, these two length scales are not proportional to each other, and a constant fraction of the CBL depth is not an appropriate proxy of the local length scale of the entrainment zone. This different scaling eventually leads to the emergence of the singularity in models developed in previous work for very strong-shear conditions. The models proposed in the present work do not suffer from this limitation.

B.6.2 *Singularity at finite wind strength in previous work*

A singularity in previous work takes place when the denominator of Eq. (B.12) equals zero, i.e., when

$$C_P\,(\Delta u^{(0)})^2 = \frac{N_0^2}{2}\left[(h^{(0)})^2 - z_{\mathrm{enc}}^2\right] \tag{B.29}$$

wherein we have already taken $C_T = 0$ (cf. table B.1) and substituted Eq. (B.18b). Under very strong-shear conditions, one can write

$$h^{(0)} - z_{\mathrm{enc}} \simeq 0.25\, z_{\mathrm{enc}}\left[1 + 4.8\left(\frac{\Delta u^{(0)}}{N_0 z_{\mathrm{enc}}}\right)^2\right]^{1/2} \simeq \sqrt{0.3}\,\frac{\Delta u^{(0)}}{N_0}\,, \tag{B.30}$$

where the first approximation follows from Eq. (B.17) with $\alpha = 1$, and the second approximation holds for $\Delta u^{(0)}/(N_0 z_{\mathrm{enc}}) \gtrsim 1.0$ with less than 10% error. Substituting

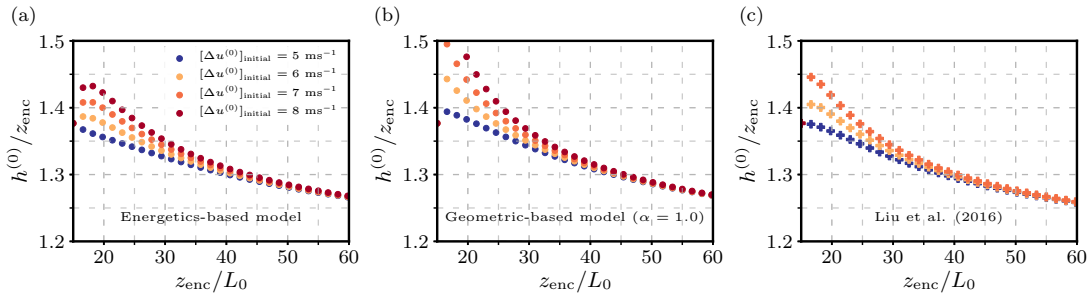

Figure B.3: Temporal evolution of the zero-order CBL depth obtained from different ZOMs with different initial conditions.

the expression for $\Delta u^{(0)}$ in terms of $h^{(0)}$ and z_{enc} from Eq. (B.30) in Eq. (B.29) and solving the achieved equation for $h^{(0)}$ gives

$$\frac{h^{(0)}}{z_{\text{enc}}} \simeq \frac{6.6\,C_P + 1}{6.6\,C_P - 1}\,, \tag{B.31}$$

as the critical condition. For $C_P = 0.43$, which is the constant used in Liu et al. (2016), this condition yields $h^{(0)} \simeq 2\,z_{\text{enc}}$ as the critical value of the CBL depth at which the singularity takes place. This critical condition corresponds to $\Delta u^{(0)}/(N_0 z_{\text{enc}}) \simeq 1.8$, according to Eq. (B.29). Such an extreme shear condition might happen during the morning in a windy day, when the well-mixed CBL is still shallow, and the velocity increment at the CBL top is strong.

Another relevant aspect is that, even though the entrainment closures in previous and present work have been derived for the quasi-steady regime, bulk models are likely initialized in atmospheric models with conditions that are far from the quasi-steady regime. This might be problematic in models proposed in previous work because they can also develop a singularity or become unrealistic when the initial conditions are far from the quasi-steady regime even in moderate-shear conditions. This occurs when

$$\left[\frac{(\Delta u^{(0)})^2}{\Delta b^{(0)} h^{(0)}}\right]_{\text{initial}} \geq \frac{1}{C_P} \tag{B.32}$$

according to Eq. (B.12) with $C_T = 0$.

To address these issues, we evaluate our ZOMs and the one by Liu et al. (2016) (as a representative of the models in group I) with different initial velocity increments at the CBL top, ranging from 5 ms^{-1}, which corresponds to the quasi-steady regime retrieved from Pino et al. (2006), to 8 ms^{-1} in intervals of 1 ms^{-1}. Results are shown in Fig. B.3. We observe that all models smoothly relax towards the quasi-equilibrium solutions, with deviations on the order of 10% in the CBL depth or less, except for Liu et al. (2016)'s model with $\Delta u^{(0)} = 8\ \text{ms}^{-1}$, which predicts unrealistically small CBL depths (out of the shown scale). This result illustrates that the singularity or unrealistic results might occur in previous models even for moderate-shear conditions.

B.6.3 *Dependence on environmental conditions of sheared CBL properties*

For the purpose of illustration, we explicitly discuss the dependence of sheared CBL bulk properties on environmental conditions using one of the ZOMs developed in

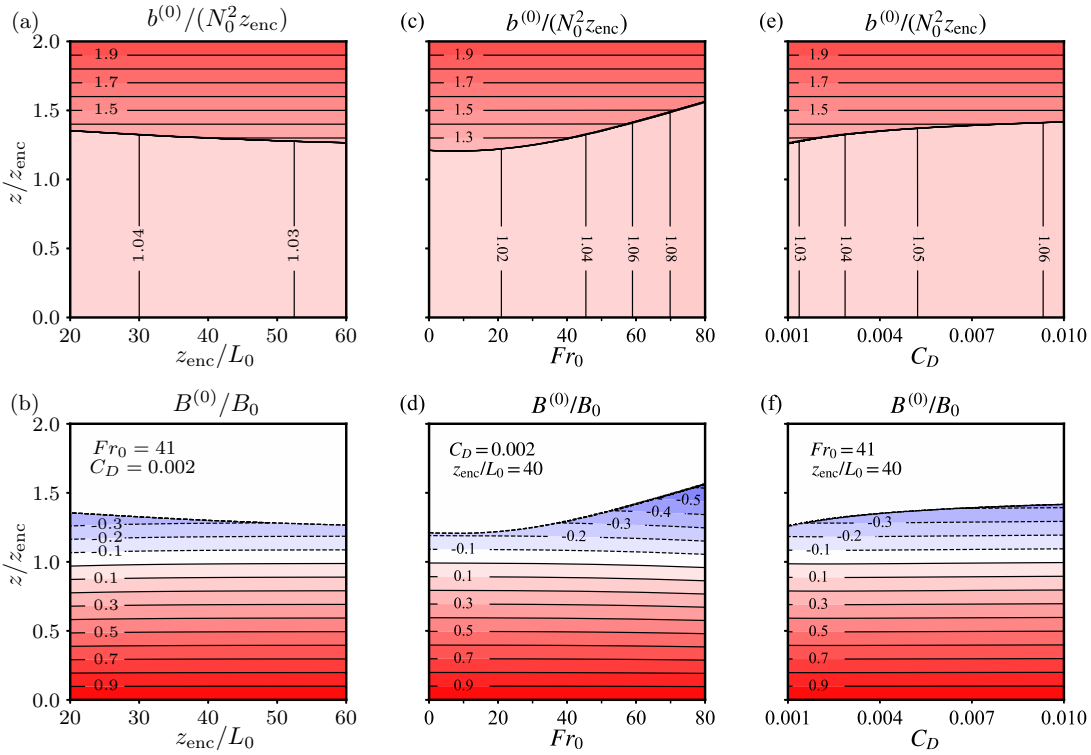

Figure B.4: Contour plots of (top panel) the normalized zero-order buoyancy and (bottom panel) its zero-order vertical flux as a function of the normalized distance from the surface and in panel (a,b) z_{enc}/L_0, in panel (c,d) Fr_0, and in panel (e,f) C_D.

this work. We employ the energetics-based model and scan the whole parameter space corresponding to midday atmospheric conditions over land (cf. section B.2.2). As indicated before, dynamical properties of the described CBL, once the initial conditions are sufficiently forgotten and the quasi-steady regime is reached, depend on two non-dimensional parameters, namely Fr_0 and C_D, and the non-dimensional independent variable z_{enc}/L_0. In addition, the non-dimensional parameter φ characterizes moisture properties.

We consider the case $\{Fr_0 = 41, C_D = 0.002\}$ at $z_{enc}/L_0 = 40$ as reference state and vary one non-dimensional parameter at a time. The model is always initialized with the initial condition provided in section B.5.2. Because this initial condition is not the exact one corresponding to the quasi-steady regime for all the parameter space, we illustrate the CBL properties at $z_{enc}/L_0 = 40$, which is sufficiently beyond the initial state of the CBL development, $z_{enc}/L_0 = 15$ (cf. Fig. B.3). This assures that the initial conditions have been sufficiently forgotten, and the discussed data are in the quasi-steady regime.

B.6.3.1 *Buoyancy*

The dependence of the normalized buoyancy and buoyancy flux on Fr_0, C_D, and z_{enc}/L_0 are provided graphically in Fig. B.4. This dependence is very small for the buoyancy and buoyancy flux within the mixed layer. The dependence is, however, of the order of one for the entrainment-flux ratio and the buoyancy increment at the CBL top. This behavior illustrates one of the main features of the barotropic CBL,

namely, wind-shear effects on the CBL structure and buoyancy-related properties remain localized at the CBL top.

We also observe that, with increasing $z_{\rm enc}/L_0$, the entrainment enhancement due to wind shear diminishes, and hence, wind-shear effects on CBL properties reduce and we approach the shear-free limit (cf. section B.5.1). The CBL depth and the mixed-layer buoyancy reduce, respectively, by $\simeq 7\%$ and $\simeq 1\%$, and the entrainment-flux ratio decreases by $\simeq 25\%$ over the interval of $z_{\rm enc}/L_0$ shown in Fig. B.4(a,b).

Wind-shear effects on CBL properties, as expected, grow when the reference Froude number or the surface-drag coefficient increase, because both non-dimensional parameters directly or indirectly lead to the larger velocity increment at the CBL top. The CBL depth and the mixed-layer buoyancy increase, respectively, by $\simeq 25\%$ and $\simeq 10\%$ and the entrainment-flux ratio grows by $\simeq 200\%$ for the interval of Fr_0 shown in Fig. B.4(c,d). For the case $Fr_0 = 80$, $C_D = 0.002$ and $z_{\rm enc}/L_0 = 40$, the independent variable $\Delta u^{(0)}/(N_0 z_{\rm enc})$ is approximately 1.14, which is still below the critical condition to observe the singularity in previous ZOMs. Further analysis (not shown) indicated that the critical condition, $\Delta u^{(0)}/(N_0 z_{\rm enc}) \simeq 1.8$, takes place, for instance, for $Fr_0 = 80$ and $C_D = 0.005$ in the early state of the CBL development.

The effect of Fr_0 and C_D on the CBL evolution differs in that the CBL depth grows with C_D asymptotically towards a finite value (see Fig. B.4*e*, *f*), whereas the growth of the CBL with Fr_0 is unbounded (see Fig. B.4*c*, *d*). The reason is that growing C_D with fixed Fr_0 causes wind-shear effects to emerge earlier (at a smaller $z_{\rm enc}/L_0$) because the velocity increment at the CBL top increases fast. Wind-shear affects are, however, limited since the reference Froude number, or equivalently the velocity in the free atmosphere, is fixed.

B.6.3.2 *Moisture*

To address the dependence of moisture properties of the sheared CBL on environmental conditions, we first consider $\varphi = 0$, which corresponds to the pure-drying regime. Figure B.5 shows graphically the dependence of the normalized moisture and moisture flux on Fr_0, C_D, and $z_{\rm enc}/L_0$. There are two features worth mentioning in this figure. First, given that the free atmosphere is dry and the wind shear enhances entrainment, the CBL dries more when the Froude number or the surface-drag coefficient increase (see Fig. B.5*c*, *e*). The entrainment enhancement due to the wind shear, however, diminishes as the CBL grows, and hence, the sheared CBL dries less as $z_{\rm enc}/L_0$ increases (see Fig. B.5*a*). Second, wind-shear effects on the mixed-layer specific humidity, $q_{\rm ml}^{(0)}$, are much larger than their effects on mixed-layer buoyancy, $b_{\rm ml}^{(0)}$ (cf. Figs. B.4 and B.5). The reason is that $\varphi = 0$ corresponds to $F_{q,0} = 0$, i.e., there is no surface flux of moisture but only the entrainment flux, so the entrainment enhancement due to the wind shear is more relevant in the moisture field than in the buoyancy field.

Figure B.6(a,b) illustrates graphically the dependence of moisture bulk properties on the flux-ratio parameter for $Fr_0 = 41$, $C_D = 0.002$, and $z_{\rm enc}/L_0 = 40$. For $\varphi \lesssim 1.2$, the CBL dries because the flux of moisture out of the CBL (entrainment drying) dominates over the surface flux into the CBL (surface moistening); the flux increases from the surface to a maximum at the CBL top. By increasing φ, the surface flux of moisture grows and for $\varphi \simeq 1.2$, the surface moistening equals the entrainment

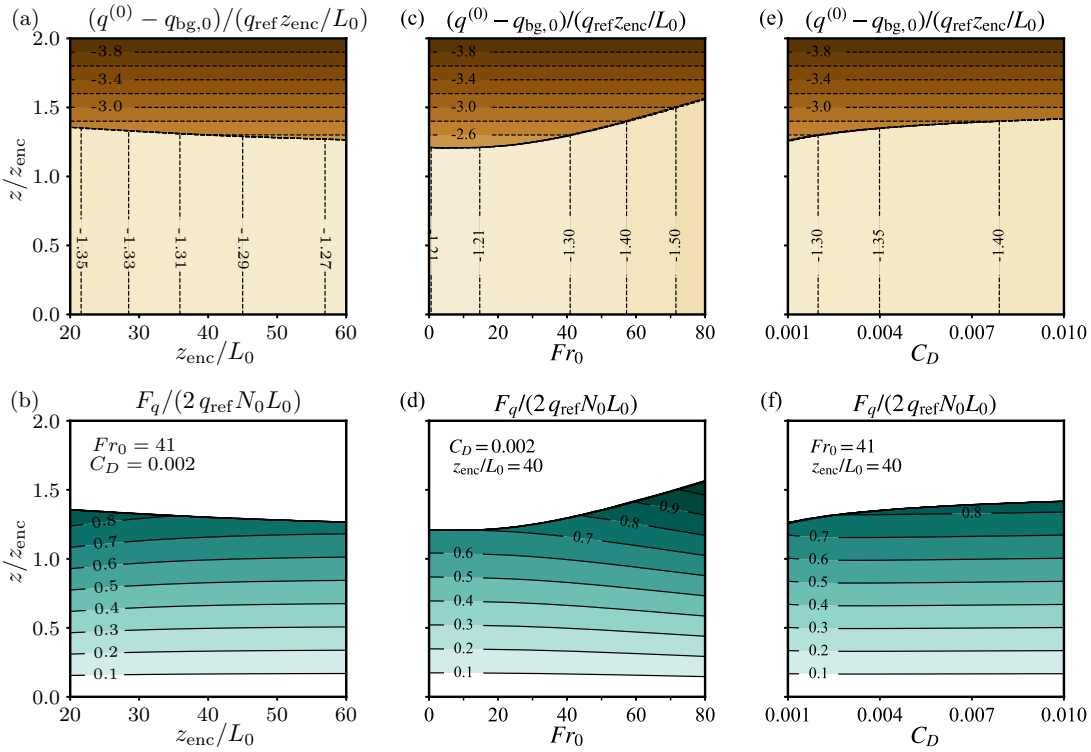

Figure B.5: Contour plots of (top plot) the normalized zero-order specific humidity and (bottom plot) its zero-order vertical flux as a function of the normalized distance from the surface and in panel (a) z_{enc}/L_0, in panel (b) Fr_0, and in panel (c) C_D for the condition $\varphi = 0$.

drying (Fig. B.6*b*). For $\varphi \gtrsim 1.2$, the CBL moistens because the surface flux of moisture into the CBL (surface moistening) dominates the flux of moisture out of the CBL (entrainment drying); the flux decreases from surface to the CBL top.

The cross-over value, $\varphi_{cr}^{(0)} \simeq 1.2$, for the considered sheared CBL is slightly larger than $\varphi_{cr}^{(0)} \simeq 1.17$ for the shear-free limit, since entrainment of dry air increases with the wind shear. Figure B.6(c) illustrates this behaviour more clearly, as the critical flux-ratio parameter enhances with increase of the Froude number. This enhancement, however, diminishes as the CBL grows.

B.7 SUMMARY AND CONCLUSIONS

Two zero-order bulk models (ZOM) with different entrainment closures have been developed for a cloud-free barotropic convective boundary layer (CBL) that grows into a linearly stratified atmosphere. In the first one, the negative and positive areas of the buoyancy flux were assumed to match between the model and the actual CBL. In the second one, the CBL depth was the variable chosen to match between the model and the actual CBL. Non-singular parameterizations for these properties derived in Haghshenas & Mellado (2019) have been employed as the entrainment-closure equation in each model. We referred to these models as energetics- and geometric-based models, respectively.

The main advantage of the proposed models is that they are free from the potential singularity at finite wind strength that has often been reported as a major limitation

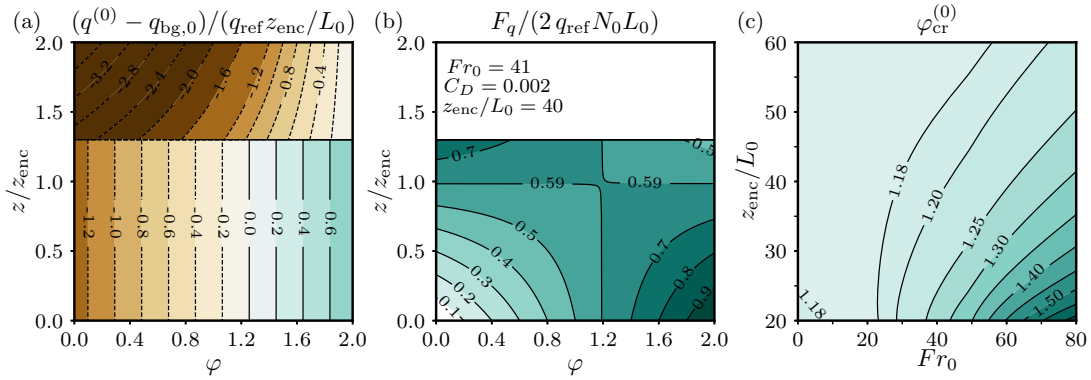

Figure B.6: Contour plots of (a) the normalized zero-order specific humidity and (b) its zero-order vertical flux as a function of the normalized distance from the surface and the flux-ratio parameter φ, defined by Eq. (B.5), for the sheared CBL characterized by $Fr_0 = 41$, $C_D = 0.002$, and $z_{\mathrm{enc}}/L_0 = 40$. Panel (c) demonstrates the contour plot of $\varphi_{\mathrm{cr}}^{(0)}$ as a function of Fr_0 and z_{enc}/L_0 with $C_D = 0.002$.

in previous work. We eliminated the potential singularity by performing an integral analysis of the TKE budget equation in the actual structure of the CBL and, in particular, by considering the local length scale of the entrainment zone when estimating the integral of the negative buoyancy flux and of the shear production across the entrainment zone. We discussed the potential singularity in the entrainment-closure equation of previous work analytically and numerically. Using the parameterizations for different CBL properties, we have shown that the singularity takes place under very strong-shear conditions when the sheared CBL depth becomes nearly two times larger than the encroachment length scale, or equivalently when $\Delta u^{(0)}/(N_0 z_{\mathrm{enc}})$, as the independent variable that characterizes wind-shear effects, equals 1.8. In addition, we have shown that considering initial conditions far away from the quasi-steady regime also leads to the singularity or unrealistic results in the models proposed in previous work even for moderate-shear conditions.

We have shown that the temporal evolution of different CBL properties obtained from the energetics-based model agrees very well with predictions of those models in previous work that appropriately considered the contribution of the entrainment-zone shear in the entrainment-closure equation. The best match was observed with predictions of Liu et al. (2016)'s model wherein 43% of generated turbulence by entrainment-zone shear was assumed to be used for entrainment.

One potential disadvantage of the energetics-based model and also the models in previous work, in which the energetics are matched between the actual and the modeled CBL, is that the modeled CBL depth cannot be *a priori* associated to any actual CBL-top height. This uncertainty might become important when the bulk model is intended to include more complexity like cloud formation. We developed the geometric-based model to address this issue. We considered three options for the CBL depth in the geometric-based model, namely, the height of the minimum buoyancy flux, the height that marks the transition from the lower to the upper entrainment-zone sublayer, and the height of the maximum buoyancy gradient. These heights differ by few hundred meters under typical midday atmospheric conditions over land. Predictions of the geometric-based model suggested that the CBL depths

in the energetics-based model and also models in previous work correspond better to the height that marks the transition from the lower to upper entrainment-zone sublayer, rather than the height of the minimum buoyancy flux. This finding helps explain the approximately 5% deviation of the zero-order CBL depth from the height of the minimum buoyancy flux reported in Conzemius & Fedorovich (2007).

An important conclusion of this study is that the zero-order bulk model, despite its simplicity, can appropriately represent bulk properties of sheared CBLs, meaning that a finite transition layer between the mixed layer and the free atmosphere is not explicitly required. This is because the relevant shear-induced features of the actual entrainment zone are considered in the entrainment closure. If needed, the vertical structure of the actual entrainment zone of the sheared CBL can be reconstructed *a posteriori* using the zero-order CBL depth predicted from any of the ZOMs and using the relationships between the zero-order CBL depth and various actual CBL heights provided in Haghshenas & Mellado (2019).

Acknowledgements

The authors gratefully acknowledge the Gauss Centre for Supercomputing (GCS) for providing computing time through the John von Neumann Institute for Computing (NIC) on the GCS share of the supercomputer JUQUEEN at Jülich Supercomputing Centre (JSC). Funding was provided by the Max Planck Society through its Max Planck Research Groups program. Primary data and scripts used in the analysis and other supporting information that may be useful in reproducing the author's work are archived by the Max Planck Institute for Meteorology and can be obtained by contacting publications@mpimet.mpg.de.

APPENDIX BA

Parameterization for the area ratio of the negative and positive buoyancy flux in the actual CBL

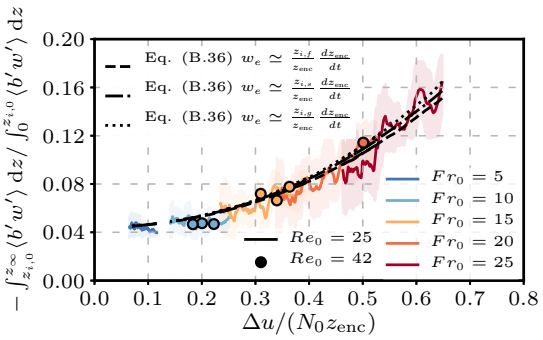

Figure B.7: Verification with DNS data of the parameterization for the area ratio of negative and positive buoyancy flux. Only data for $z_{\mathrm{enc}}/L_0 \gtrsim 15$, corresponding to the quasi-steady regime, is plotted. Symbols and lines indicate the average within an interval $\Delta z_{\mathrm{enc}}/L_0 = 2$, and shadow regions indicate the interval of two standard deviations around that average. $z_{\mathrm{i,0}}$ is the zero-crossing height, $z_{\mathrm{i,f}}$ is the height of the minimum buoyancy flux, $z_{\mathrm{i,s}}$ marks the transition from the lower EZ sublayer to the upper EZ sublayer, and $z_{\mathrm{i,g}}$ is the height of the maximum buoyancy gradient.

Several cloud-free barotropic CBLs over an aerodynamically smooth surface forced by a constant surface buoyancy flux growing into a linearly stratified atmosphere have been simulated by means of direct numerical simulation in Haghshenas & Mellado (2019). Each case was characterized by a reference buoyancy Reynolds number, $Re_0 = N_0 L_0^2/\nu$, and a reference Froude number, $Fr_0 = U_0/(N_0 L_0)$, setting the Prandtl number to one. Here ν is the kinematic viscosity. They have studied the quasi-steady regime of several cases scanning the parameter space $0 \leq Fr_0 \leq 25$ with two Re_0 of 25 and 42.

In order to derive the parameterization for the area ratio of the negative and positive buoyancy flux, we consider Eq. (5.4) of Haghshenas & Mellado (2019)

$$\int_{z_{i,0}}^{z_\infty} \left[\langle b'w'\rangle_c - \langle b'w'\rangle\right] \mathrm{d}z \sim \int_{z_{i,0}}^{z_\infty} -\langle u'w'\rangle \frac{\partial\langle u\rangle}{\partial z}\,\mathrm{d}z\,, \tag{B.33}$$

which implies that the entrainment enhancement in sheared CBLs is due to the additional TKE generated by the wind shear in the entrainment zone. Here $z_{i,0}$ is the reference height at which the buoyancy flux becomes zero. Primes indicate turbulent fluctuation fields, and subscript c denotes the shear-free limit.

In agreement with previous work, the negative area of the buoyancy flux in the shear-free limit is scaled by the convective scales as $-\int_{z_{i,0}}^{z_\infty}\langle b'w'\rangle_c\,\mathrm{d}z \simeq 0.02\,B_0 z_{\mathrm{enc}}$, where the coefficient of proportionality is obtained from the DNS data. Thus, the area of the negative buoyancy flux in sheared CBLs can be approximated as

$$-\int_{z_{i,0}}^{z_\infty}\langle b'w'\rangle\,\mathrm{d}z \simeq 0.02\,B_0 z_{\mathrm{enc}} + c_1\,w_e(\Delta u)^2\,, \tag{B.34}$$

using Eq. (B.33) and the well-known scaling argument for the integral of the shear production term (see e.g. Boers et al., 1984). Here $w_e \equiv \mathrm{d}\,z_{i,f}/\mathrm{d}\,t$ is the growth rate of the CBL depth, where $z_{i,f}$ is the height of the minimum buoyancy flux. To avoid the poor statistical convergence associated with determining w_e by taking the time derivative of $z_{i,f}$, we use the approximation provided in Haghshenas & Mellado (2019) as $w_e \simeq (z_{i,f}/z_{\mathrm{enc}})\mathrm{d}\,z_{\mathrm{enc}}/\mathrm{d}\,t$. The DNS data supports the ansatz in Eq. (B.34) and shows $c_1 \simeq 0.09$.

The fact that wind shear only modifies the vertical structure of the entrainment-zone indicates that the positive area of the buoyancy flux in sheared CBLs, consistent with shear-free CBLs, is scaled as

$$\int_0^{z_{i,0}}\langle b'w'\rangle\,\mathrm{d}z \simeq 0.46\,B_0 z_{\mathrm{enc}}\,, \tag{B.35}$$

where the coefficient of proportionality is obtained from the DNS data. The parameterization for the area ratio then reads as

$$-\frac{\int_{z_{i,0}}^{z_\infty}\langle b'w'\rangle\,\mathrm{d}z}{\int_0^{z_{i,0}}\langle b'w'\rangle\,\mathrm{d}z} \simeq 0.044 + 0.2\,\frac{w_e\,(\Delta u)^2}{B_0\,z_{\mathrm{enc}}}\,. \tag{B.36}$$

We obtain a value $\simeq 0.044$ for the area ratio in the shear-free limit, which is consistent with previous work (Conzemius & Fedorovich, 2006a). Figure B.7 supports this parameterization with DNS data, showing that the dependence of the proportionality coefficient, c_1, on the choice of the reference definition of the CBL height in w_e is smaller than the achieved statistical convergence. This sensitivity analysis allows

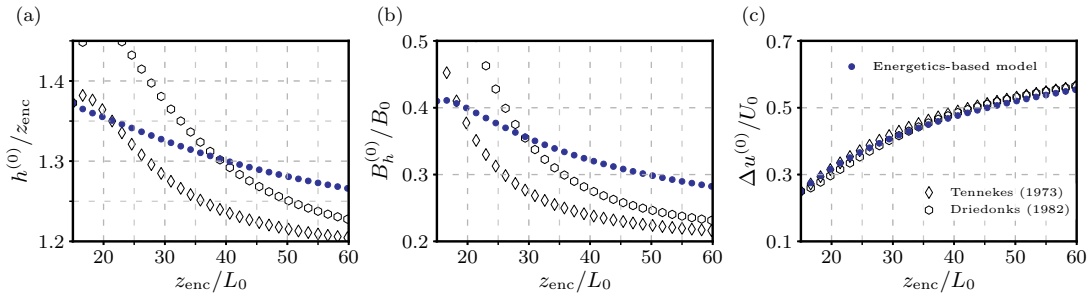

Figure B.8: Comparison of different properties of the sheared CBL ($Fr_0 = 41$ and $C_D = 0.002$) obtained from ZOMs developed in the present and previous work classified as Group II.

us to consider Eq. (B.36) as the entrainment closure in the energetics-based model, regardless of knowing *a priori* to which definition of the actual CBL height, the modeled CBL depth can be associated. In addition, Comparing the data from cases $Re_0 = 25$ and cases $Re_0 = 42$ shows that the Reynolds-number dependence of this parameterization is small, less than the achieved statistical convergence (see Fig. B.7).

APPENDIX BB

Geometric-based model corresponding to the height of the maximum buoyancy gradient

As explained in the main text, we also develop a geometric-based model with the model CBL depth chosen to be equal to the actual height of the maximum buoyancy gradient, for the sake of completeness. The corresponding closure equation is obtained from Eqs. (5.17) and (5.18) in Haghshenas & Mellado (2019) as

$$\frac{h^{(0)}}{z_{enc}} \simeq \underbrace{0.94}_{\text{I}} + \underbrace{0.25 \times X}_{\text{II}} + \underbrace{1.78 \times Y \times Z}_{\text{III}}, \tag{B.37}$$

where

$$X = \left[1 + 4.8 \left(\frac{\Delta u^{(0)}}{N_0 z_{enc}}\right)^2\right]^{1/2},$$

$$Y = \left[0.23 \left(\frac{L_0}{z_{enc}}\right)^2 - 0.85 \left(\frac{L_0}{z_{enc}}\right)^3\right]^{1/2},$$

$$Z = \left[1.34 \frac{\mathrm{d}\, h^{(0)}}{\mathrm{d}\, z_{enc}} - \frac{0.53}{X^2}\right]^{1/2}.$$

The first term (I) in Eq. (B.37) corresponds to the depth of the actual mixed layer, the second term (II) corresponds to the thickness of the lower entrainment-zone sublayer, and the third term (III) corresponds to the thickness of the upper entrainment-zone sublayer. Even though employing the geometric-based model with the aforementioned closure is straightforward, it is more convenient to use those two geometric-based models explained in the main text and reconstruct the height of the maximum buoyancy gradient from the results of those models and Eq. (B.37).

APPENDIX BC

Evaluation of ZOMs classified in group II

In this section, we evaluate the results of the ZOMs classified in group II that only takes the surface wind shear into account in the entrainment parameterization, Eq. (B.12). Figure B.8 illustrates the temporal evolution of the CBL properties obtained from these models. The result of the energetics-based model is incorporated in the figure to facilitate the comparison. Driedonks (1982) produces large values of the CBL depth and concomitantly the entrainment-flux ratio early on, followed by a sharp reductions over the remainder of the CBL development. Tennekes (1973) appears to work better in the early stage of the CBL development, however their predictions undergo a sudden decline in time as well. The reason for such a behavior is as follows. The surface wind shear, which fully determines the shear enhancement of entrainment in these models, is initially large. This results in a large entrainment-flux ratio and hence a large CBL depth. However, the surface wind shear decreases rapidly as time proceeds, and it is not anymore an appropriate proxy of the entrainment-zone shear, which, as discussed in recent previous work, is responsible for the entrainment enhancement by wind shear. Note that the velocity increments at the CBL top fall approximately on top of each other as a result of having the same surface closure, Eq. (B.11), in all models and the little sensitivity of this closure to the CBL depth.

BIBLIOGRAPHY

Ayotte, K. W. et al. (1996). "An evaluation of neutral and convective planetary boundary-layer parameterizations relative to large eddy simulations." In: *Bound.-Layer Meteor.* 79.1, pp. 131–175.

Batchvarova, E. & S.-E. Gryning (1994). "An applied model for the height of the daytime mixed layer and the entrainment zone." In: *Bound.-Layer Meteor.* 71.3, pp. 311–323.

Betts, A. K. (1974). "Reply to comment on the paper 'Non-precipitating cumulus convection and its parameterization'." In: *Quart. J. Roy. Meteor. Soc.* 100, pp. 469–471.

Boers, R., E. W. Eloranta & R. L. Coulter (1984). "Lidar Observations of Mixed Layer Dynamics: Tests of Parameterized Entrainment Models of Mixed Layer Growth Rate." In: *J. Appl. Meteor.* 23, pp. 247–266.

Carson, D. & F. Smith (1975). "Thermodynamic model for the development of a convectively unstable boundary layer." In: *Advances in Geophysics* 18, pp. 111–124.

Conzemius, R. J. & E. Fedorovich (2006a). "Dynamics of sheared convective boundary layer entrainment. Part I: Methodological background and large eddy simulations." In: *J. Atmos. Sci.* 63, pp. 1151–1178.

– (2006b). "Dynamics of sheared convective boundary layer entrainment. Part II: Evaluation of bulk model predictions of entrainment flux." In: *J. Atmos. Sci.* 63, pp. 1179–1199.

– (2007). "Bulk models of the sheared convective boundary layer: evaluation through large eddy simulations." In: *J. Atmos. Sci.* 64, pp. 786–807.

Conzemius, R. & E. Fedorovich (2004). "Numerical models of entrainment into sheared convective boundary layers evaluated through large eddy simulations." In: *16th Symposium on Boundary Layers and Turbulence*.

De Roode, Stephan R., A. Pier Siebesma, Sara Dal Gesso, Harm J. J. Jonker, Jerôme Schalkwijk & Jasper Sival (2014). "A mixed-layer model study of the stratocumulus response to changes in large-scale conditions." In: *Journal of Advances in Modeling Earth Systems* 6.4, pp. 1256–1270.

Deardorff, J. W. (1970). "Preliminary results from numerical integration of the unstable boundary layer." In: *J. Atmos. Sci.* 27, pp. 1290–1211.

– (1979). "Prediction of Convective Mixed-Layer Entrainment for Realistic Capping Inversion Structure." In: *J. Atmos. Sci.* 36, pp. 424–436.

Deardorff, J. W., G. E. Willis & D. K. Lilly (1969). "Laboratory investigation of non-steady penetrative convection." In: *Journal of Fluid Mechanics* 35.1, pp. 7–31.

Driedonks, A. G. M. (1982). "Models and observations of the growth of the atmospheric boundary layer." In: *Bound.-Layer Meteor.* 23, pp. 283–306.

Fedorovich, E. (1995). "Modeling the Atmospheric Convective Boundary Layer within a Zero-Order Jump Approach: An Extended Theoretical Framework." In: *Journal of Applied Meteorology* 34.9, pp. 1916–1928.

Fedorovich, E. & R. J. Conzemius (2008). "Effects of wind shear on the atmospheric convective boundary layer structure and evolution." In: *Acta Geophysica* 56, pp. 114–141.

Fedorovich, E., R. Conzemius & D. Mironov (2004). "Convective entrainment into a shear-free linearly stratified atmosphere: Bulk models reevaluated through large-eddy simulation." In: *J. Atmos. Sci.* 61, pp. 281–295.

Flamant, C., J. Pelon, B. Brashers & R. A. Brown (1999). "Evidence of a Mixed-Layer Dynamics Contribution to the Entrainment Process." In: *Bound.-Layer Meteor.* 93.1, pp. 47–73.

Garcia, J. R. & J. P. Mellado (2014). "The two-layer structure of the entrainment zone in the convective boundary layer." In: *J. Atmos. Sci.* 71, pp. 1935–1955.

Garratt, J. R. (1992). "The Atmospheric Boundary Layer." In: *Cambridge University Pres*.

Garratt, J. R., J. C. Wyngaard & R. J. Francey (1982). "Winds in the Atmospheric Boundary Layer-Prediction and Observation." In: *J. Atmos. Sci.* 39.6, pp. 1307–1316.

Haghshenas, A. & J. P. Mellado (2019). "Characterization of wind-shear effects on entrainment in a convective boundary layer." In: *J. Fluid Mech.* 858, pp. 145–183.

Haltiner, G. J. & R. T. Williams (1980). "Numerical Prediction and Dynamic Meteorology." In: John Wiley and Sons, 477 pp.

Huang, J., X. Lee & E. G. Patton (2011). "Entrainment and budgets of heat, water vapor, and carbon dioxide in a convective boundary layer driven by time-varying forcing." In: *Journal of Geophysical Research: Atmospheres* 116.D6.

Kantha, L. H., O. M. Phillips & R. S. Azad (1977). "On turbulent entrainment at a stable density interface." In: *Journal of Fluid Mechanics* 79.4, pp. 753–768.

Kato, H. & O. M. Phillips (1969). "On the penetration of a turbulent layer into stratified fluid." In: *Journal of Fluid Mechanics* 37.4, pp. 643–655.

Kim, S. W., S. U. Park & C. H. Moeng (2003). "Entrainment processes in the convective boundary layer with varying wind shear." In: *Bound.-Layer Meteor.* 108, pp. 221–245.

Kim, S. W., S. Park, D. Pino & J. Vilà-Guerau De Arellano (2006). "Entrainment parameterization in a sheared convective boundary layer by using a first-order jump model." In: *Bound.-Layer Meteor.* 120, pp. 455–475.

Lilly, D. K. (1968). "Models of cloud-topped mixed layers under a strong inversion." In: *Quart. J. Roy. Meteor. Soc.* 94, pp. 292–309.

Liu, P., J. Sun & L. Shen (2016). "Parameterization of sheared entrainment in a well-developed CBL. Part I: Evaluation of the scheme through large-eddy simulations." In: *Adv. Atmos. Sci.* 33, pp. 1171–1184.

Mahrt, L. (1991). "Boundary-layer moisture regimes." In: *Quart. J. Roy. Meteor. Soc.* 117.497, pp. 151–176.

Mahrt, L. & D. H. Lenschow (1976). "Growth dynamics of the convective mixed layer." In: *J. Atmos. Sci.* 33, pp. 41–51.

Mellado, J. P., C. C. van Heerwaarden & J. R. Garcia (2016). "Near-Surface Effects of Free Atmosphere Stratification in Free Convection." In: *Bound.-Layer Meteor.* 159.1, pp. 69–95.

Mellado, J.P., M. Puche & C. C. van Heerwaarden (2017). "Moisture statistics in free convective boundary layers growing into linearly stratified atmospheres." In: *Quarterly Journal of the Royal Meteorological Society* 143.707, pp. 2403–2419.

Naumann, Ann Kristin, Bjorn Stevens, Cathy Hohenegger & Juan Pedro Mellado (2017). "A Conceptual Model of a Shallow Circulation Induced by Prescribed Low-Level Radiative Cooling." In: *Journal of the Atmospheric Sciences* 74.10, pp. 3129–3144.

Pelly, J. L. & S. E. Belcher (2001). "A Mixed-Layer Model Of The Well-Mixed Stratocumulus Topped Boundary Layer." In: *Bound.-Layer Meteor.* 100.1, pp. 171–187.

Pino, D. & J. Vilà-Guerau De Arellano (2008). "Effects of shear in the convective boundary layer: analysis of the turbulent kinetic energy budget." In: *Acta Geophysica* 56, pp. 167–193.

Pino, D., J. V. G. de Arellano & P. J. Duynkerke (2003). "The contribution of shear to the evolution of a convective boundary layer." In: *J. Atmos. Sci.* 60, pp. 1913–1926.

Pino, D., J. V. G. de Arellano & S. W. Kim (2006). "Representing sheared convective boundary layer by zeroth- and first-order-jump mixed-layer models: Large-eddy simulation verification." In: *J. Appl. Meteor. Clim.* 45, pp. 1224–1243.

Suarez, Max J., Akio Arakawa & David A. Randall (1983). "The Parameterization Of the Planetary Boundary Layer in the UCLA General Circulation Model: Formulation and Results." In: *Monthly Weather Review* 111.11, pp. 2224–2243.

Sullivan, P., C. H. Moeng, B. Stevens, D. H. Lenschow & S. D. Mayor (1998). "Structure of the entrainment zone capping the convective atmospheric boundary layer." In: *J. Atmos. Sci.* 55, pp. 3042–3064.

Sun, J. & Q. Xu (2009). "Parameterization of Sheared Convective Entrainment in the First-Order Jump Model: Evaluation Through Large-Eddy Simulation." In: *Bound.-Layer Meteor.* 132.2, pp. 279–288.

Tennekes, H. (1973). "A Model for the Dynamics of the Inversion Above a Convective Boundary Layer." In: *J. Atmos. Sci.* 30, pp. 558–567.

Tennekes, H. & A. G. M. Driedonks (1981). "Basic entrainment equations for the atmospheric boundary layer." In: *Bound.-Layer Meteor.* 20.4, pp. 515–531.

Van Heerwaarden, Chiel C. & Juan Pedro Mellado (2016). "Growth and Decay of a Convective Boundary Layer over a Surface with a Constant Temperature." In: *Journal of the Atmospheric Sciences* 73.5, pp. 2165–2177.

Willis, G. E. & J. W. Deardorff (1974). "A Laboratory Model of the Unstable Planetary Boundary Layer." In: *Journal of the Atmospheric Sciences* 31.5, pp. 1297–1307.

Zanten, Margreet C. van, Peter G. Duynkerke & Joannes W. M. Cuijpers (1999). "Entrainment Parameterization in Convective Boundary Layers." In: *J. Atmos. Sci.* 56.6, pp. 813–828.

Zeman, O. & H. Tennekes (1977). "Parameterization of the turbulent energy budget at the top of the daytime atmospheric boundary layer." In: *J. Atmos. Sci.* 34, pp. 111–123.

ACKNOWLEDGMENTS

The only reason that I succeeded in doing this project is the incredible support I received from my surrounding people who accompanied me in this long journey. First and foremost I would like to express my very great appreciation to my advisor Juan Pedro Mellado for his invaluable, tremendous support and guidance over the last three and half years and for making my PhD an enjoyable and rewarding experience. Apart from all infinite scientific insights he shared with me, I always appreciate his personality, and in particular his determination, patience, and kindness. Thanks Juan Pedro for believing in me and providing me such an unbelievable opportunity. I would also like to offer my special thanks to my co-advisors, Cathy Hohenegger and Felix Ament, for their useful and constructive recommendations and extremely encouraging and helpful panel meetings. I am particularly grateful for Bjorn Stevens's encouraging feedbacks and for sparking the idea of developing a bulk model as the second part of my dissertation. It was a great pleasure to be part of a department led by him. My special acknowledgment goes to Bernhard Schulz. Bernhard was not only an incredible, considerate office-mate, but also a wonderful, supporting companion, who offered me his help, whenever I needed. We learned a lot from each other out of our tough, time-consuming discussions. My special thanks are extended to the staff of the International Max Planck Research School and specifically: Antje Weitz, Cornelia Kampmann, Michaela Born and Wiebke Bohem. I would also like to thank all previous and current members of the Turbulent Mixing Processes group for their readiness to help and willingness to share their knowledge. Advices given by Alberto de Lozar and Chiel van Heerwaarden at the beginning of my PhD have been a great help. Katherine Fodor is especially thanked for being the first and the main reviewer of my work and for her great effort in the proof-reading of my papers and this thesis and for her valuable suggestions. Contribution of Moritz Hartmann to the bulk-model paper and our intensive discussions on the moisture is greatly appreciated.

Last but not least, I would like to acknowledge my lovely parents, who have always been supportive and encouraging in every step of my life. Above all, I would like to thank my amazing wife Shiva for her love and constant support, for making me feel like the luckiest man in the world every single day, and most of all, for being my best friend. I owe Shiva everything.

DECLARATION

Versicherung an Eides statt
Declaration of oath

Hiermit versichere ich an Eides statt, dass ich die vorliegende Dissertation mit dem Titel: „On Entrainment in Sheared Convective Boundary Layers “ selbstständig verfasst und keine anderen als die angegebenen Hilfsmittel – insbesondere keine im Quellenverzeichnis nicht benannten Internet-Quellen – benutzt habe. Alle Stellen, die wörtlich oder sinngemäß aus Veröffentlichungen entnommen wurden, sind als solche kenntlich gemacht. Ich versichere weiterhin, dass ich die Dissertation oder Teile davon vorher weder im In- noch im Ausland in einem anderen Prüfungsverfahren eingereicht habe und die eingereichte schriftliche Fassung der auf dem elektronischen Speichermedium entspricht.

Hamburg,

Armin Haghshenas

Hinweis / Reference

Die gesamten Veröffentlichungen in der Publikationsreihe des MPI-M
„Berichte zur Erdsystemforschung / Reports on Earth System Science“,
ISSN 1614-1199

sind über die Internetseiten des Max-Planck-Instituts für Meteorologie erhältlich:
http://www.mpimet.mpg.de/wissenschaft/publikationen.html

All the publications in the series of the MPI -M
„Berichte zur Erdsystemforschung / Reports on Earth System Science“,
ISSN 1614-1199

are available on the website of the Max Planck Institute for Meteorology:
http://www.mpimet.mpg.de/wissenschaft/publikationen.html